

PETROGENESIS OF THE BONANZA MAGMA CHAMBER,
SAN JUAN VOLCANIC FIELD,
SOUTHWESTERN COLORADO

A Thesis

Presented in Partial Fulfillment of the Requirements for
the degree Master of Science in the
Graduate School of the Ohio State University

by

Martha Louise McKnight, B.S.

The Ohio State University

1987

Master's Examination Committee

Michael Barton

Douglas E. Pride

Jeffrey Daniels

Approved by

Handwritten signature of Michael Barton in black ink, consisting of the initials 'MB' followed by 'Barton' in a cursive script.

Michael Barton
Department of
Geology and Mineralogy

"Glasses are the only rocks of which we can say with complete confidence that they correspond in composition with a liquid"

--- N.L. Bowen, 1928

ACKNOWLEDGMENTS

Many thanks to all of the people who have helped in this study: to Kim Randall and Doug Pride for their help in the field; to Joep Huijsmans for the XRF-analyses; to ARCO, Sigma Xi, and Friends of Orton Hall for their generous monetary support; to Mike Barton for his guidance throughout the project, and to Doug Pride for reviewing the manuscript; to Dennis Schucker and Dave Bernosky for allowing me to take over their computers; to Phil Jagucki for moral support; and special thanks to Paul Wyers for answering thousands of questions and for spending many sleepless nights with me in Mendenhall 302.

VITA

February 2, 1962 Born - Dallas, Texas
1984 B.S., Trinity University,
San Antonio, Texas
1984-1986 Graduate Teaching
Assistant, The Ohio State
University, Columbus,
Ohio

FIELDS OF STUDY

Major Field: Geology

Studies in Igneous Petrology, Dr. Michael Barton

TABLE OF CONTENTS

ACKNOWLEDGEMENTS.....	ii
VITA.....	iii
LIST OF TABLES.....	vi
LIST OF FIGURES.....	vii
LIST OF PLATES.....	x
 CHAPTER	 PAGE
I. INTRODUCTION.....	1
Geologic importance of ash flows.....	1
Unusual features of the Bonanza Tuff.....	2
Purpose.....	4
 II. GEOLOGIC SETTING OF THE SAN JUAN MOUNTAINS...	 5
Geologic history of the San Juan Mountains	5
Geophysical data.....	13
Lipman et al.'s model.....	14
 III. GEOLOGIC SETTING OF THE BONANZA REGION.....	 19
Location.....	19
History of the town.....	19
Geophysical data.....	21
Stratigraphy.....	25
Basement rocks.....	25
Rawley Andesite.....	27
Bonanza Tuff.....	31
Intracaldera facies.....	32
Distal facies.....	33
Source.....	41
Upper volcanics.....	42
Intrusive rocks.....	44
Mineralization.....	48
 IV. PETROGRAPHY AND MINERAL CHEMISTRY.....	 50
Introduction and analytical methods.....	50
Rawley Andesite (Tra).....	51
Lower Bonanza Tuff (Tbl).....	53
Upper Bonanza Tuff (Tbu).....	71
Upper volcanics (Tuv).....	75
Origin of observed petrographic features.	77
Resorption features.....	77

	Zoning in feldspars.....	82
	Oxidation features.....	87
	Secondary silicification.....	89
V.	GEOTHERMOMETRY AND GEOBAROMETRY.....	90
	Two-feldspar geothermometer.....	90
	Stormer's (1975) method.....	90
	Brown and Parson's (1981) method.....	99
	Accuracy of the two-feldspar geothermometer.....	103
	Application to the Bonanza volcanics..	104
	Biotite thermometer.....	106
	Application.....	107
	Determination of water content.....	110
VI.	WHOLE-ROCK CHEMISTRY.....	115
	Introduction.....	115
	Major element chemistry.....	115
	Alteration.....	119
	K ₂ O contents compared.....	120
	Variation diagrams.....	120
	Trace element chemistry.....	127
	Compositional trends with time.....	138
	Isotope chemistry.....	146
VII.	DISCUSSION.....	158
	Introduction.....	158
	Early eruption of the Bonanza Tuff.....	159
	Lack of Plinian airfall.....	159
	Chemistry vs. mineralogy.....	161
	Magmatic processes.....	161
	Lithic accumulation.....	163
	Eolian winnowing.....	165
	High K ₂ O.....	166
	Magmatic processes.....	167
	Alteration.....	169
	Chemistry of the Tbu.....	171
	Mineral chemistry trends.....	174
VIII.	CONCLUSIONS.....	177
	LIST OF REFERENCES.....	179

LIST OF TABLES

TABLE		PAGE
1.	Feldspar Temperatures for Samples from the Lower and Upper Bonanza Tuff.105
2.	Biotite Temperatures for Samples from the Lower and Upper Bonanza Tuff.109
3.	Whole-Rock Major Element Chemistry for the Bonanza Volcanic Units.116
4.	CIPW Norms for the Bonanza Volcanics.117
5.	Trace Element Chemistry of the Bonanza Volcanic Units Compared to Trace Element Abundances of Orogenic Silicic Volcanics. . .	.128
6.	$^{87}\text{Sr}/^{86}\text{Sr}$ Values for Rocks of the Bonanza Area.156

LIST OF FIGURES

FIGURES	PAGE
1. Geologic map of the San Juan volcanic field.	3
2. Histograms of SiO ₂ contents for the major phases of Tertiary volcanism in the San Juans.	8
3. Eruption rates for the San Juan volcanics. . .	11
4. Residual profile of the gravity anomaly, profile of magnetic anomaly, and model of batholith dimensions.	15
5. Model for the evolution of the San Juan batholith.	16
6. Topographic map of the Bonanza region. . . .	20
7. Gravity map of the Bonanza area.	22
8. Model of the configuration of the Bonanza caldera.	24
9. Stratigraphic column of the Paleozoic sedimentary rocks in the Bonanza district. .	26
10. Stratigraphic relationships of igneous rocks in the Bonanza region.	28
11. Geologic map of the Bonanza district.	30
12. Stratigraphic column of the Findley Ridge section.	38
13. Zones of welding within a typical ash flow. .	39
14. Reconstructed flow directions of the Bonanza Tuff ash flows.	43
15. Variations in mineralogy with stratigraphic height for the Bonanza Tuff.	55
16. Ternary plot of plagioclase and alkali feldspar compositions within the Bonanza Tuff and Upper Volcanic lava flows.	57

17.	Ternary plot of K-Mg-Fe components in biotite samples.	60
18.	Ti content of biotite versus stratigraphic height.	61
19.	Ulvospinel content of opaques versus stratigraphic height.	61
20.	Mg content of opaques versus stratigraphic height.	64
21.	Cr content of opaques versus stratigraphic height.	64
22.	Ternary plot of pyroxene compositions.	65
23.	Mol fraction of Mg in pyroxene versus stratigraphic height.	65
24.	Mol percent of ferrosilite in pyroxene versus stratigraphic height.	67
25.	Average ratio of Fe^{3+}/Fe^{2+} in pyroxene versus stratigraphic height.	67
26.	P-T diagram for the Ab-An system.	79
27.	P-T diagram for the Ab-An system showing the pressure sensitivity of the Ab melting curve relative to An.	79
28.	Fo-Di-SiO ₂ phase equilibria diagram.	81
29.	The effects of mixing on the cusped MORB melting curve.	83
30.	X-T diagram for the Ab-An system showing the effects of pressure on composition.	85
31.	X-T diagram for the Ab-An system showing the effects of water content on composition.	85
32.	Comparison of activity-composition relationships for real and ideal solutions.	94
33.	Phase diagram for the Ab-An system showing regions of unmixing.	96
34.	Graphical two-feldspar geothermometer.	102

35.	Comparison of biotite and feldspar temperatures to determine pressure of magma equilibration.	111
36.	Comparison of biotite and feldspar temperatures to determine the water pressure at which the magma equilibrated.	113
37.	AFM diagram of major element chemistry.	118
38.	Variation diagram comparing K_2O and SiO_2 content of Bonanza units to other orogenic volcanics.	121
39.	Harker variation diagrams of major element chemistry.	122
40.	Harker variation diagrams of trace element chemistry.	130
41.	Plots of incompatible elements vs. ppm Th.	137
42.	Cyclic trends exhibited by composition of Santorini lavas vs. stratigraphic height.	140
43.	Plots of major element compositions vs. stratigraphic height.	141
44.	Plots of trace element compositions vs. stratigraphic height.	147
45.	Plot of volume percent lithics vs. stratigraphic height.	164
46.	Plot of volume percent matrix vs. stratigraphic height.	164
47.	Plot of K_2O/Na_2O ratio vs. wt. percent H_2O	172
48.	Model for eruption of the Bonanza magma chamber.	175

LIST OF PLATES

PLATE		PAGE
1.	Intracaldera Facies of the Lower Bonanza Tuff.	34
2.	Ridge Between Elkhorn and Copper Gulches: Intracaldera Sample Site.	35
3.	Photograph of Findley Ridge Showing the Eight Ash Flows Recognized by Marrs (1973). . .	37
4.	Eutaxitic Flow Texture in the Distal Facies of the Lower Bonanza Tuff.	40
5.	Outcrop Pattern of Upper Volcanic Lava Flows.	45
6.	Outcrop of Porphyry Peak Rhyolite Showing Platy Flow Structure.	47

CHAPTER 1
INTRODUCTION

Geologic Importance of Ash Flows

Ash flow deposits offer a unique opportunity for petrogenic studies because the sudden eruption of an ash flow preserves a quenched sample of the underlying magma chamber, and generally evacuates a larger proportion of the chamber than is emptied by a lava eruption (Cox, Bell, and Pankhurst, 1979). A sample from the crystallized and denuded pluton itself is of lesser value for the study of magmatic processes because the original character of the magma has been altered during slow cooling as the minerals re-equilibrated to lower temperatures.

During a pyroclastic eruption, the shallow, more evolved magmas are usually tapped first, with successive eruptions drawing from deeper, less differentiated zones within the chamber. This eruptive sequence results in stratigraphic zonation of the ash flow deposit, as has been documented in the Bishop Tuff of California (Hildreth, 1981), as well as in ash flows in Japan (Katsui, 1963), New Zealand (Martin, 1965), and Ethiopia (Gibson, 1970). Smith (1979) noted that, generally, zoned ash flows demonstrate:

- 1) an increase in phenocryst content
- 2) an increasingly mafic composition, and
- 3) hotter mineral-equilibrium temperatures

at successively higher stratigraphic levels.

Unusual Features of the Bonanza Tuff

The Bonanza Tuff is an early Oligocene ignimbrite deposit located in the northeastern corner of the San Juan volcanic field (Fig. 1), and it is anomalous in many aspects. According to K/Ar dates, the Bonanza Tuff is at least five million years older than any other ignimbrite in the San Juan field (Varga and Smith, 1984). In addition, the compositional zoning is inverted relative to the expected felsic-to-mafic upward sequence suggested by Smith (1979); the Bonanza Tuff exhibits an abrupt transition from a lower composite sheet of phenocryst-rich high-K dacite ignimbrite to an upper, phenocryst-poor sheet of rhyolitic composition (Varga and Smith, 1984). According to Smith (1979), the transition between the lower and upper flow sheets of the Bonanza Tuff represents a larger gap in SiO₂ content than is known for any ignimbrite erupted from a zoned magma chamber. Finally, the Bonanza Tuff contains virtually no Plinian ash fall component, although such deposits usually precede a large ash flow eruption (Fisher and Schmincke, 1984).

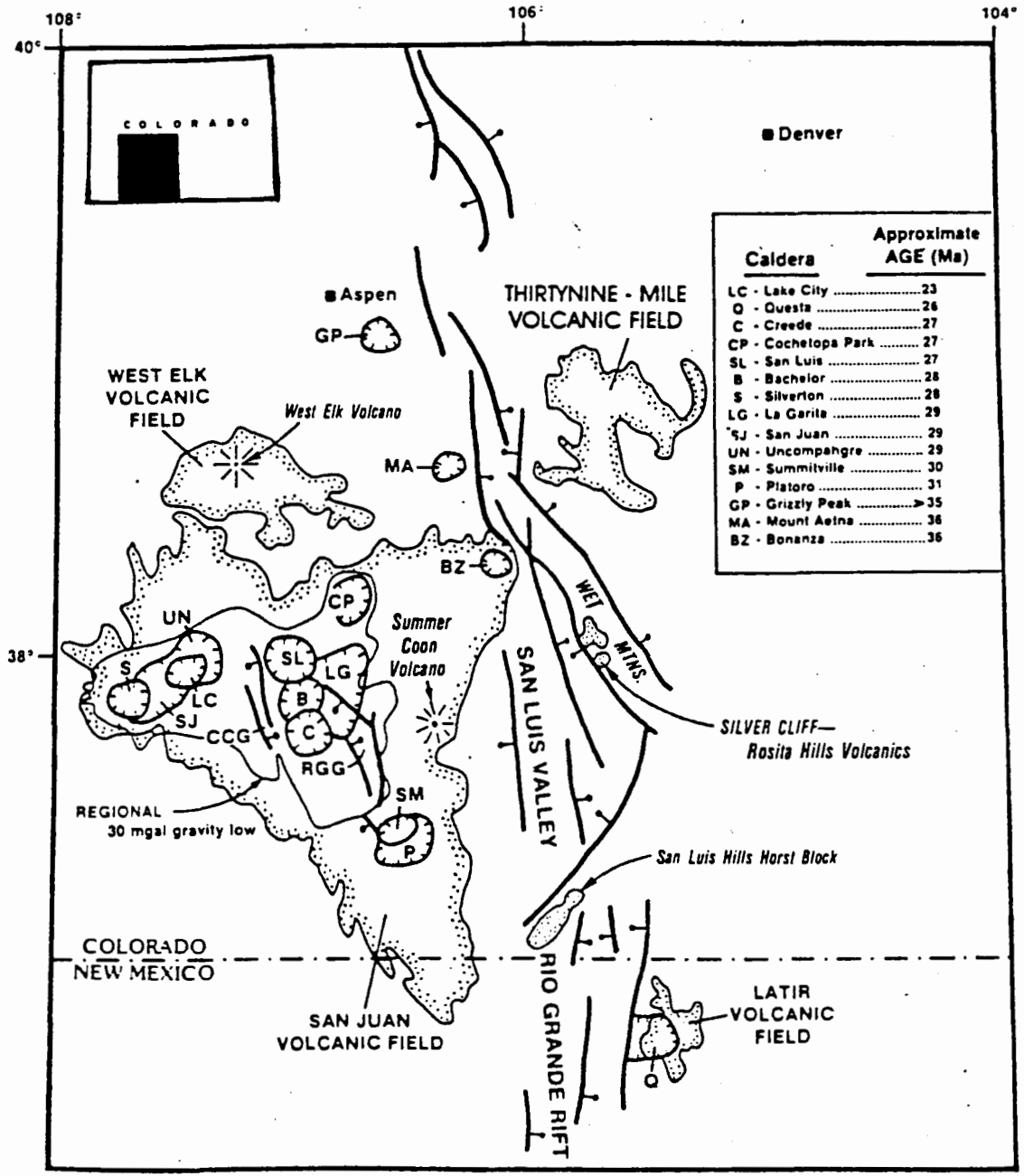


Fig. 1. Map of the San Juan volcanic field in southwestern Colorado, showing calderas (circular hachured areas), Cenozoic tectonic features, and the Bouguer gravity anomaly from Plouff and Pakiser's (1965) study (modified from Varga and Smith, 1984).

Purpose

The purpose of this study is to develop a petrogenic model for the Bonanza magma chamber that is consistent with the anomalous zoning of the Bonanza Tuff, its early emplacement, and its lack of Plinian ash fall deposits. Whole rock major and trace elements are used to investigate possible petrogenic processes relating the upper and lower units of the Bonanza Tuff. Microprobe analyses of minerals are used to estimate the depth of the magma chamber, to evaluate thermal zonation within the chamber, and to construct the oxygen fugacity and the water content of the magma prior to eruption.

CHAPTER 2

GEOLOGIC SETTING OF THE SAN JUAN MOUNTAINS

Geologic History of the San Juan Mountains

The San Juan mountains are located in southwestern Colorado (Fig. 1). From earliest time, this region has been an area of active tectonism. Precambrian rocks record at least two episodes of mountain-building approximately 2.5 and 1.5 billion years ago, during which intense folding and metamorphism were accompanied by the intrusion of many granitic plutons (Chronic, 1980).

A long period of crustal stability followed in the late Precambrian, during which extensive erosion exposed the roots of the early mountains. Later, as Paleozoic seas began to creep across the region, the Precambrian crystalline rocks were buried by thick sequences of marine sediments (Chronic, 1980).

A zone of crustal weakness seems to bisect Colorado, for when sea-floor spreading along the eastern margin of the North American plate became unusually intense during Pennsylvanian time (300 million years ago), the ancient Precambrian orogenic zone was reactivated. The crust was fractured and uplifted to form two extensive island ranges,

known as the Ancestral Rockies, which rose above the Paleozoic sea. During the late Paleozoic and Mesozoic, the Ancestral Rockies were leveled by erosion and contributed to fluvial and lacustrine sediments that were deposited as the epic seas retreated (Chronic, 1980).

The San Juan Mountains began forming in the late Cretaceous to early Tertiary (60 million years ago) with the onset of another period of rapid sea-floor spreading. The opening of the Atlantic Ocean pushed the North American plate 1500 miles westward over the edge of the Pacific plate, causing stresses that culminated in the Laramide Orogeny and formed the Rocky Mountains (Chronic, 1980). At this time the southwestern part of Colorado was uplifted into a vast dome spanning 100 miles, known as the Brazos-Uncompahgre uplift (Lipman et al., 1978). Erosion of the dome began in the Eocene, eventually exposing its Precambrian core and creating an erosion surface with 500 feet of relief (Chronic, 1980).

Volcanic activity in the San Juans occurred in three stages, beginning abruptly approximately 38 million years ago in the early Oligocene with the extrusion of vast quantities of intermediate-composition lavas onto the Eocene erosion surface. These early lavas were erupted from clustered composite volcanoes which, as they grew, shed aprons of laharic breccias and reworked volcanic debris that collected in the intervening basins (Lipman et

al., 1978).

The intermediate flows and the associated debris are collectively known as the Conjechos Formation, and are also temporally equivalent with the San Juan and Lake Fork Formations of the western San Juans, and the West Elk Breccia to the north. Lavas of the Conjechos and related formations range in composition from alkali andesite to low-silica rhyodacite (Fig. 2), with flows becoming more silicic higher in the stratigraphic sequence. Eventually the intermediate lava flows and associated debris merged laterally to produce a broad composite field covering more than 25,000 km² (Lipman et al., 1970). This area includes the present-day San Juan Mountains, West Elk volcanic field, White River Plateau (Chronic, 1980), Thirtynine-Mile volcanic field, Wet Mountains, and the San Luis Hills (Varga and Smith, 1984) (Fig. 1). These early deposits had an estimated original volume of 40,000 km³ and comprise approximately two-thirds of all the volcanic material that was ever deposited in the San Juans (Lipman et al., 1970).

The second stage of volcanism began 31 million years ago (Varga and Smith, 1984), when clusters of composite volcanoes in the northeastern and southern parts of the San Juan field ceased to passively erupt intermediate-composition lavas and began to expel explosive pyroclastic materials. In many instances the rapid eruption of pyroclastics caused simultaneous caldera collapse, with

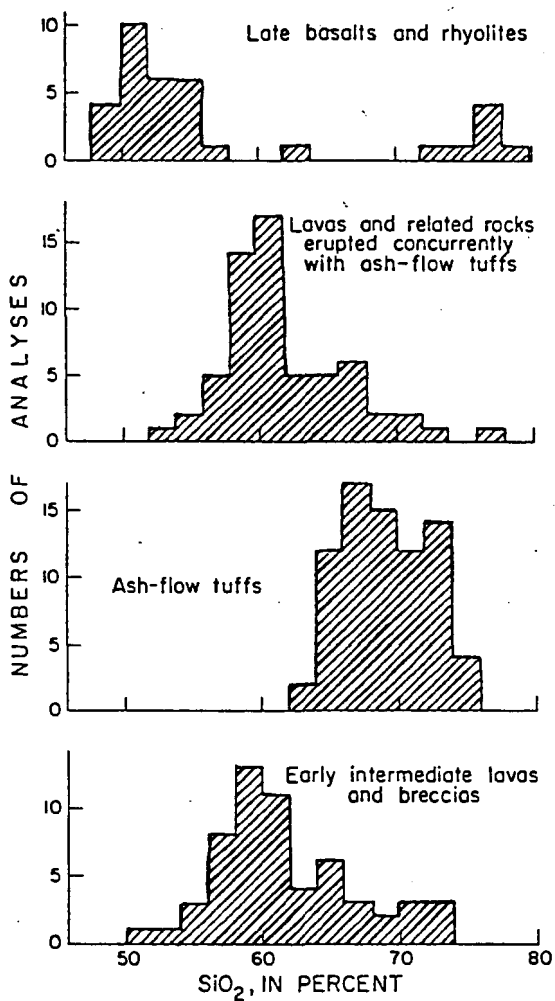


Fig. 2. Histograms of SiO₂ contents for each of the major phases of Tertiary volcanism in the San Juan Mountains (after Lipman et al., 1970).

later pyroclastic flows becoming ponded in the caldera. The calderas formed by these first ash-flow eruptions are the Bonanza and the nested Platoro and Summitville calderas. The sizes of the calderas are roughly proportional to the volume of the corresponding ash-flow deposits. Explosive volcanism moved to the western part of the field 29 million years ago, where the Ute Creek, Lost Lake, San Juan, Uncompahgre, and Silverton calderas formed in less than two million years (Steven and Lipman, 1976).

Post-subsidence lavas were erupted following almost every major ash-flow sheet in the San Juans. In the eastern and western parts of the volcanic field, the post-subsidence eruptions were composed of intermediate composition lavas and breccias, much like the initial andesitic eruptions of the San Juans.

Twenty-eight million years ago, while explosive volcanism was still occurring in the western San Juans, pyroclastics began erupting in the central part of the field, forming eight major ash-flow sheets and eight major calderas over a span of two million years (Steven and Lipman, 1976). Post-subsidence lavas in the central San Juan field were generally quartz latites, similar in composition to the corresponding ash flows. It was at this time that the La Garita caldera collapsed after erupting 3000 km³ of pyroclastic material, forming the Fish Canyon Tuff, the most voluminous ignimbrite deposit in the San

Juan field (Lipman et al., 1978).

Explosive volcanism ended 26 million years ago, after the formation of fifteen to eighteen calderas over a span of five million years. Volcanism must have been very intense during this period, as is indicated by the eruption rates calculated by Lipman et al. (1970) (Fig. 3). The sixteen or more ash-flow sheets erupted during the Oligocene formed a welded tuff plateau which was as extensive as the underlying intermediate lavas, but only half as thick. These ash flows range in composition from quartz latite to low-silica rhyolite, and several of the individual flow sheets are chemically zoned, becoming more mafic with increasing stratigraphic height (Lipman et al., 1978).

As the episode of explosive volcanism in the San Juans ended, the tectonic character of the region also changed, perhaps in response to the collision of the North American plate with the East Pacific Rise (Lipman et al., 1970). A period of uplift occurred from Miocene to Pliocene time, during which Colorado and parts of the surrounding states were uplifted at least 5000 feet to their present elevation and tilted to the east (Chronic, 1980). At the same time, basin and range faulting began along the Rio Grande Rift (Lipman et al., 1970), forming a complex series of grabens extending through New Mexico and west Texas into northern Mexico (Karig, 1965). The San Luis Valley is the northern

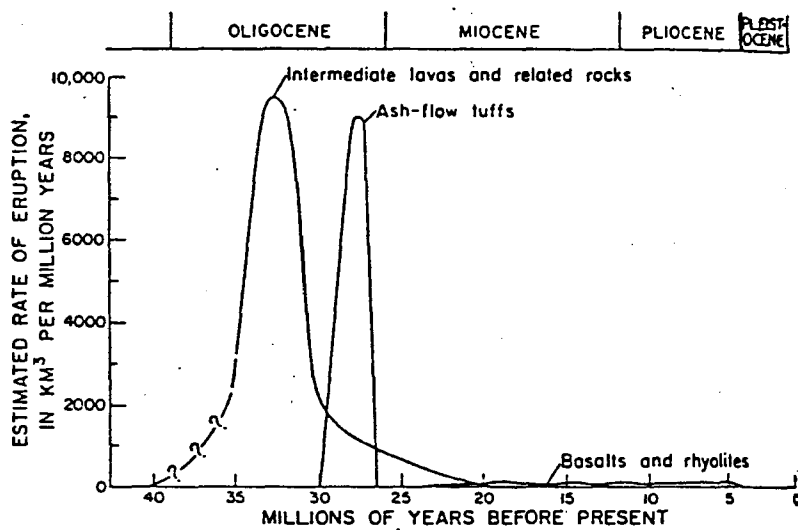


Fig. 3. Calculated eruption rates for the three main petrologic units in the San Juan volcanic field (after Lipman et al., 1970).

extension of this rift zone, although today the down-faulted graben structure lies buried beneath thousands of feet of alluvium and volcanic debris.

The third phase of San Juan volcanism began approximately 25 million years ago in early Miocene time. As compressional tectonic forces gave way to extensional faulting, explosive pyroclastic eruptions were replaced by quiet bimodal basalt and high silica rhyolite flows (Lipman et al., 1978). The early bimodal flows, known today as the Hinsdale Formation, capped the area with a thin basaltic veneer. Compositions of the mafic lavas range from alkali olivine basalt to basaltic andesite, with rhyolite magmas forming local flows and plug domes (Lipman et al., 1970).

Only one large pyroclastic eruption occurred during the Miocene. This took place 22.5 million years ago in the western San Juans when the violent extrusion of the Sunshine Peak Tuff led to the formation of the Lake City caldera. Although pyroclastic in nature, the Sunshine Peak Tuff is classified with the Miocene bimodal rhyolites rather than with the Oligocene ash-flow deposits; Miocene rhyolites are more silicic ($\text{SiO}_2 \geq 75$ percent) than Oligocene tuffs (Fig. 2) and contain numerous quartz and very sodic sanidine phenocrysts, but lack the plagioclase phenocrysts that are so abundant in the Oligocene deposits (Lipman et al., 1970).

More recent basalt flows have a tholeiitic composition

and are generally restricted to the Rio Grande Rift zone. These flows are classified separately as the Servilleta Formation (Lipman et al., 1970), and continued erupting intermittently until approximately five million years ago (Chronic, 1980). Since that time, Pleistocene glaciation and stream erosion have worked to shape the present topography of the San Juan Mountains.

Geophysical data

A study by Plouff and Pakiser in 1972 revealed that a large negative Bouguer gravity anomaly underlies most of the area covered by volcanic deposits in the San Juan Mountains (Fig. 1). The gravity low has an area of approximately 100 by 150 kilometers, and the geology of the region plus the geometry of the gravity low led Plouff and Pakiser to reach the following conclusions:

"Because of the types and thicknesses of volcanic rock units involved and the small density contrast between the volcanic rocks and the surrounding near-surface rocks, the volcanic rocks alone are probably not sufficient to explain the magnitude and shape of the anomaly. An inverse correlation between the Bouguer gravity anomaly and the altitude above sea level exists in this area, but gradients along the edges of the gravity low are too steep to explain the anomaly entirely in terms of isostatic compensation by a crustal root. Therefore, a low density igneous complex consisting of numerous coalescing calderas underlain by a concealed batholith is suggested as the primary cause of the anomaly. The calderas filled with volcanic rocks were formed in the subsiding roof of the formerly molten batholith."

Plouff and Pakiser also calculated a possible subsurface geometry of the batholith from the gravity data and supplementary magnetic studies. They assumed a density contrast between the batholith and the country rock of 0.1 g/cm^3 , and subtracted the regional gravity gradient to produce a more accurate, residual gravity profile of the anomaly (Fig. 4A). The magnetic field was analyzed along the same cross-section as the gravity profile, and a magnetic high that correlates with the gravity data, was found (Fig. 4C). Using a magnetization contrast of $.001$ electromagnetic units/cm³, a model of the batholith's dimensions was created (Fig. 4D). According to both gravity and magnetic data, the batholith lies only two to seven kilometers below the surface, and is shallowest beneath the Lake City caldera. The batholith seems to be nineteen kilometers thick at the center, which is almost half of the thickness of the earth's crust in the San Juan area.

Lipman et al.'s model

Lipman et al. (1978) integrated the subsurface geophysical data of the San Juans with the stratigraphic, chemical, and isotopic data to generate a model for the evolution of the volcanic field. A summary of their model is shown in Figure 5.

Lipman et al. believed that the evolution of a large batholith beneath the San Juan field was first marked by the

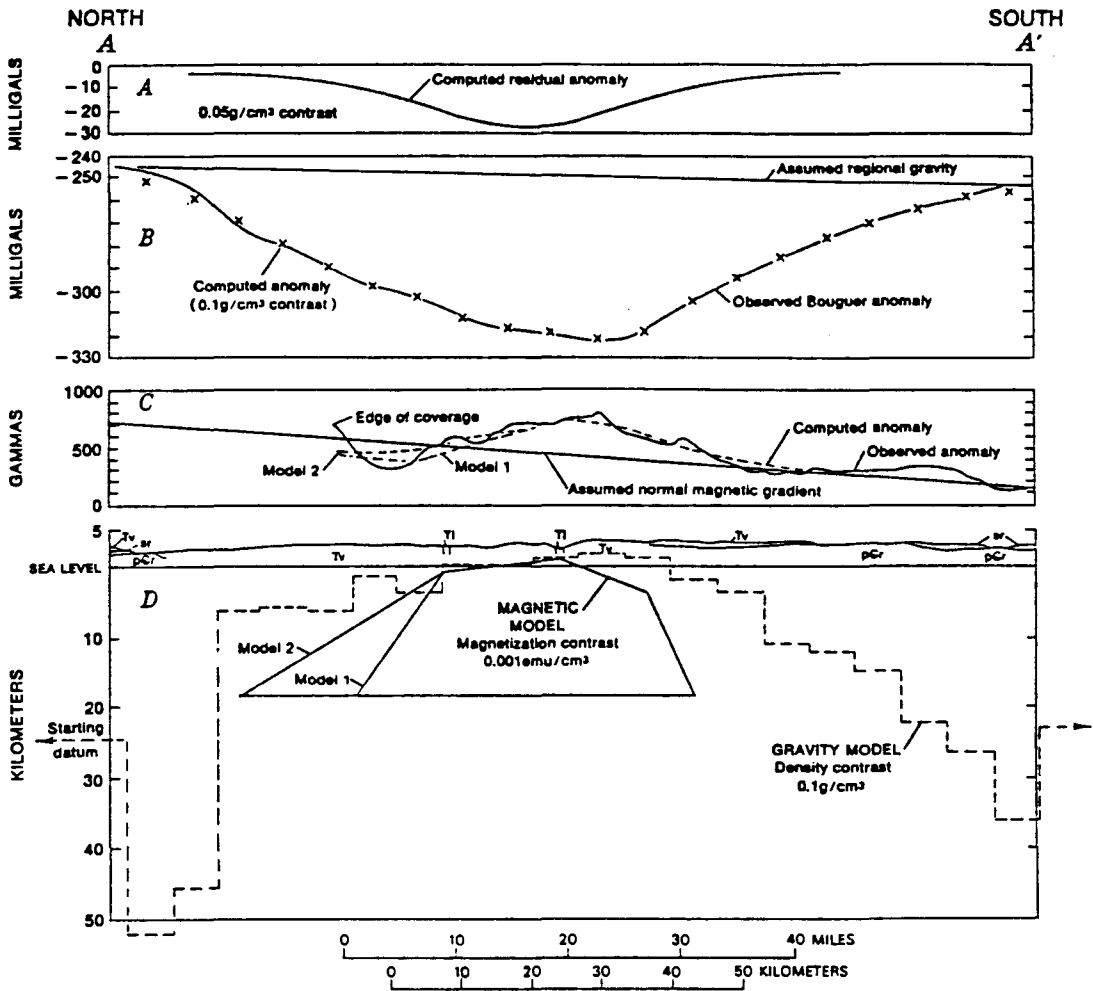


Fig. 4. A and B: Residual profiles of gravity anomaly. C: Magnetic high along same cross-section. D: Model of batholith's dimensions using gravity and magnetic data. Batholith is 19 km thick and lies only 2 to 7 km below the surface (after Plouff and Pakiser, 1965).

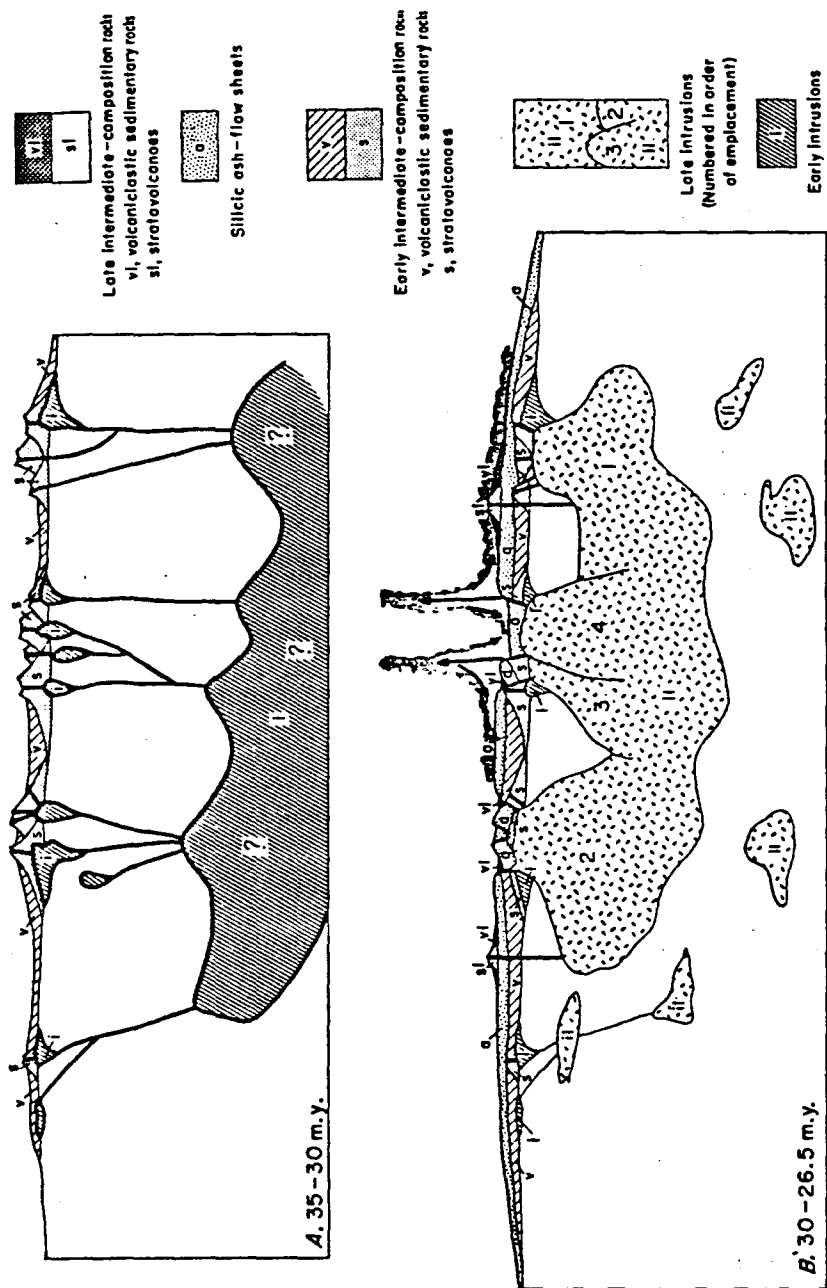


Fig. 5. Model for evolution of Oligocene batholith beneath the San Juan Mountains. A: 35-30 m.y. ago pockets of intermediate-composition magma accumulated at shallow crustal levels and erupted from clustered composite volcanoes. B: 30-26 m.y. ago ash flow eruptions with concurrent caldera collapse were caused by the emplacement of the batholith at shallow depths (after Lipman et al., 1978).

eruption of the intermediate-composition Conjechos volcanics. These lavas were generated in the lower crust or upper mantle, and then rose rapidly to shallow levels, with little modification during the ascent. Early composite volcanoes marked sites of local accumulations of magma beneath the surface.

The first calderas that formed in the eastern part of the field fall outside of the Bouguer gravity anomaly and therefore represent local silicic magma chambers that separated from the batholith and were emplaced at shallow levels before the main part of the San Juan batholith began to ascend. When the main batholith did rise towards the surface, the western part ascended first, with magmatic differentiation occurring in separate cupolas within the roof of the batholith. The silicic magmas within these cupolas were soon evacuated by the eruption of ash flows, causing concurrent caldera collapse (29-27 million years BP). After the silicic differentiates within the western part of the batholith were depleted, intermediate-composition lavas from deeper parts of the chamber were extruded as post-subsidence lavas.

Calderas forming 28-26 million years BP within the central part of the San Juan field mark the final emplacement of the batholith at shallow levels. Silic post-subsidence lavas in this area indicate that differentiated magmas in shallow levels of the batholith had by this time

increased significantly in volume because they were not depleted by the voluminous eruptions in this area.

Later, partial melting of the upper mantle produced the basaltic Hinsdale lavas. These lavas ponded below the lower sialic crust, providing the heat to partially melt the lower crust and form the Miocene-Pliocene rhyolites (Lipman et al., 1978).

CHAPTER 3

GEOLOGIC SETTING OF THE BONANZA REGION

Location

Bonanza is located in Saguache County, Colorado, along the western edge of the Rio Grande rift system. Although the Bonanza region comprises the northeastern corner of the San Juan volcanic field, it lies outside of the closed gravity low recognized by Plouff and Pakiser (1972) (Fig. 1). Because Bonanza is not situated above the batholith that underlies most of the San Juan field, Lipman et al. (1978) suggested that the Bonanza magma chamber was an early satellite pluton of the San Juan batholith.

History of the Town

The town of Bonanza began as a mining camp in 1880, when miners travelling west to Gunnison, Colorado were attracted by promising outcrops along Kerber Creek (Fig. 6). Soon 1500 claims were staked, and the population soared to an estimated 40,000 between 1880 and 1888 as hopeful families flooded the area (Kempner, 1978).

The town prospered during its first years, as more than \$9,000,000-worth of lead, silver, copper, and zinc

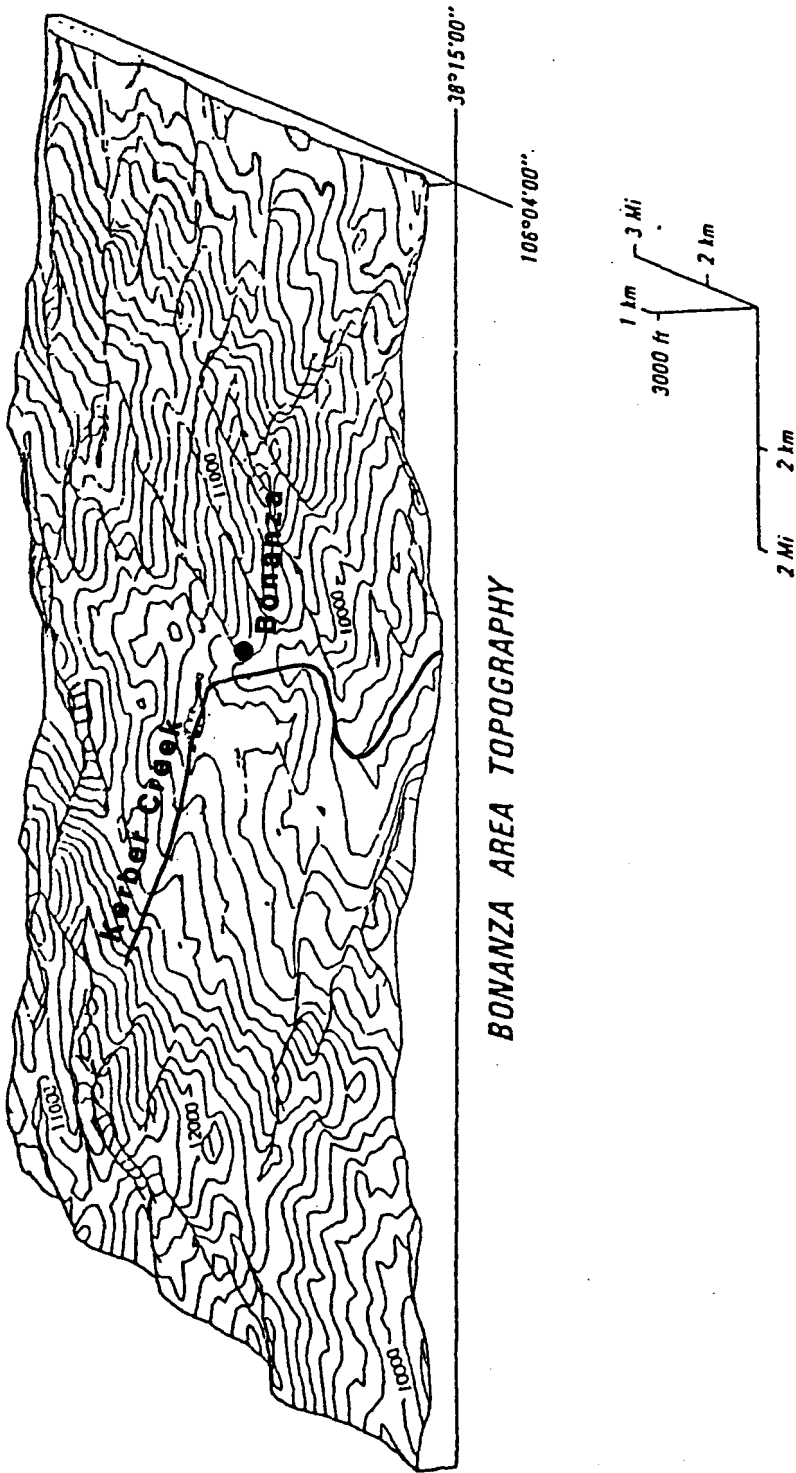


Fig. 6. Topographic map of the Bonanza region. The row of peaks that encircle the town of Bonanza roughly mark the rim of the caldera (after Varga and Smith, 1984).

were produced (Cook, 1960); yet, eventually the inaccessibility of the area and the low grade of the ores led to the decline of the mining town. The most prosperous mine in the district, the Rawley Mine, finally closed in 1930 (Burbank, 1932), and today only a few houses (and several tailing piles and ponds) remain as evidence of the once bustling town.

Geophysical Data

The presence of a collapse structure in the Bonanza area was mentioned as early as 1932, when Burbank noted the complex faulting and fissuring of the Tertiary volcanic deposits, and that these deposits seemed to be dipping radially away from a central area near the town of Bonanza. Burbank thought that these features were the result of the intrusion of a large magma body at a depth of several thousand feet. This intrusion caused the crust to dome upwards, faulting the pre-volcanic rocks and tilting them outward. When the magma finally reached the surface, the release of pressure caused the crustal bulge to collapse and intense fracturing occurred (Burbank, 1932).

Karig (1965) confirmed Burbank's findings when he conducted a gravity survey of the San Luis Valley region during the summer of 1963. Karig discovered a closed gravity low, defined by the -286 milligal contour (Fig. 7), centered over the Bonanza area. This gravity low is

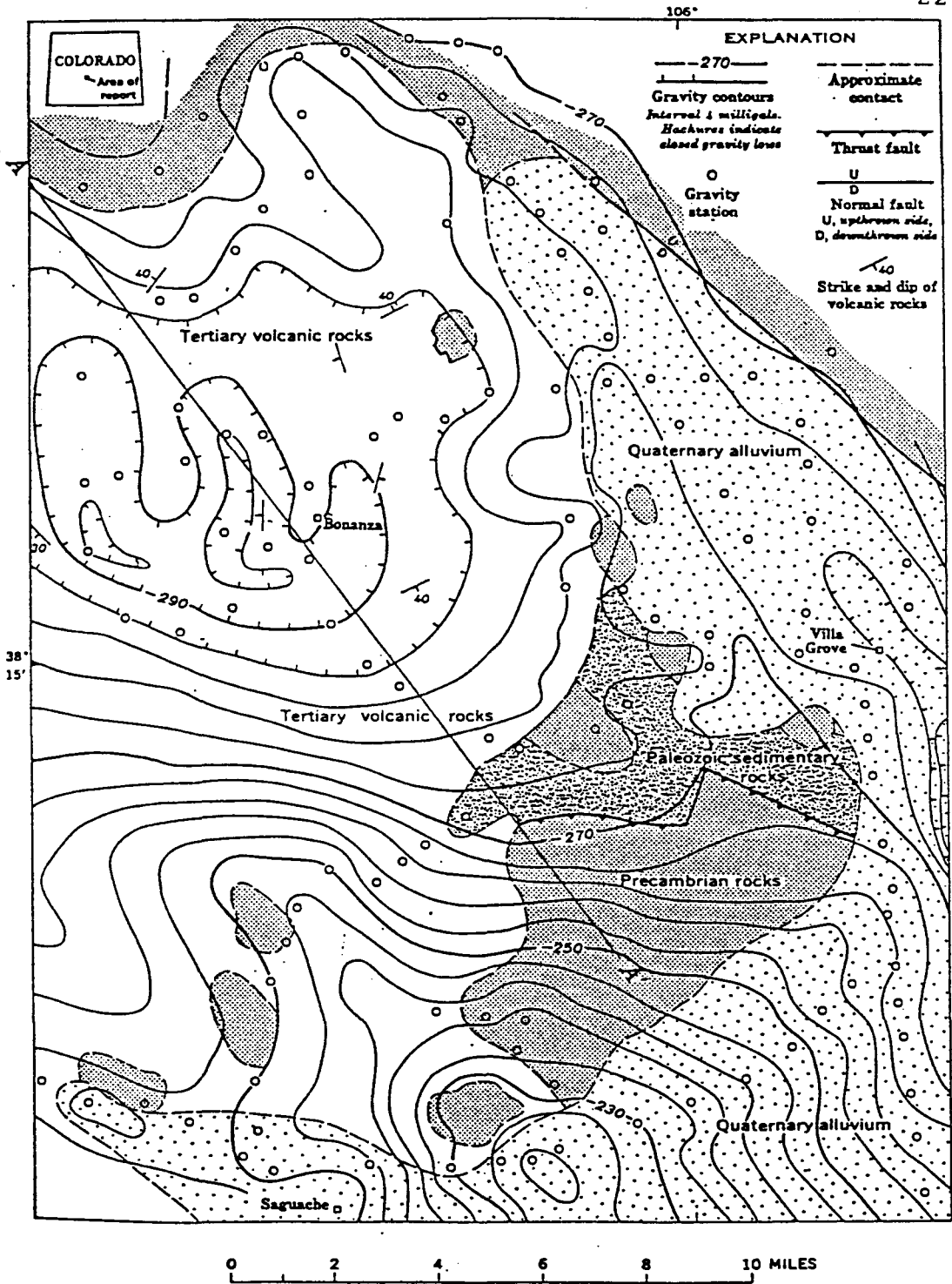


Fig. 7. Gravity map of the Bonanza area showing general geology. A closed gravity low is defined by the -286 milligal contour (after Karig, 1965).

elliptical with dimensions of eight by ten miles, and several smaller gravity lows are present within the area of closure.

Although most of the San Juan calderas are not associated with distinctive gravity anomalies, Plouff and Pakiser (1972) believe that the Precambrian rocks which outcrop on the north, south, and east sides of the Bonanza region accentuate the anomaly here by creating a greater density contrast between the country rock and the down-dropped volcanics. To estimate volumes, average densities of 2.70 and 2.50 g/cm^3 were assigned to the Precambrian bedrock and the down-dropped volcanics, respectively. Thus, a density contrast of 0.2 g/cm^3 is obtained, which means that the low-density volcanics must be approximately 8000 feet thick to cause the observed gravity low (Fig. 8) (Karig, 1965).

Karig (1965) also noted additional geologic evidence supporting the presence of a collapse structure in the Bonanza area:

1. A belt of peaks with an average diameter of seven miles surrounds the town of Bonanza, approximating the outline of the gravity low. A topographic basin occupies the region of the gravity anomaly itself, and Kerber Creek runs through this low area (Fig. 6). Although the present topography has certainly been modified by erosion, this configuration may represent the initial relief of the area.
2. The uppermost Precambrian rocks within the gravity low are at a considerably

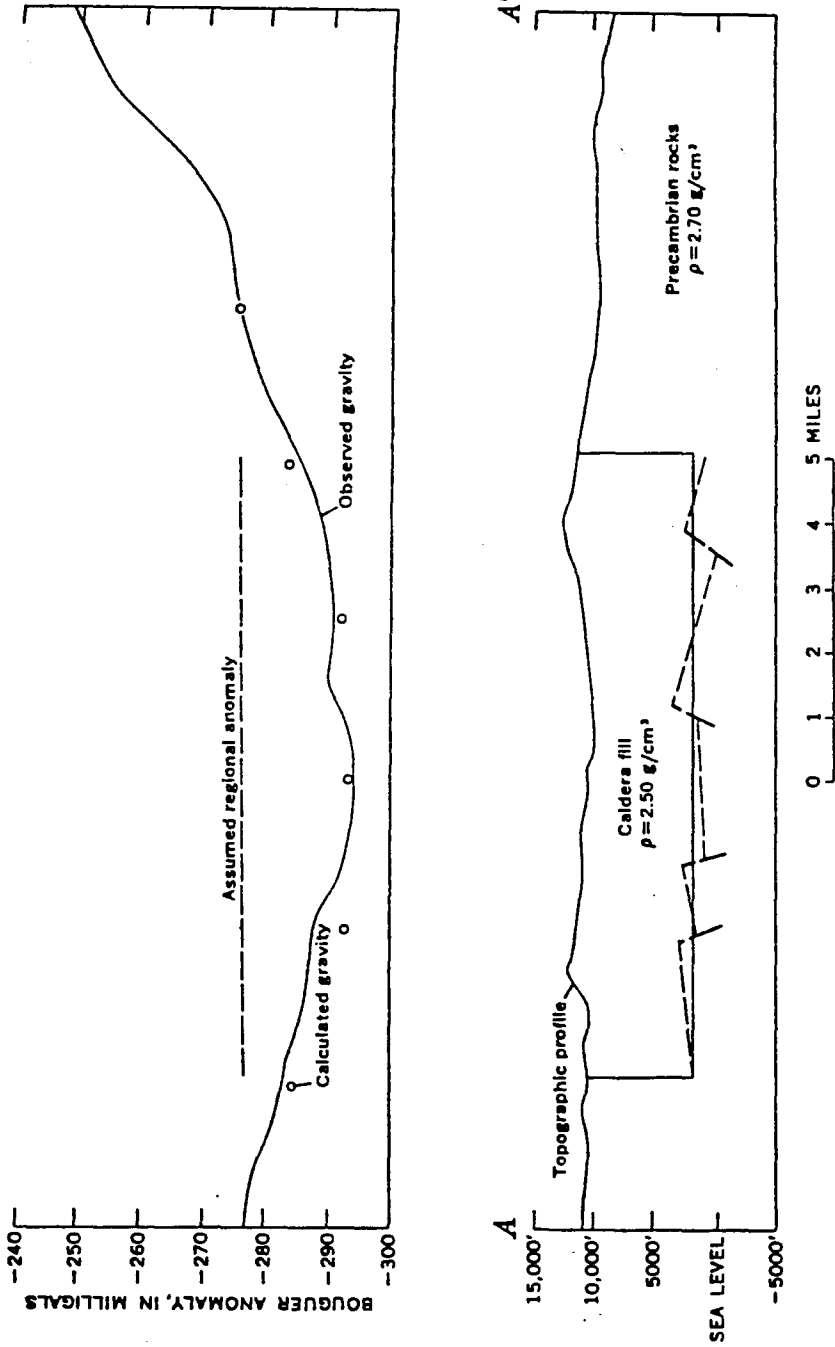


Fig. 8. Profile along cross-section A-A' (from Fig. 7) showing the caldera configuration necessary to produce the observed gravity anomaly in the Bonanza area (after Karig, 1965).

lower elevation than outcrops of the same Precambrian rocks exposed outside of the gravity anomaly. This suggests that the central area may be down-faulted. Data from mines in the district indicate that large listric faults run adjacent to the topographic rim.

3. Tertiary-age silicic flows and intrusions in the Bonanza region are restricted to the margins of the gravity low, similar to the ring intrusions discussed by Smith and Bailey (1968).

The relative thicknesses of certain Tertiary volcanic units also support the interpretation of a caldera in the central Bonanza area. This information will be presented in the following section.

Stratigraphy

Basement rocks

The volcanic deposits of Bonanza lie upon a basement of Precambrian and Paleozoic rocks. The Precambrian rocks consist of hornblende-mica gneisses and schists that have been intruded by aplitic, granitic, and pegmatitic dikes. Overlying these rocks are at least 5000 feet of Paleozoic sedimentary rocks that range from lower units of chiefly limestone to upper beds of Pennsylvanian sandstone and conglomerate. Burbank divided these sedimentary rocks into five formations (Fig. 9), among them being the well-known Leadville Limestone of Mississippian age and the Permian Maroon Formation.

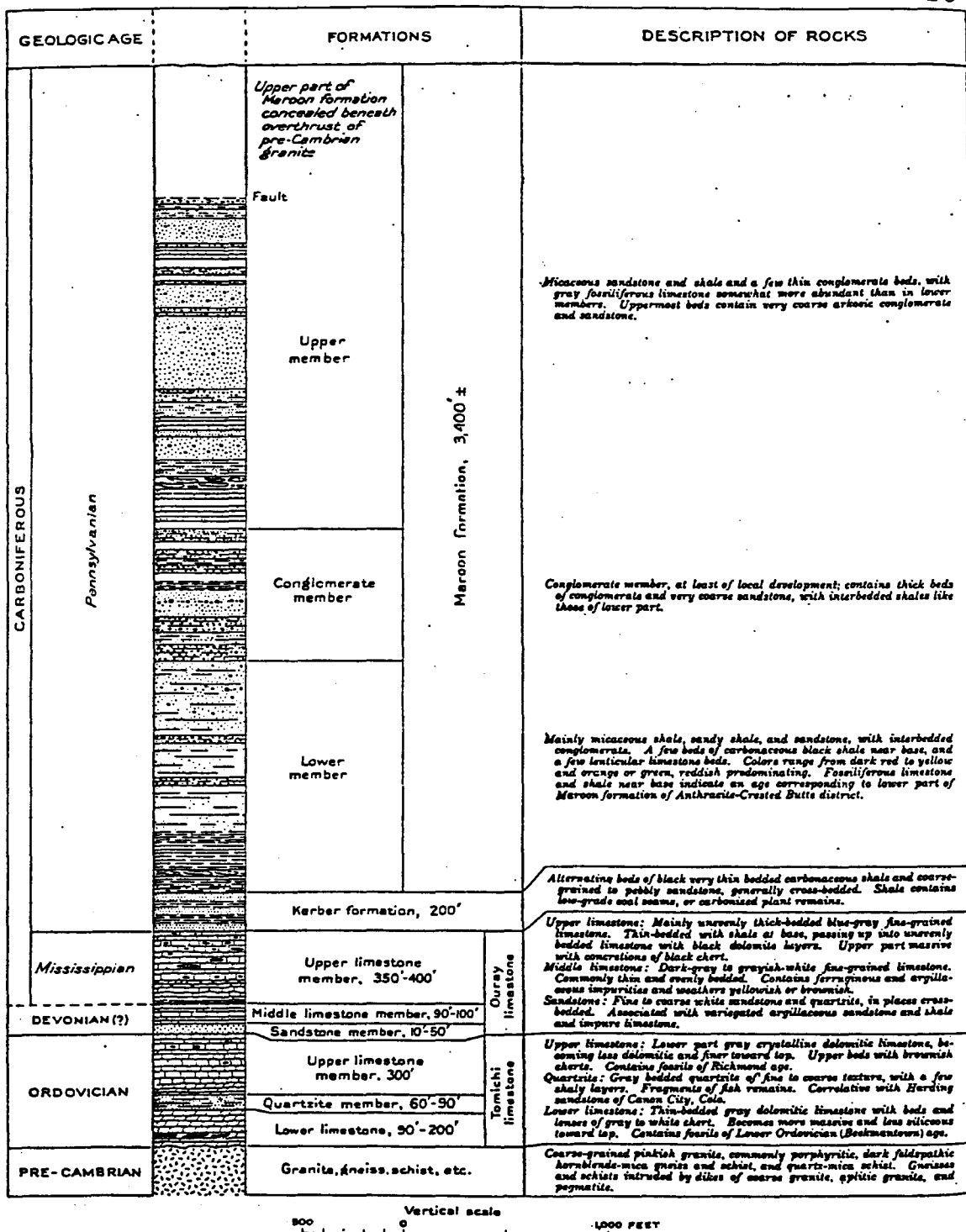


Fig. 9. Stratigraphic column of the Paleozoic sedimentary rocks in the Bonanza district (after Burbank, 1932).

The Laramide Orogeny, which occurred in late Cretaceous and Eocene time, consisted to two main periods of deformation that affected the pre-Tertiary rocks. During the first period of deformation, the rocks were folded into asymmetrical anticlines and synclines with north-northwest- trending axes. In the second period, thrust sheets overrode the earlier folds obliquely to their axes. Large-scale erosion in the late Eocene denuded the area of Paleozoic sedimentary rocks, except for those that were downfolded within synclines, and created an erosional surface with 500 feet of relief (Burbank, 1932).

Today, Paleozoic rocks are exposed in areas fringing the Bonanza volcanic deposits; however, clasts of the sedimentary units do not show up within the Tertiary flows and tuffs. Inclusions of Precambrian crystalline rocks are quite common, though, suggesting that Paleozoic sediments do not underlie the vent areas for the later volcanics (Varga and Smith, 1984).

Rawley Andesite

Volcanism in the Bonanza region followed the same general pattern as in the rest of the San Juans (Fig. 10). The eruptive sequence began with the extrusion of the Rawley Andesite, which initially covered much of the northeastern part of the San Juan volcanic field (Burbank, 1932). Varga and Smith determined a potassium-argon age of

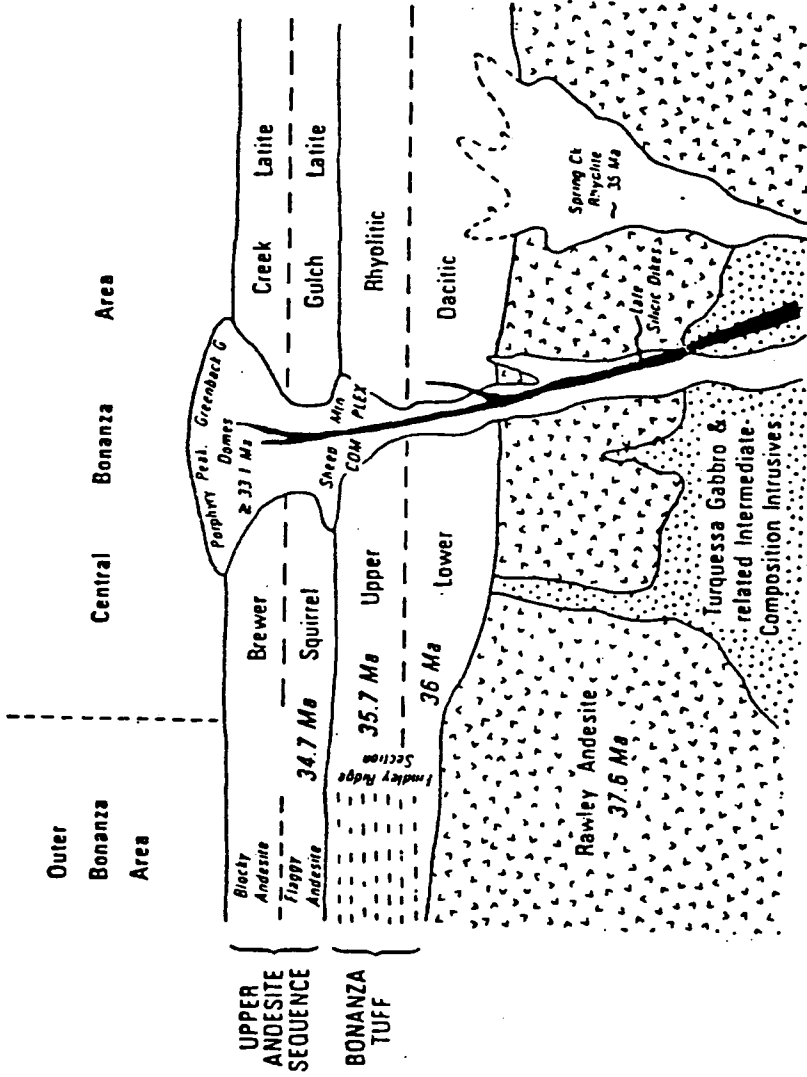


Fig. 10. Schematic stratigraphic relationships of igneous rocks in the Bonanza region. Dashed lines represent cooling breaks (after Varga and Smith, 1984).

approximately 37.6 million years BP (early Oligocene) for the Rawley Andesite, supporting Bruns' (1971) conclusion that this lava flow is slightly older than, but correlative with, the early, intermediate-composition Conjejos volcanics of the main San Juan field.

The Rawley Andesite consists of a thick series of lava flows, basal flow breccias, laharic breccias, and small amounts of tuff, all of which have a high-K basaltic-andesite composition according to the classification scheme of Peccerillo and Taylor (1976). Individual flows may be from ten to 100 feet thick and range in texture from fine-grained to porphyritic (Burbank, 1932). Fresh exposures are black or dark gray, and are very dense so that they break with a conchoidal fracture. Weathered surfaces have a gray, tan, or rusty brown color, and phenocrysts are very noticeable. Near fractures, the Rawley Andesite frequently has a greenish color indicating alteration by hydrothermal fluids.

Steep contacts between the Rawley Andesite and the underlying rocks indicate that, at the time of the first eruptions, the topography in the Bonanza area was as rugged as that of today (Cook, 1960); yet, the widespread Rawley Andesite eventually covered even the tallest of peaks (Burbank, 1932).

Today the Rawley Andesite is exposed throughout the Bonanza region (Fig. 11), where it often forms blocky

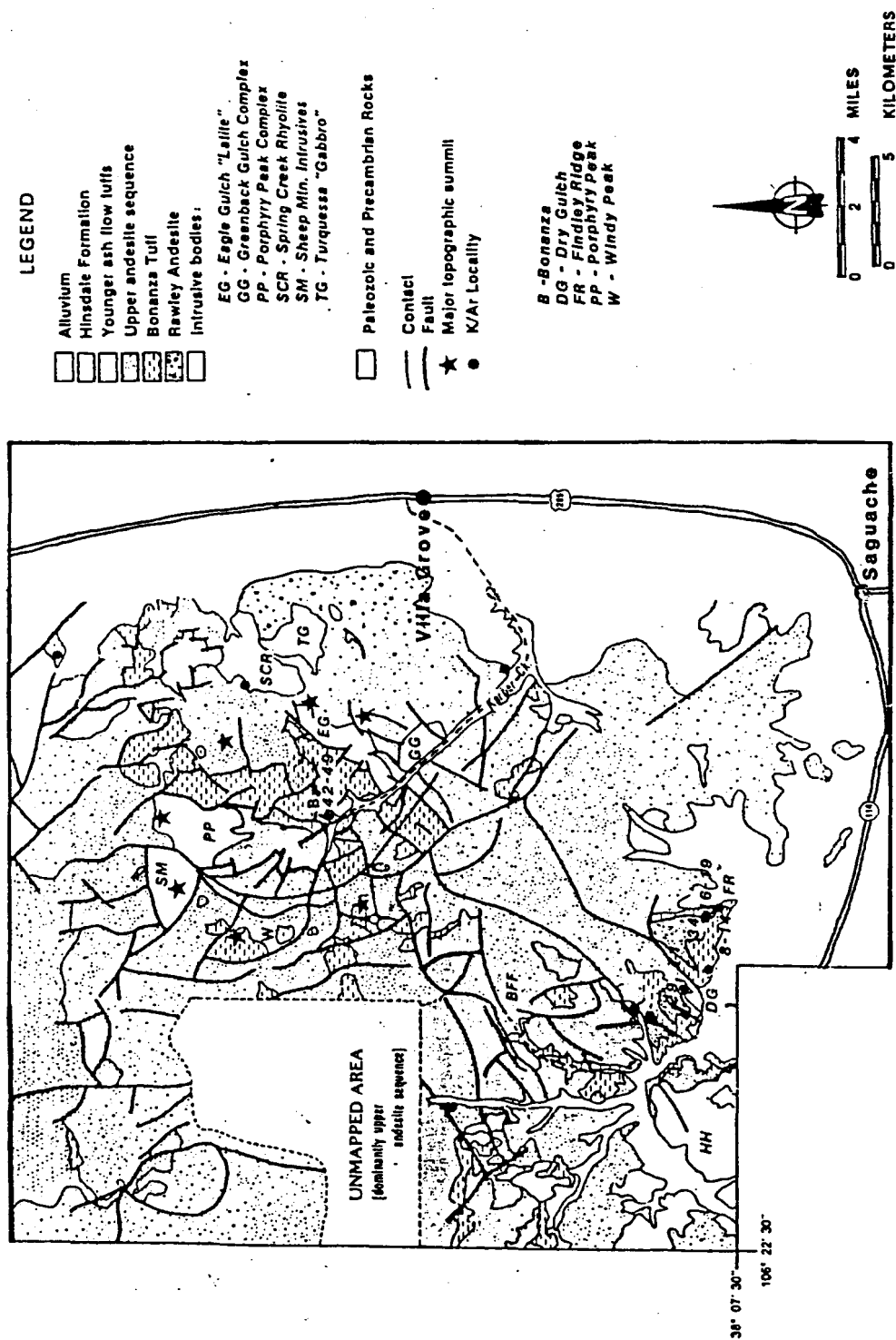


Fig. 11. Geologic map of the Bonanza district. Numbers represent sample locations (modified from Varga and Smith, 1984).

ridges and steep slopes. The deposit reaches a maximum thickness of more than 2280 feet in the central Bonanza area, but in the outer regions the flows thin and laharic breccias are more common. This suggests that the main source(s) of the Rawley Andesite lie within the central Bonanza area (Varga and Smith, 1984). Marrs (1973) believed that the Rawley Andesite was erupted from numerous vents in a large shield volcano that was centered over the Bonanza area.

Bonanza Tuff

The Bonanza Tuff was erupted onto the eroded surface of the Rawley Andesite (Marrs, 1973). Varga and Smith (1984) calculate that the original volume of the Bonanza Tuff was as much as 50 km³, however, today extensive erosion has reduced the Bonanza Tuff to discontinuous outcrops throughout the Bonanza area (Fig. 11).

Varga and Smith (1984) used potassium-argon methods to determine an age of 36 million years BP for the deposition of the entire Bonanza Tuff sequence. The Treasure Mountain Tuff, the first ash flow to be deposited in the southern San Juans, was erupted from the Platoro caldera 31 million years ago. This means that the Bonanza Tuff is at least five million years older than any other pyroclastic deposit in the San Juan field (Varga and Smith, 1984). Because the Bonanza Tuff is much thicker within the central Bonanza

area, it is believed that collapse of the Bonanza caldera was coeval with the eruption of the tuff, with later pyroclastic flows becoming ponded within the caldera (Lipman et al., 1970).

The Bonanza Tuff is divided into two distinct petrographic units: a lower composite sheet of phenocryst-rich high-K dacite ignimbrite, and an upper ash flow unit of phenocryst-poor, rhyolitic composition (Varga and Smith, 1984). The two units have very different outcrop patterns, and the intracaldera and distal facies of both units are also quite distinct. The characteristics of the upper and lower members of the Bonanza Tuff will be discussed in the following paragraphs.

1) intracaldera facies

Within the caldera, the lower member of the Bonanza Tuff is highly welded, indicating a sequence of eruptions so rapid that individual ash flows did not have time to cool. The lower unit is so dense that Patton (1915) and Burbank (1932) first mapped it as a latitic lava flow, mistaking the eutaxitic texture caused by the flattened pumice for flow structure. It was not until Mayhew (1969) examined the unit microscopically that the Bonanza formation was recognized to be an ash flow tuff.

At first glance, the lower Bonanza Tuff seems to be indistinguishable from the Rawley Andesite because the

colors in outcrop are very similar. However, the Bonanza Tuff has a decidedly fragmental texture (Plate I). Angular inclusions of Rawley Andesite are frequently seen on fresh surfaces, and weathered surfaces have a chunky appearance. The lower tuff reaches a maximum thickness of more than 500 feet on the ridge between Copper and Elkhorn Gulch (Burbank, 1932), and here the unit displays its characteristic blocky, ridge-forming outcrop pattern (Plate II). Samples of the intracaldera facies of the lower Bonanza Tuff were gathered along this ridge, which can be reached by car from RD LL56 that turns west off of Route 285, just north of Villa Grove (Fig 11).

The only major cooling break within the caldera occurs between the lower and upper units of the Bonanza Tuff (Marrs, 1973). The upper member is also highly welded within the caldera, however, the upper Bonanza Tuff is much softer than the lower unit, and forms gentle, covered slopes. Where it is exposed in a rare outcrop, the upper tuff is a chalky white color, and is very crumbly. Together, the lower and upper members of the Bonanza Tuff reach a thickness of approximately 1000 feet within the caldera (Marrs, 1973).

2) distal facies

Tuff deposits are much thinner in the outer Bonanza region, ranging from zero to 500 feet (Marrs, 1973); yet it

Plate I. The intracaldera facies of the lower Bonanza Tuff. Note the highly fragmental texture of the rock and the large inclusion of Rawley Andesite to the left of the hammer.



Plate II. The ridge between Elkhorn and Copper Gulches, where samples of the intracaldera facies of the lower Bonanza Tuff were collected. The blocky, ridge-forming outcrop pattern is typical for this unit. (Photo taken from Road LL56.)



is the distal facies that offer the most complete stratigraphic sections. Here the Bonanza Tuff is easily recognizable because it displays characteristically pyroclastic features, and cooling breaks exist between separate flows. Also, lack of vegetation in the arid, southeastern portion of the district offers excellent exposures of the rock.

Samples of distal facies were collected for this study from Findley Ridge and Dry Gulch, which lie approximately 2.5 miles west of Saguache, just north of highway 114 (Fig. 11). Four hundred and eighty-eight feet of tuff are exposed at Findley Ridge, and it is here that Marrs (1973) originally described the type section of the Bonanza Tuff.

Marrs (1973) recognized eight distinct ash flows at Findley Ridge on the basis of petrography, cooling breaks, and zones of welding (Plate III, Fig. 12). Typically, a single flow may contain the zones of welding shown in Figure 14. The vitrophere zone may extend to the base of the flow if the ash was erupted at very high temperatures, and often the unwelded top of the flow is eroded or reworked (Smith, 1979).

In the Findley Ridge area, the welded zones form benches, often with crude columnar joints and eutaxitic texture (Plate IV). These welded zones have a dark-colored matrix of gray, purple, or black and weather to a brown color. Poorly welded zones vary from light gray to pink in

Plate III. Findley Ridge, the type locality of the Bonanza Tuff. The eight ash flows recognized by Marrs (1973) are indicated. Welded zones of the ash flows tend to form benches.



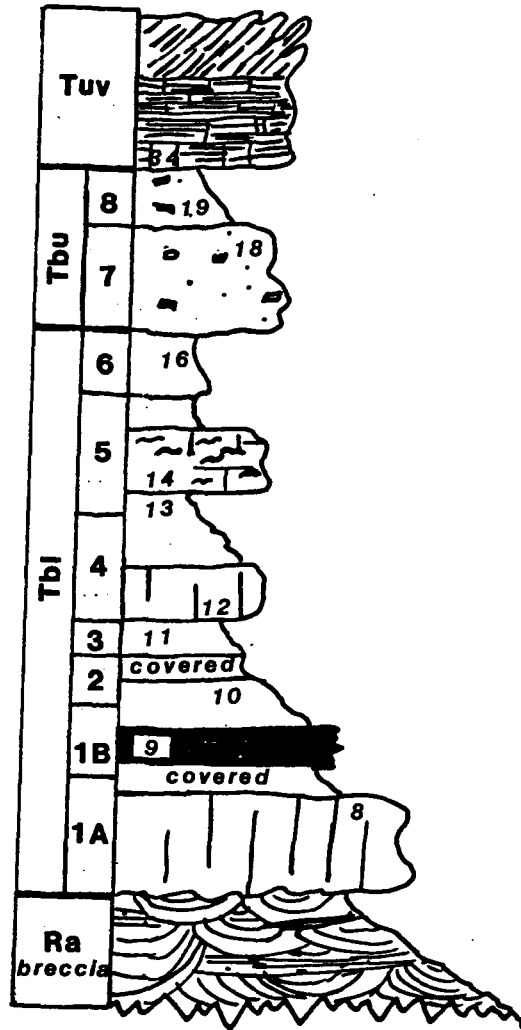


Fig. 12. Stratigraphic column of the Findley Ridge section. Thicknesses of the units are not to scale. Numbers designate samples collected in the present study, and the eight ash flows recognized by Marrs (1973) are indicated.

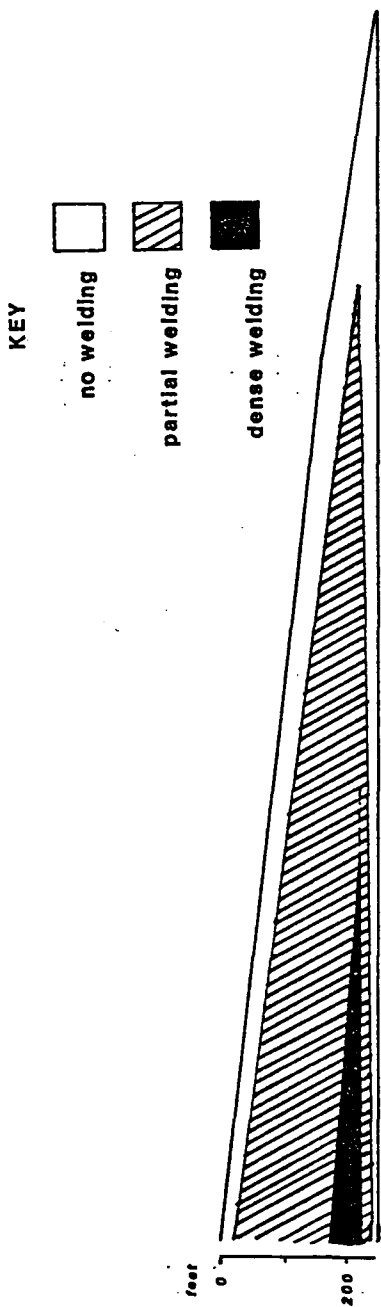
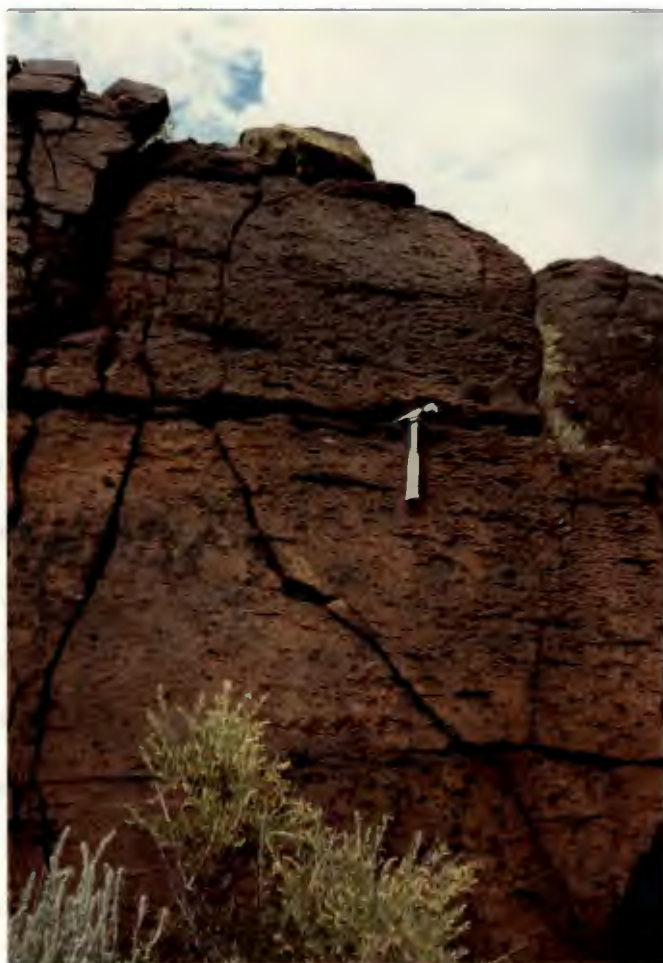


Fig. 13. Zones of welding within an ash flow. Most flows will not contain all these zones; the vitrophere zone may extend to the base of the flow if the ash was emplaced at very high temperatures. Often the unwelded top of the flow is eroded and reworked (modified from Smith, 1979).

Plate IV. Eutaxitic texture caused by the preferential weathering of flattened pumices. This welded ash flow outcrops at Findley Ridge and is characteristic of the distal facies of the lower Bonanza Tuff.



color and, because they are less resistant, form rubble-covered slopes.

The upper and lower members of the Bonanza Tuff are readily distinguishable in the distal facies. Plagioclase and biotite phenocrysts are evident throughout the lower petrographic sheet, and purple to dark gray inclusions of Rawley Andesite are common in the bottoms of individual flows (Marrs, 1973). Fragments of Rawley Andesite and phenocrysts are not as abundant in the upper member, however. Relative proportions of biotite and plagioclase crystals decrease in the upper member of the Bonanza Tuff, and clear, glassy sanidine crystals and amphibole phenocrysts increase.

Although slightly deformed pumices suggest that the distal facies of the upper Bonanza Tuff is only poorly welded, intense silicification has made the unit quite resistant in the southeastern part of the district (in contrast to its slope-forming intracaldera character). The upper tuff forms a bench which is 60 feet high at Findley Ridge, and ranges in color from red to light gray or pink.

3) source

Marrs (1973) believed that the Bonanza Tuff was erupted from the central Bonanza area, due to the thinning of ash flows and a decrease in welding intensity away from this area. Varga and Smith (1984) further investigated

this theory by examining both macroscopic and microscopic indications of flow direction within the Bonanza Tuff (Fig. 14). They determined that a major portion of the lower Bonanza Tuff was erupted from a vent in the present Porphyry Peak/Sheep Mountain area, and that minor eruptions also originated from the area now occupied by the Spring Creek Rhyolite intrusion. The upper tuff was also erupted from the Porphyry Peak/Sheep Mountain vent.

Upper Volcanics

Post-caldera lavas consist of local, intertonguing flows of andesite that unconformably overlie the Bonanza Tuff throughout the region, reaching thicknesses of more than 500 feet in the central caldera area (Marrs, 1973). These flows were erupted 34.7 million years ago (Lipman, et al., 1978), and include the Squirrel Gulch Latite and the overlying Brewer Creek Latite described by Burbank (1932).

The Squirrel Gulch Latite consists of hornblende-biotite latite flows that are quite dense and break with a conchoidal fracture. Fresh surfaces are black, but the rocks turn light brown upon weathering, making hornblende phenocrysts much more evident. The Brewer Creek Latite has a similar appearance within the caldera, but has a quartz-mica latite composition (Burbank, 1932).

Within the caldera the post-caldera flows are quite massive, but in the outer region, the Squirrel Gulch Latite

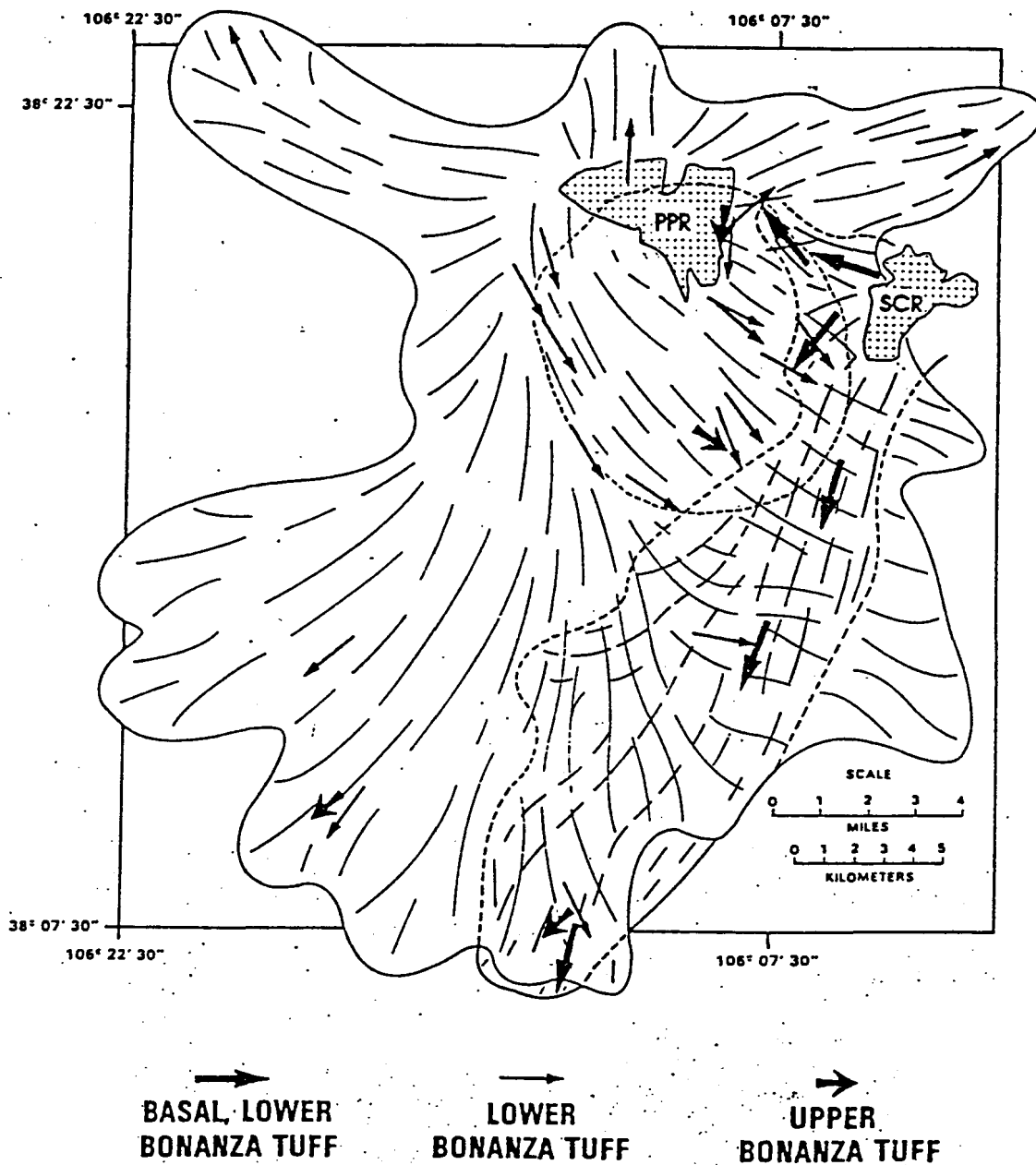


Fig. 14. Reconstructed flow directions of the Bonanza Tuff ash flows. Flow vectors were determined microscopically. The caldera margin is indicated by the circular dashed line, and PPR and SCR indicate the locations of the Porphyry Peak Rhyolite (PPR) and Spring Creek Rhyolite (SCR) intrusions (after Varga and Smith, 1984).

becomes very flaggy and the Brewer Creek Latite is blocky. These flows are quite resistant to erosion in both inner- and outer-caldera areas, and tend to cap ridges (Plate V). To the west of the Bonanza region, the upper volcanic flows grade into laharic breccias (Varga and Smith, 1984).

Varga and Smith (1984) believe that the source for the upper volcanic flows may lie in the central Bonanza area, because the post-caldera flows are mineralogically and chemically similar to the flows of Rawley Andesite that originated in the central region. Also, the upper volcanics are similar in composition to some of the later intrusions in the caldera area (for example, the Eagle Gulch Latite, Fig. 11). Perhaps these intrusions mark the location of vents for the post-caldera lavas (Varga and Smith, 1984).

Intrusive Rocks

Several generations of intermediate-composition stocks and dikes dissect the Bonanza area. These intrusions were probably emplaced continuously throughout the period of Tertiary volcanic activity, with intrusive activity ending 33 million years ago (Varga and Smith, 1984). Examples include the Eagle Gulch and Hayden Peak Latites, described by Burbank (1932). These intrusions are similar in chemistry and mineralogy to the intermediate lavas and ash flows of the area (Varga and Smith, 1984). Burbank (1932)

Plate V. Upper volcanic lava flow capping the ridge on the left. Picture taken looking southeast from Dry Gulch.



suggested that these intrusions formed as lava from the underlying magma chamber squeezed between the many fault blocks produced by caldera collapse.

Silicic stocks, domes, dikes, and sills also occur in the Bonanza caldera region, yet they are especially abundant along the margins of the caldera. The Spring Creek Rhyolite is one such intrusion, along with the three rhyolite bodies near Porphyry Peak. These rhyolite plutons are interpreted as being shallow ring-intrusions which were emplaced after caldera collapse (Varga and Smith, 1984), similar to those described by Smith and Bailey (1968). The rhyolite that comprises Porphyry Peak itself may have an extrusive as well as intrusive facies. This unit displays platy foliation parallel to a complex flow structure, dipping away from a central point (Plate VI) (Perry, 1971). The Porphyry Peak Rhyolite may represent lava flows that comprised a resurgent dome at the surface (Varga and Smith, 1984). Today the Porphyry Peak Rhyolite is intensely sericitized and silicified (Burbank, 1932).

The Sheep Mountain Rhyolite is mineralogically similar to the Porphyry Peak Rhyolite, but the coarser texture of the Sheep Mountain unit suggests that it was emplaced at a deeper, subsurface level, and has been moved by faulting to an elevation equal with the Porphyry Peak Rhyolite (Varga and Smith, 1984).

Plate VI. Outcrop of Porphyry Peak Rhyolite. Platy foliation is parallel to flow structure.



Mineralization

A mineralized district covering approximately 30 square miles is centered near the town of Bonanza (Cook, 1960). The following information concerning the mineralization has been obtained from Burbank's (1932) study of the Bonanza mining district.

Because mineralized veins are seldom offset by faulting in the Bonanza district, mineralization of the region must have occurred after the main period of caldera collapse. The faults produced by the caldera subsidence merely acted as conduits for the mineralizing fluids. The rocks that were the most mechanically susceptible to faulting, the Rawley Andesite and the lower Bonanza Tuff, are the units in which economic concentrations of ore have been found.

Mineralization occurred in two stages soon after the development of faults and fissures in the area. From fluid inclusion studies, Baker (1987) concluded that mineralization was initiated by the circulation of meteoric water at shallow levels. This water ranged in temperature from 164 to 346°C, and was probably heated by the ring intrusions along the caldera margins (Baker, 1987).

The first stage of mineralization occurred when acidic hot-spring waters added silica directly to the rocks near the faults (Burbank, 1932). This caused decomposition of the primary silicates, converting the immediate wallrock

into white or gray silica or commonly jasper. Ferric and ferrous oxides in the solution gave the jasper its reddish color. This first stage of mineralization was barren and produce no ore. However, silicified volcanic rock does indicate the presence of a nearby fissure that existed prior to ore formation.

The second stage of mineralization consisted of brecciation of jasper near large veins, followed by sericitic alteration of the wallrock. This alteration appears to be the result of alkaline or neutral solutions flowing through the fissures (Burbank, 1932). At the same time, veins were filled with gangue and metal sulfides including pyrite, sphalerite, galena, chalcopyrite, covellite, pyrargyrite, silver-bearing tennantite, and stromeyerite. Native tellurium, gold- and silver-bearing tellurides (Burbank, 1932), and disseminated molybdenum (Baker, 1987) were also deposited at this time. (In fact, empressite is a gold-silver telluride mineral that was named for the Empress Josephine Mine in the Bonanza district, where its occurrence was first described.) The mineralized veins were mined for lead, zinc, copper, silver, and gold in the Bonanza region, with lead and silver bringing the greatest profit.

CHAPTER 4

PETROGRAPHY AND MINERAL CHEMISTRY

Introduction and analytical methods

Several workers have described the petrographic features of the volcanic units in the Bonanza area (Mayhew, 1969; Perry, 1971; Marrs, 1973; Varga and Smith, 1984), however, no one has reported any mineral chemistry data. I will supplement the existing petrographic data with rock descriptions compiled from 20 thin sections. These samples were collected from the stratigraphic sections at Elkhorn Gulch, Findley Ridge, and Dry Gulch. Rock units will be discussed in order of increasing stratigraphic height, with Figure 13 providing relative sample locations within the stratigraphic section. Modal data were determined by visual estimation.

I will also report mineral compositions for the feldspar, biotite, opaque, and pyroxene phenocryst phases. These data were obtained at the University of Michigan, Ann Arbor, using a Cameca automated microprobe with a wavelength dispersive system and three spectrometers. Standard operating conditions were employed. Sample microprobe analyses can be obtained from Dr. Michael Barton at The Ohio State University in Columbus.

Compositions of opaque minerals have been recalculated in terms of magnetite-ulvospinel and hematite-ilmenite solid solutions according to Stormer's (1983) scheme, in order to compare the observed compositions with available experimental data. Compositions will be presented in terms of mole percent ulvospinel (Usp) and ilmenite (Ilm).

Rawley Andesite (Tra)

The Rawley Andesite is a porphyritic lava composed of phenocrysts of sanidine, plagioclase, an opaque phase, and highly altered pyroxene in a hypocrySTALLINE, trachytic matrix. Phenocrysts comprise an estimated 30 percent of the total rock volume, and lithic inclusions are rare. Because the tuff sequence was the main focus of reaearch, only one thin section of the Rawley Andesite flow was examined. This sample was collected from an outcrop on the northwest side of Copper Gulch road, midway between the St. Louis Mine and the point where the power line crosses the road. In hand sample, this specimen of Rawley Andesite seemed to be relatively fresh, however, in thin section it appears to have been severely altered by hydrothermal fluids.

plagioclase: Plagioclase is the most abundant phenocryst in the Rawley Andesite, comprising approximately 24 percent of the rock. It occurs as euhedral crystals up to 2.5 mm in length that are frequently clustered into

glomeroporphy. A few crystals are untwinned, but most exhibit some combination of albite, Carlsbad, or penetration twins. Using the Michel-Levy method, core compositions ranging from An₃₈ (andesine) to An₆₅ (labradorite) were recognized. Phenocrysts with no compositional zoning predominate, but oscillatory reverse zoning is also prevalent. Crystal edges are frequently rounded or embayed and their centers are often sieve-textured, indicating resorption. Occasional inclusions of opaques and apatite are present, and all plagioclase phenocrysts have been variably altered to clay, sericite, and calcite.

opaques: An opaque phase occurs as subhedral crystals which comprise about four percent of the rock volume. Crystals have a maximum length of .5mm, and have resorbed edges. Apatite frequently occurs as inclusions. Crystals of the opaque mineral are commonly associated with altered pyroxenes, and in many cases form obvious replacement or alteration features such as rims around pyroxenes and biotites or granules exsolving along cleavage planes of the host mineral.

apatite: Apatite occurs as hexagonal, rounded, or prismatic crystals of up to .15mm in length, comprising one percent of the total rock volume. It occurs as frequent inclusions in the other phenocryst phases and is also present as microphenocrysts in the groundmass.

altered phenocrysts: The remaining phenocrysts comprise eight percent of the Rawley Andesite, but all have been altered beyond recognition to products of quartz, carbonate, and chlorite ± opaques. The crystals reach a maximum length of 3.25mm, and many have retained euhedral tabular or diamond-shaped outlines. Inclusions of less-altered Rawley Andesite in the overlying pyroclastic flows provide insight into the unit's original phenocryst assemblage by revealing light greenish-brown pyroxene (augite) crystals as well as phenocrysts of tan to reddish brown biotite. Varga and Smith (1984) also report hornblende phenocrysts in their description of the Rawley Andesite which correlates with the diamond-shaped crystals observed in this study.

matrix: The matrix has a hypocrySTALLINE, hyalopilitic texture and is composed of plagioclase microlites and opaque grains. Many primary features of the matrix have been obscured by alteration to carbonate, sericite, and clay.

Lower Bonanza Tuff (Tb1)

The lower Bonanza Tuff is a high-K dacitic pyroclastic unit containing abundant phenocrysts of plagioclase, magnetite, and biotite ± sanidine ± pyroxene ± anorthoclase in a matrix of pumice, glass shards, and ash. Variations

in mineralogy with stratigraphic height are presented in Figure 15. The phenocryst to matrix ratio varies greatly in the lower Bonanza Tuff from 1/1 to 1/3, but seems to be in part a function of welding; greater ratios occur in the more densely welded units. All phenocrysts show resorption features. Rock fragment inclusions are abundant in all samples, but seem to be most densely concentrated near the base of each ash flow (Marrs, 1979).

plagioclase: Plagioclase is by far the most abundant phenocryst phase in the lower stratigraphic units, where it comprises 40 percent of the rock volume. It becomes less common upsection, however, declining to only five percent in samples 14 and 28. Plagioclase laths vary in size randomly throughout the Tbl flows, with maximum lengths ranging from 1.5 to 3.0mm. Many of these crystals are broken.

All types of compositional zoning can be observed within one rock sample. In samples 8 to 12, plagioclase crystals with no zoning predominate, and in the higher stratigraphic units oscillatory zoning superimposed on reverse and normal zoning becomes more common, along with patchy replacement by more albitic material. Occasionally crystals have a more albitic or more anorthitic rim.

Plagioclase compositions are plotted in terms of molar proportions of albite, anorthite, and orthoclase

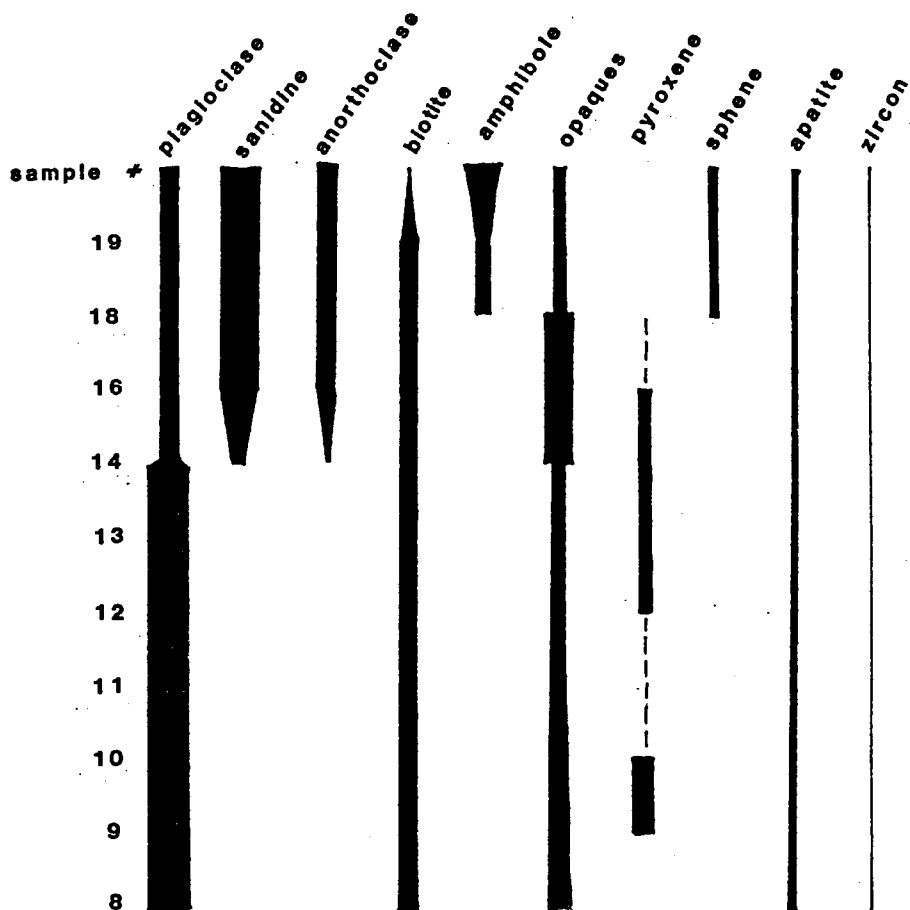


Fig. 15. Variations in mineralogy with stratigraphic height. Samples 8-16 are lower Bonanza Tuff and 18-19 are upper Bonanza Tuff. Thicknesses of the lines represent the relative abundances of these mineral phases, and dashed lines represent resorbed minerals.

in Figure 16. Core compositions become slightly more albitic upsection, ranging from an average of An₄₃ in sample 9 to An₄₁ in sample 14. Crystal rim compositions are quite variable with respect to core compositions. Plagioclase crystals exist that have increasing Or content from the core (Or_{1.1}) to the rim (Or_{7.3}), or increasingly anorthitic rims (An_{43.3} core; An_{45.0} rim); however, crystals with more albitic rims predominate, usually with orthoclase content increasing simultaneously. The largest such change from core to rim is an increase of 5.6 percent Ab.

Resorption features are seen in all plagioclase crystals, including embayed and rounded edges and sieve-textured centers. Inclusions of magnetite and apatite are also common. The phenocrysts themselves are usually quite fresh, but in some samples they have been slightly altered to clay.

alkali feldspars: Sanidine. As plagioclase crystals decrease in abundance upsection, sanidine content increases to a maximum of 37 volume percent in sample 28. Indeed, sanidine is the most abundant phenocryst phase in the three uppermost samples of Tbl, and appears only as rare, extremely resorbed crystals in the lower flows. The intracaldera tuffs contain subequal amounts of sanidine and plagioclase, although it is impossible to compare the stratigraphic position

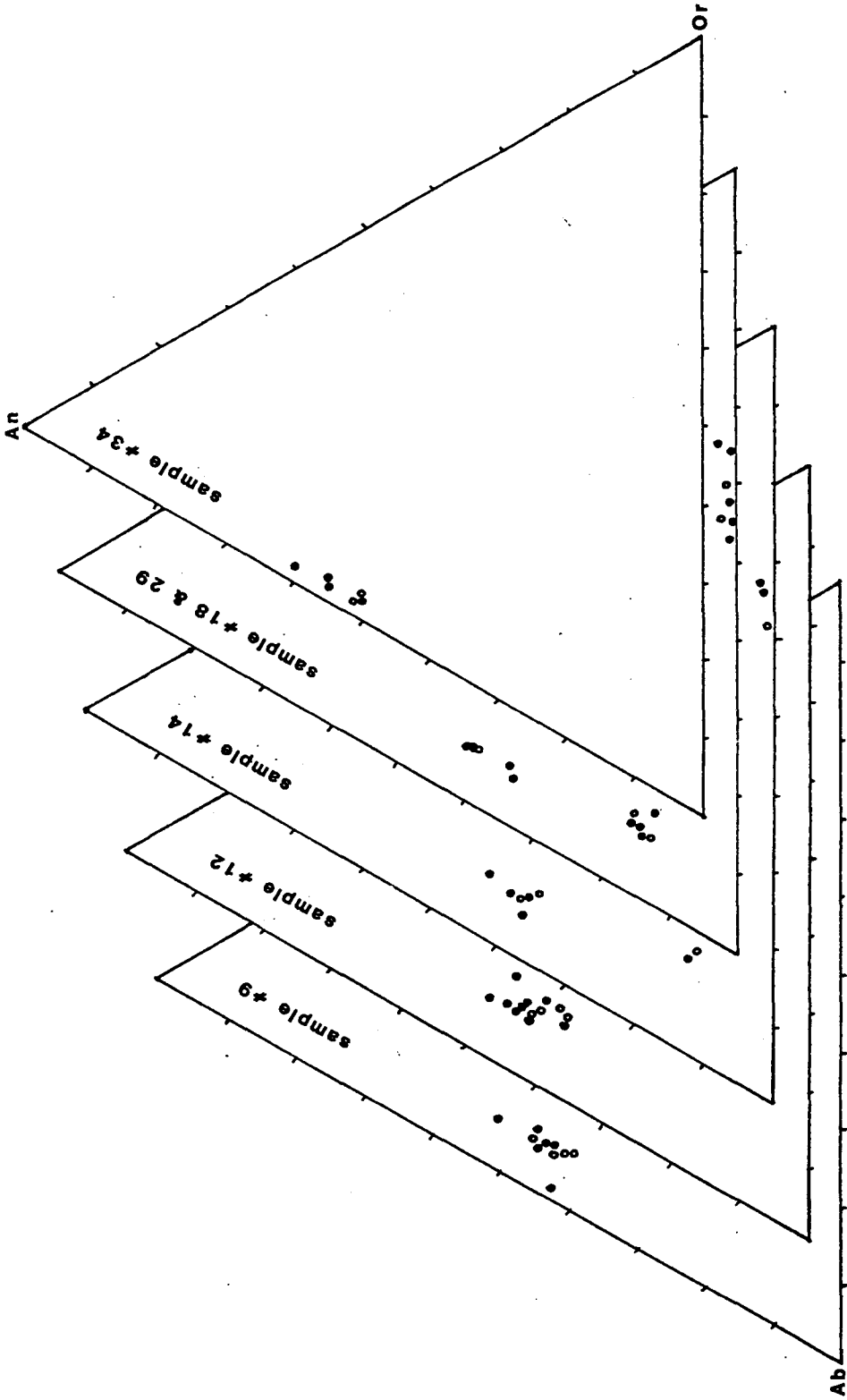


Fig. 16. Ternary plot of plagioclase and alkali feldspar compositions within the lower Bonanza Tuff (samples 9-14), upper Bonanza Tuff (samples 18 and 29), and Upper Volcanic lava flows (sample 34). Compositions are given in terms of molar proportions of Ab, An, and Or.

of the intracaldera samples to those collected at Findley Ridge and Dry Gulch.

Sanidine occurs as subhedral to euhedral tabular crystals which are frequently broken and resorbed. Crystals range in size from 1.5 to 2.8mm, and have only occasional Carlsbad twins. Crystals in some samples are slightly altered to clay.

Chemical analyses of sanidine phenocrysts are also plotted on the ternary diagram of Figure 16. The cores in sample 14 have an average composition of $Or_{65}-Ab_{32}-An_{2.5}$, and the rims contain approximately seven percent more albite than the cores.

Anorthoclase. A second population of alkali feldspar phenocryst compositions is present in sample 14. These feldspars have compositions of $Ab_{75}-An_{12}-Or_{13}$, and plot in the anorthoclase field. They exhibit reverse zoning, but have rims that are slightly more potassic than the cores and are somewhat resorbed. Petrographically, anorthoclase can be distinguished from sanidine by double polysynthetic twins which form a grid pattern. The twin laminae are narrower than those of microcline, however, and have a different crystallographic orientation. Anorthoclase typically forms at much lower temperatures than sanidine, and must be xenocrystal.

biotite: Biotite is a very common phenocryst phase in the

lower Bonanza Tuff, comprising two to eight volume percent of the rock. No correlation exists between abundance and stratigraphic height. Crystal size also varies randomly, ranging from a maximum length of 0.9 to 2.5mm. Phenocrysts are commonly subhedral, and are elongated or hexagonal in shape.

Biotite color varies from sample to sample, ranging in pleochroic scheme from a honey brown, a red brown, or a dark greenish brown to a dark brown color. Crystals are usually surrounded by an opaque rim and smaller phenocrysts will be completely black. Crystals are often embayed, and inclusions of apatite and magnetite are common. Occasionally crystals are broken and have been bent around other phenocrysts during compaction. Biotites in intracaldera samples have been severely altered to chlorite and calcite.

The mol fraction of magnesium in biotite (x_{Mg}^{bi}) decreases upsection from values of .78 in the lower units to .63 in the upper ash flows. This indicates that the iron content is increasing with stratigraphic height (Fig. 17), suggesting that the later-erupted magmas were more evolved. The number of atoms per formula unit (afu) of Ti generally decreases upsection, ranging from .7195 to .5243 (Fig. 18). This is unusual because Ti normally correlates with Fe. Significant amounts of fluorine have substituted for OH^- in the

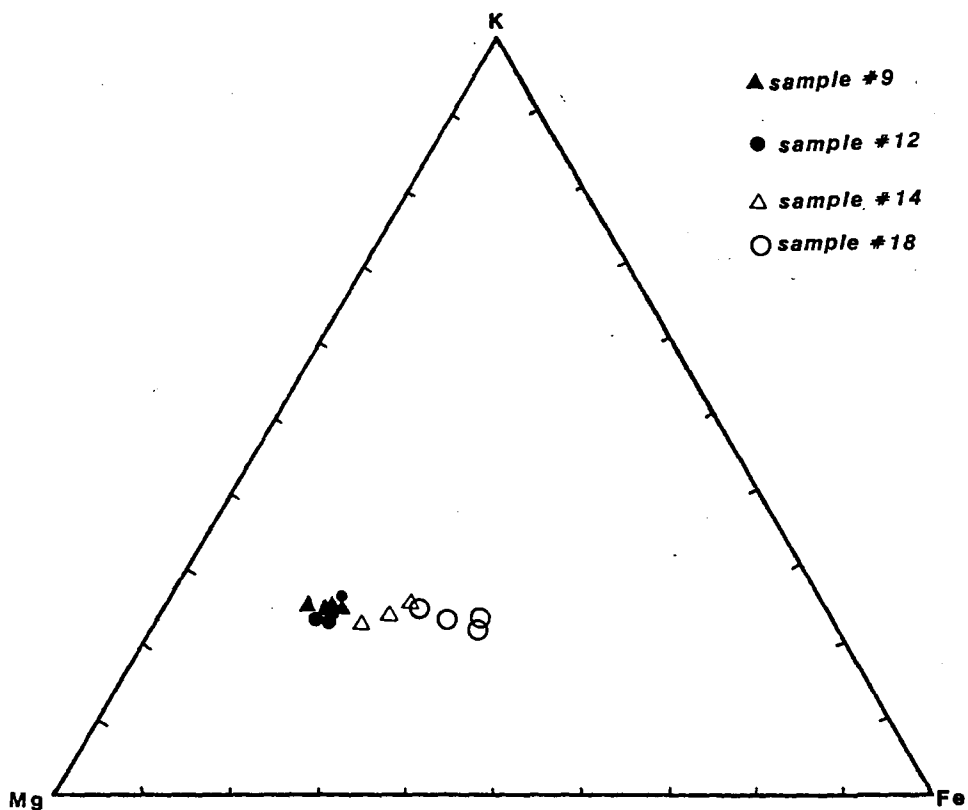


Fig. 17. Ternary plot of K-Mg-Fe components in biotite samples. Samples 9 through 13 were collected from increasing stratigraphic heights.

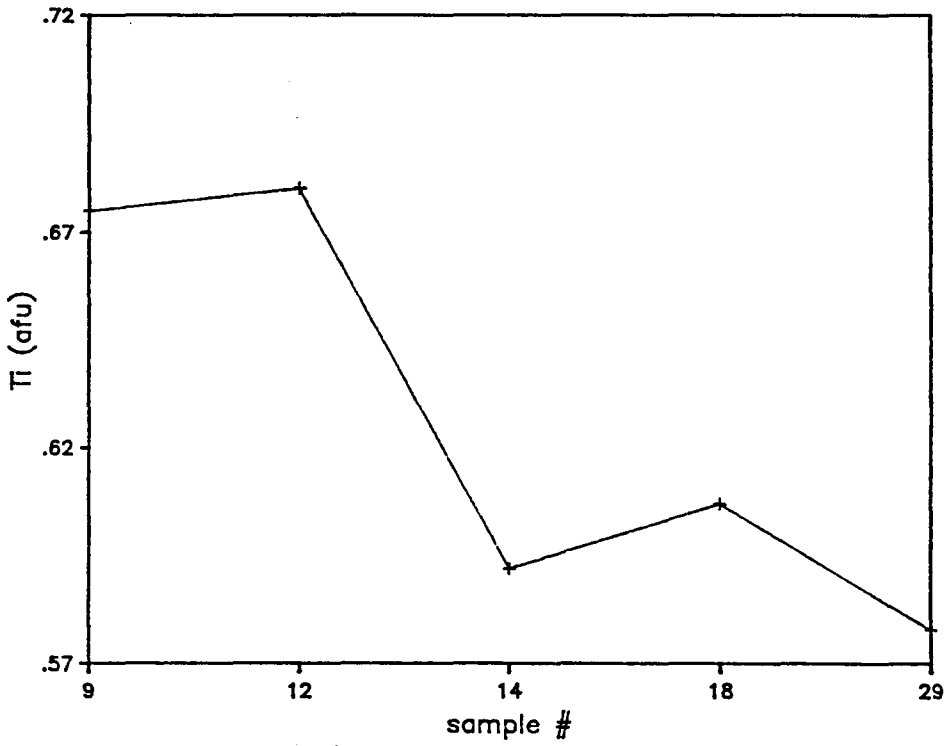


Fig. 18. Average Ti atoms per formula unit of biotite versus stratigraphic height.

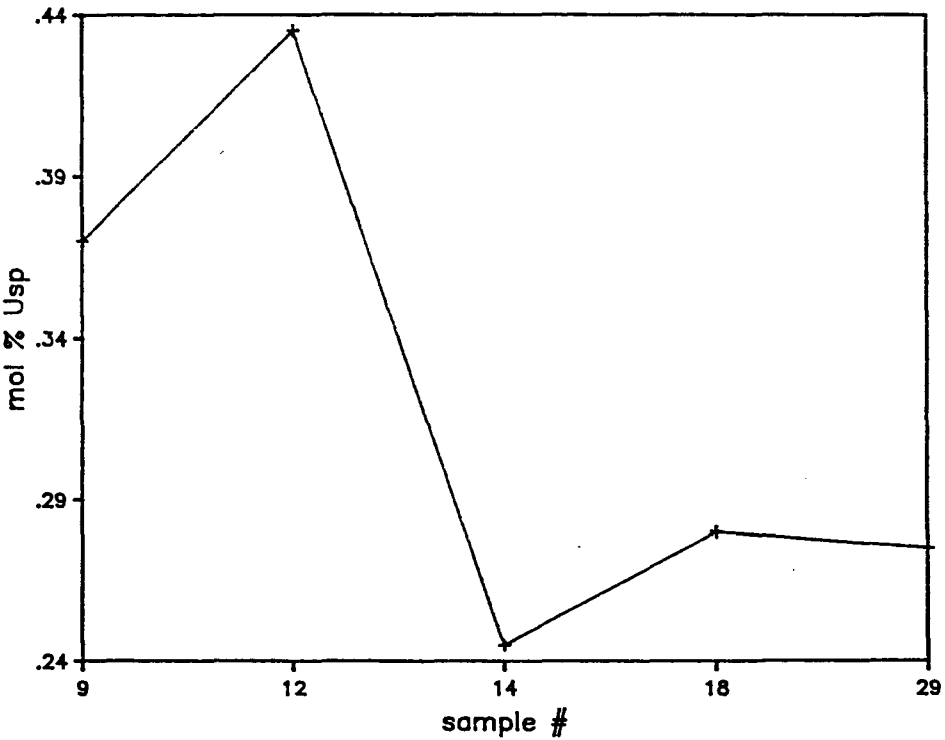


Fig. 19. Average mol percent of Usp in opaques versus stratigraphic height.

biotite crystals. The F content ranges from an average wt. percent of .0305 to .0530, with no systematic variation with stratigraphic height.

opaques: Subhedral to anhedral opaques are a prevalent phase in all samples, ranging in abundance from 0.3 to 2 volume percent, with no systematic variation with stratigraphic height. Crystals occur as phenocrysts, ranging in size from .45 to 1.0 mm, and also as small inclusions in biotite, pyroxene, and plagioclase. The opaques also seem to be alteration products in some cases. Opaques form granules throughout altered pyroxenes in sample 13, and also form dark rims around biotites in all thin sections. Opaque crystals are very fresh in outer caldera samples, but are always embayed or rounded by resorption. Inclusions of apatite are common. Opaques in intracaldera samples have been severely altered to chlorite.

The opaque grains in the probed samples are all titanomagnetites, ranging in composition from an average value .237 mol percent ulvospinel (Usp) to a maximum value of .466 percent Usp (Fig. 19). Usp values are highest for sample 12 which is about midway stratigraphically in the Tbl, and values are lowest in sample 14. Mol percent Al_2O_3 varies from .305 to 1.374, with no correlation to stratigraphic height. Atoms of Mg per formula unit tend to decrease with stratigraphic

height from values of 1.437 to .0487 (Fig. 20), and Cr similarly decreases from a maximum value of .0202 to .0151 afu, and then increases slightly (Fig. 21). Some magnetites contain no chromium. Intergrowths of hercynite ($\text{Fe}^{+2}\text{Al}_2\text{O}_4$) are also present in some opaque phases, with an Al_2O_3 content of 9.881, MgO of 4.281, and Cr_2O_3 of .0025 mol percent.

Most crystals show "exsolution" features of more titanium-rich material as lamellae in the (111) planes of the host magnetite. The most Ti-rich lamellae present has the composition of Ilm .660

pyroxene: Only samples 9 and 12 from the Tbl contain appreciable amounts of pyroxene (1.2 to 4.0 volume percent). In these rocks fresh, euhedral to anhedral crystals are easily distinguished by their pale green color and prevalent cleavage. Some simple twinning is also evident, and crystals are frequently rounded and embayed. Pyroxenes frequently contain abundant inclusions of magnetite and apatite.

The pyroxenes from the Lower Bonanza Tuff all plot in the augite composition field (Fig. 22), with the mol fraction of Mg ($X_{\text{Mg}}^{\text{PYX}}$) ranging from .746 to .782, becoming slightly greater with increasing stratigraphic height (Fig. 23). The mol percent of wollastonite (CaSiO_3) also increases stratigraphically, ranging from .4047 in sample 9 to .4571 in sample 14. Mol percent

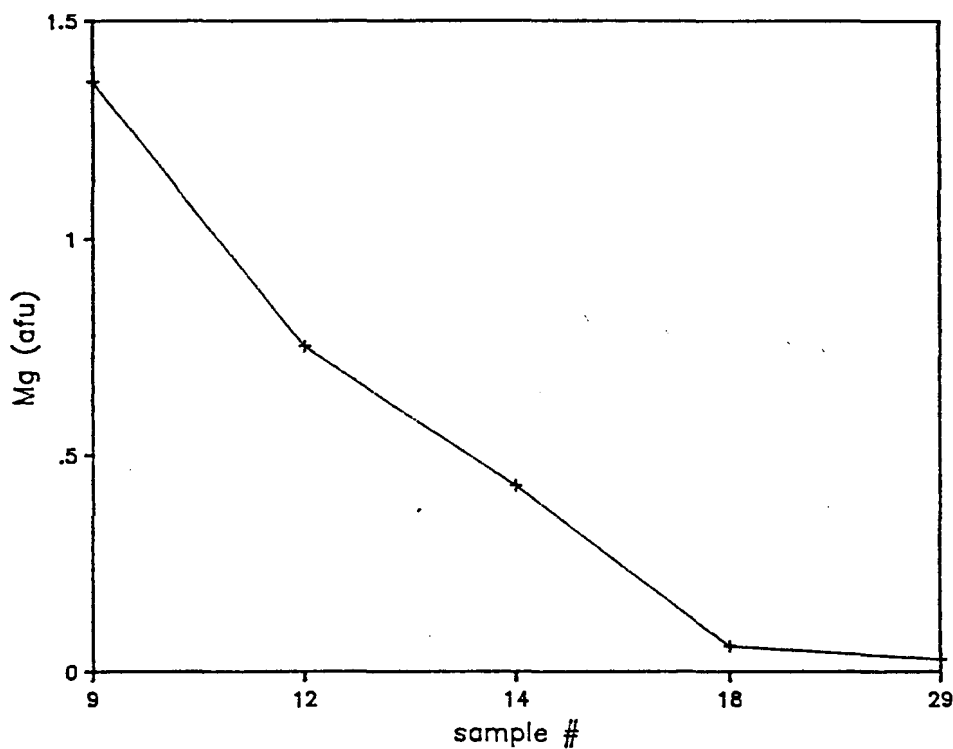


Fig. 20. Average atoms of Mg per formula unit of titanomagnetite versus stratigraphic height.

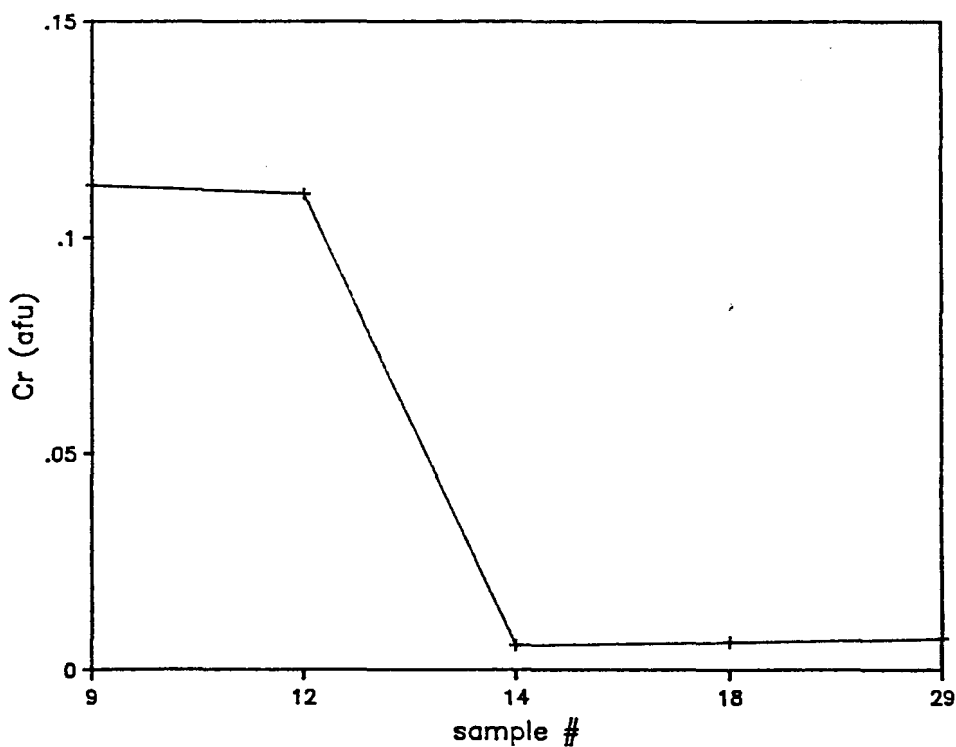


Fig. 21. Average Cr in titanomagnetite versus stratigraphic height.

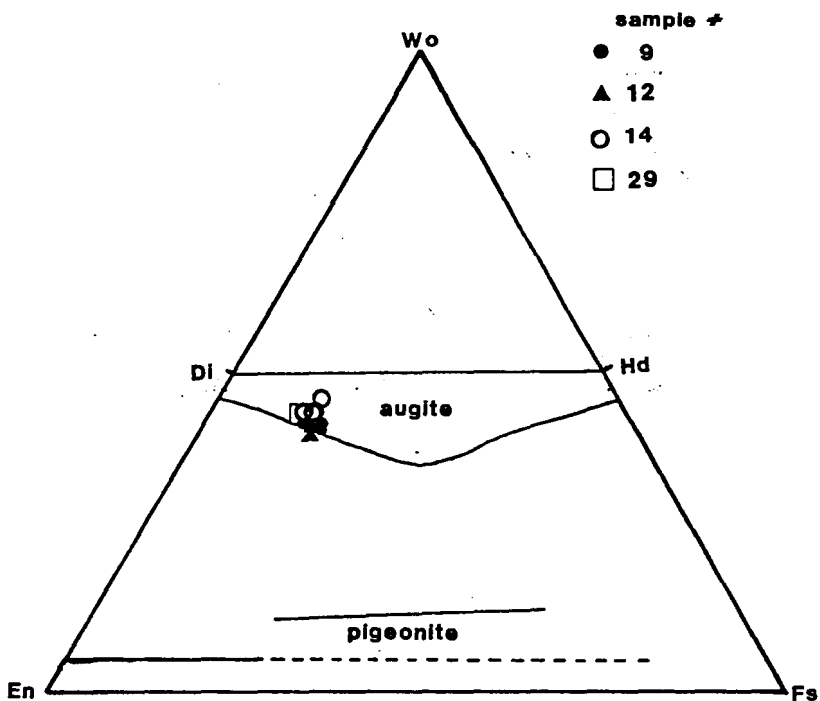


Fig. 22. Ternary plot of pyroxene compositions. Compositions are given in terms of mol percent ferrosilite, enstatite, and wollastonite.

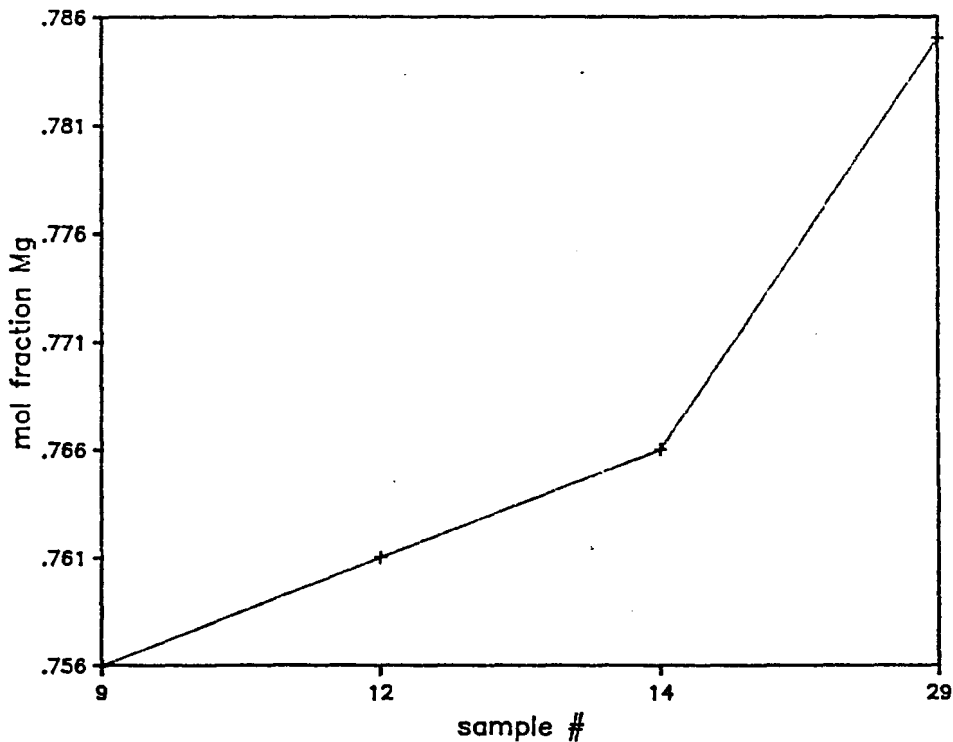


Fig. 23. Average mol fraction of Mg in pyroxene versus stratigraphic height.

enstatite (MgSiO_3) and ferrosilite (FeSiO_3) both generally decrease with greater stratigraphic height, ranging from .4045 to .4485 and .1296 to .1542 respectively (Fig. 24).

The decrease of mol percent FeSiO_3 and the increase of mol percent Mg with stratigraphic height is opposite of the chemical trend observed in the biotite crystals. Perhaps this discrepancy is caused by the effects of Fe^{3+} in the magma. As a magma becomes more evolved, the Fe content of the melt increases, tending to lower the value of $X_{\text{Mg}}^{\text{PYX}}$. At the same time, a larger percent of Fe in the melt is Fe^{3+} . Because Fe^{3+} is not easily incorporated into the pyroxene structure, greater amounts of Fe^{3+} in the melt tend to increase $X_{\text{Mg}}^{\text{PYX}}$ values. This trend must have dominated the pyroxene chemistry, resulting in the observed decrease in mol percent ferrosilite with stratigraphic height. This hypothesis can be verified by calculating the amount of Fe^{3+} in the pyroxenes from stoichiometric constraints and plotting the average $\text{Fe}^{3+}/\text{Fe}^{2+}$ value for each sample against stratigraphic height (Fig. 25).

The ferric/ferrous iron ratio does increase upsection, proving the importance of Fe^{3+} in controlling the mol fraction of Mg in pyroxene.

Orthopyroxene crystals are present only in sample 9, however, these grains are altered and give low wt.

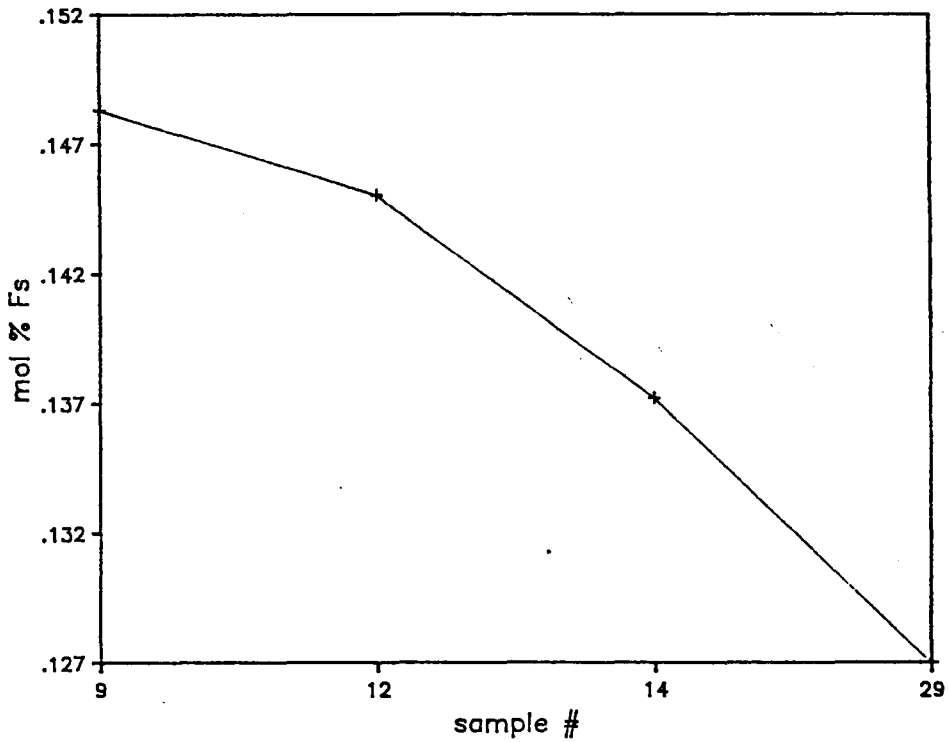


Fig. 24. Average mol percent ferrosilite versus stratigraphic height.

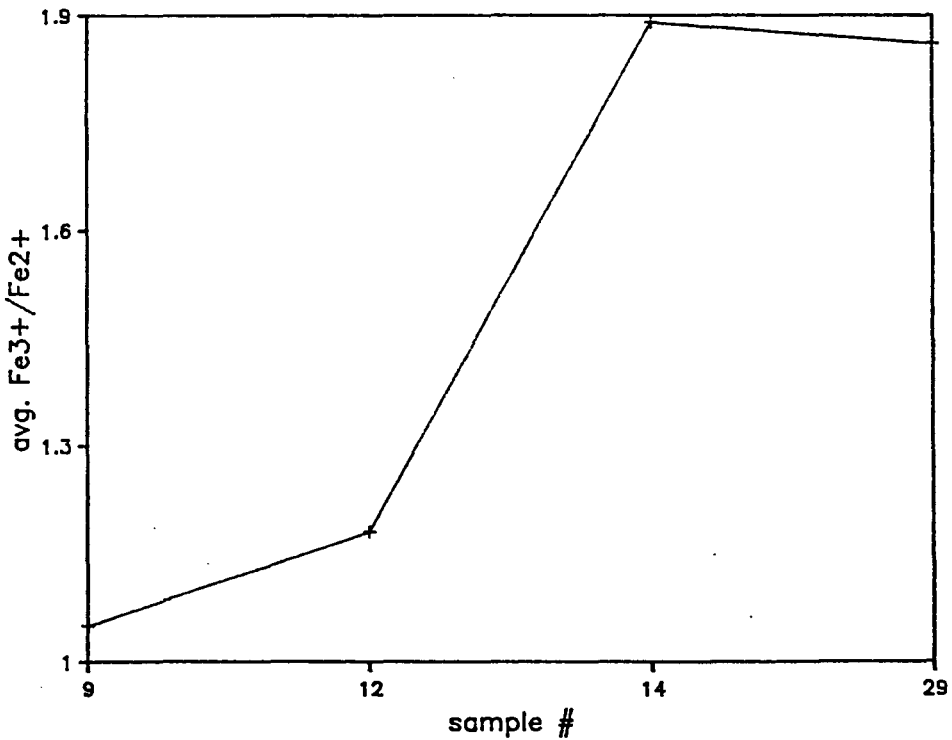


Fig. 25. Average ratio of $\text{Fe}^{3+}/\text{Fe}^{2+}$ in pyroxene versus stratigraphic height.

percent totals when probed. Therefore, reliable chemical data cannot be obtained for two coexisting pyroxenes.

In some cases the pyroxene seems to be reacting with the melt to produce a new phenocryst phase. Some augite crystals are surrounded by an opaque jacket, or have discrete grains of opaques throughout the phenocryst. Other augites contain inclusions of glass, or sometimes have feldspars in their centers. In sample 9, augites are frequently surrounded by needle-like opaque(?) quench crystals. Many of the other Tbl samples contain occasional (.1 to .6 volume percent) pyroxene phenocrysts that have been highly altered to sericite, magnetite, and clay.

accessory phases: Apatite occurs in all samples as prismatic or rounded crystals of high relief and low birefringence. It is present mainly as inclusions in magnetite, pyroxene, and biotite. A few round, high relief, high birefringence crystals of zircon are also present in the matrix.

matrix: The appearance of the matrix of the various Tbl flows is highly variable, depending upon both the nature of the eruption and the degree of welding. A few samples have a matrix that seems to be composed primarily of fine particles of glass (sample 70), whereas most flows have a groundmass of glass shards

and pumice. The shards are often flattened and bent due to compaction, especially near phenocrysts. Axiolitic recrystallization in some of the samples highlights individual shards. Pumices are distinguished by their thread-like appearance, and their color becomes darker with increased welding, giving the rock a eutaxitic texture. Samples 9 and 28 are so densely welded that no shards can be discerned, and the matrix looks like that of a holohyaline lava. Only the high percentage of lithic fragments in these two rocks indicates their pyroclastic origin.

The matrices of the lower Bonanza Tuff samples are various shades of brown that get darker with increasing welding. Occasionally pumices are replaced by chalcedony or have undergone spherulitic recrystallization. The matrix is generally fresh, with only minor sericitic alteration, however, the recrystallized pumices in the intracaldera samples have been highly altered to clay.

inclusions: The volume percent of lithic inclusions varies greatly from sample to sample. Marrs (1979) believes that inclusions are concentrated at the bottom of each individual ash flow due to greater densities, and that abnormally high lithic abundances are due to eruption from a blocked vent. Lithic fragments are common in samples 10, 14, 28, 71, and 16, and reach a maximum

abundance of 10 volume percent in sample 13. All lithic fragments have sharp contacts with their host rock, often with broken phenocrysts along the edge of the inclusion. These observations, plus the lack of vesicles or a recognizable chill margin, indicate that the lithic fragments were solids as opposed to magmas at the time of their incorporation into the Tbl.

Lithic inclusions are of six main types, and will be listed in order of abundance: 1) Samples 9, 13, 28, and 16 all contain fragments of a lava composed of plagioclase laths in a dark brown, glassy matrix. This type of lava, however, is not exposed at the surface anywhere within the Bonanza region. Fragments are from .1 to 1.25 mm wide, and are rounded to angular in shape. 2) Fragments of Rawley Andesite are quite abundant in samples 10, 13, 28, 70, and 16, and are also present as rare lapilli in sample 12. They range in size from .25mm to more than 3.2cm. Fragments are largely sub-rounded. 3) Abraded pumice fragments, probably picked up from another ash flow, are present in samples 9, 10, and 13, and range in size from .25 to 2.0mm. These foreign pumices have retained their thread-like pseudo-flow texture, but are often rounded or subangular, indicating abrasion. 4) Samples 14 and 28 contain fragments of what appears to be an earlier tuff deposit, with a glassy dust matrix which is

somewhat altered to clay. The tuff matrix contains opaque quench crystals and has phenocrysts of plagioclase and biotite. The fragments range in size from 1.0 to 5.5mm. 5) Globules of brown glass are present in flow 9. They are often rounded and seem to be inclusions, because some glass globules contain broken phenocrysts along the edges. Another explanation is that perhaps the glass is a primary feature formed when plagioclase xenocrysts acted as heat sinks and rapidly chilled the surrounding magma. Quench crystals surrounding the phenocrysts support this theory. 6) Finally, sample 46 from the intracaldera facies contains a fragment of granite that is 1.5 mm wide. The granite is composed of plagioclase, microcline, and strained quartz. It is probably a fragment of the Precambrian country rock.

Upper Bonanza Tuff (Tbu)

The upper Bonanza Tuff ranges from a high-K dacitic to a rhyolitic pyroclastic unit. It is similar in appearance to the lower Bonanza Tuff, except that it is less crystal-rich, the phenocrysts are smaller, and it contains a slightly different mineral assemblage (see Fig. 16). In the upper Bonanza Tuff alkali feldspar is the most common phenocryst, biotite is lower in abundance, and amphibole and sphene are phenocryst phases. The matrix of the upper

tuff is light gray to pink in color, and is much more recrystallized than the average Tbl sample. The mineral chemistry data presented in the following section is taken from the samples lacking secondary silicification.

alkali feldspars: Alkali feldspars are the most abundant phenocrysts in the upper Bonanza Tuff, comprising 9.2 to 32 volume percent of the rock and ranging in size from 0.9 to 2.23 mm. Crystals are often cracked and broken, or are rounded and embayed. Carlsbad twinning is common, and crystals are sometimes slightly altered to clay.

The compositions of the alkali feldspars plot in two distinct populations (Fig. 17). Sanidine, the high temperature alkali feldspar, ranges in composition from $Or_{53.1-65.3}Ab_{45-31.8}An_{1.9-3.0}$. The second group of alkali feldspars plots in the anorthoclase composition range, with values of $Or_{9.7-12.3}Ab_{74.9-76.2}An_{12.9-14.1}$.

plagioclase: Plagioclase crystals are much less common in the Upper Bonanza Tuff than in the Tbl, comprising only .2 to 12 volume percent of the unit. Crystals are also generally smaller, ranging from maximum sizes of .9 to 2.75mm in length. Most crystals are broken and embayed, and occasionally they occur as glomeroporphy. All types of zoning are again present, but crystals with no zoning are most common. Plagioclase cores range in composition from $An_{32.9-40.1}Ab_{60.4-52.9}Or_{6.7-7.1}$. Sometimes the

crystal rims are one to two percent more albitic than the core. Plagioclase crystals generally are slightly more altered to clay than the alkali feldspar crystals.

biotite: Biotite varies in abundance from .2 to 2.7 volume percent in the upper Bonanza Tuff. It is similar in appearance to biotites in the lower units, except that crystals are smaller, ranging from maximum sizes of .75 to 1.75 mm in length. Crystals frequently have dark, oxidized rims and are often embayed. x_{Mg}^{bi} ranges from .525 to .630, indicating that these crystals contain more iron than those biotites in the Tbl. Mol percent Al_2O_3 ranges from 2.3464 to 2.4249, and TiO_2 from .5885 to .6191. These values are generally lower than the TiO_2 contents of the Tbl biotites.

amphibole: Hornblende comprises .45 to 1.6 volume percent of the upper Bonanza Tuff. It is similar in appearance to the biotites, except that pleochroism ranges from light green to yellow brown to brown. Crystals range in size from .5 to .75mm, and contain inclusions of opaques and apatite. Simple twins are occasionally present. Unfortunately, no quantitative mineral chemistry data were obtained for the amphiboles in this study, other than determining that they are relatively rich in Ca, Mg, Fe, and Al.

opaques: Opaques comprise .3 to 1.2 volume percent of the Tbu samples and range in size from .2 to .5mm. Usp

content ranges from an average value of .267 to a high of .293 percent, which is generally lower than the values for the Tbl. Similarly, mol percent Al_2O_3 varies from .2429 to .4501, and MgO varies from .0364 to .1890 percent, both of which are again lower than the values obtained for Tbl opaques. Mol percent Cr_2O_3 ranges from 0.0 to .0140.

sphene: Sphene is another mineral phase which distinguishes the upper Bonanza Tuff from the lower unit. Sphene content ranges from .15 to 1.0 percent, and crystals reach a maximum size of .25mm. Sphene can be distinguished by its euhedral shape, tan color, very high relief, and very high birefringence. The presence of sphene in conjunction with the absence of ilmenite in the Tbu indicates that fairly high oxygen fugacities existed in the magma (Luhr et al., 1984).

minor phases: Other phases present include very altered pyroxene phenocrysts in samples 18 and 29, with $x_{\text{Mg}}^{\text{Pyx}}$ values of .763 to .791. Accessory phases of apatite and zircon are also present.

matrix: The matrix of the Tbu has a light gray to pink color and is composed of glass shards and pumice. More axiolitic recrystallization of shards, more spherulitic recrystallization, and more secondary replacement of pumices has occurred here than in the Tbl matrix. In the Dry Gulch samples, secondary silicification of the

groundmass gives it a lacy appearance.

inclusions: Inclusions are less numerous and smaller in the Tbu, with lapilli of Rawley Andesite and the brown plagioclase-rich lava once again present. Sample 29 also contains a xenocryst of strained quartz and a xenocryst of microcline, both of which are probably inclusions plucked from the Precambrian granite country rock.

Upper Volcanics (Tuv)

The Upper Volcanic unit is a high-K andesitic lava that is composed of phenocrysts of plagioclase, pyroxene, amphibole, and opaques, in a pilotaxitic groundmass. Phenocrysts comprise 20 percent of the rock volume. The plagioclase and pyroxene crystals often occur in glomeroporphy, and only plagioclase phenocrysts show significant evidence of resorption. No lithic fragments are present in this unit, in contrast to the inclusion-rich underlying tuffs. Only one thin section of this volcanic unit was examined, and mineral chemistry analyses of only the plagioclase phenocrysts were obtained.

plagioclase: In the Upper Volcanic unit, plagioclase is once again the most abundant phenocryst phase. It comprises 12 percent of the unit, and crystals are up to 2.5 mm in length. Phenocrysts are rounded and embayed and exhibit predominantly oscillatory and

reversed zoning. Core compositions range from $Ab_{.3712}-.4633An_{.5036}-.6075Or_{.0214}-.0331$, and rims are sometimes more anorthitic by approximately one mol percent or more albitic by about six mol percent. Crystals contain occasional opaque inclusions and are somewhat altered to clay and sericite.

pyroxene: Euhedral to subhedral pyroxene phenocrysts compose approximately four volume percent of the Uv sample. Pyroxenes frequently occur as glomeroporphy with plagioclase, with crystals up to 1.75 mm in length. The pyroxene crystals are a light green color and have moderate birefringence and inclined extinction. Simple twinning sometimes occurs. Although no chemical analyses were run on the pyroxenes in this unit, optically they appear to be of augite composition. Inclusions of apatite and opaques are common.

amphibole: All of the light brown to dark brown pleochroic crystals in this sample are hornblende; no biotite is present. This is evident from the moderate 2V of the crystals and the lack of bird's eye extinction. Frequently diamond-shaped cross-sections can be seen with prismatic cleavage, but many crystals are elongated (010) sections. Most amphibole crystals have opaque rims due to oxidation or resorption, and contain inclusions of apatite and opaques.

opagues: Subhedral to anhedral opaque phenocrysts up to .5mm wide comprise one volume percent of the Uv samples. Opagues also occur as inclusions in amphibole, pyroxenes, and plagioclase phenocrysts.

apatite: Apatite occurs as microphenocrysts in the groundmass and as inclusions in the other phenocryst phases.

matrix: The holocrystalline, pilotaxitic matrix is composed of interwoven plagioclase laths and opaque crystals.

Origin of observed petrographic features

Resorption Features

Observed resorption features in the Bonanza volcanic units include phenocrysts with rounded corners, embayed edges, and sieve-textured centers. Resorption may result from either disequilibrium or equilibrium processes.

Disequilibrium is caused by sudden changes in magma temperature, pressure, or water content. An increase in temperature may occur if crystals which formed in the cooler, upper portion of a thermally zoned magma chamber sink to hotter regions, or if xenocrysts from the country rock are incorporated into the magma. Similarly, the injection of hot, mafic magma into the chamber of a cooler, more evolved magma will raise the temperature of the chamber, and mixing of the two magmas will form a hybrid magma that is not in chemical equilibrium with the phases

that were contained in either of the two end members. The melting caused by thermal disequilibrium may occur at the crystal corners, or in the center of the crystal along cleavage planes, creating a sieve-like texture (Cox et al., 1979).

An increase in the water content of a magma due to the fractionation of anhydrous phases will lower the solidus of an anhydrous mineral, and remelting may occur (Fig. 26). The stability of hydrous minerals, on the other hand, is dependent on the amount of water present, and so a decrease in water content of the magma due to late stage devolatilization may cause resorption of hydrous minerals such as biotite and amphibole (Cox et al., 1979).

All magmas undergo pressure reduction during magma ascent. The phase boundaries of anhydrous minerals have positive slopes under dry conditions, and so the loss of pressure will cause these crystals to melt (Fig. 26). The melting point of different minerals is affected to varying degrees by changes in pressure, as can be observed in the case of the two plagioclase endmembers (Fig. 27); the melting point of albite is much more sensitive to pressure than that of anorthite. Conversely, a drop in pressure may cause the crystallization of anhydrous phases if water is present, due to the negative slope of such phase boundaries (Wyllie, 1971).

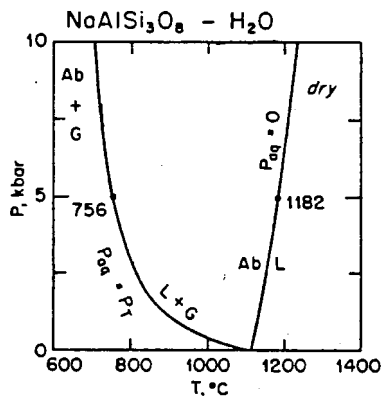


Fig. 26. P-T diagram for the Ab-An system showing the melting curve of Ab under dry conditions and in the presence of a gas phase (after Morse, 1980).

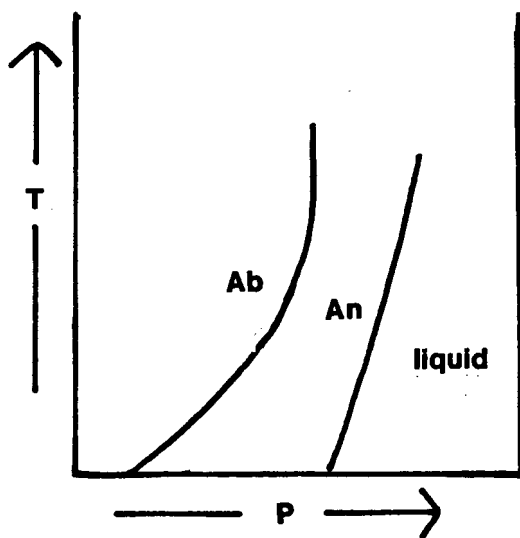


Fig. 27. P-T diagram for the melting of albite and anorthite under dry conditions. The melting temperature of Ab is more sensitive to pressure than that of An (from Barton, personal communication, 1986).

Resorption can occur while crystals are still in equilibrium with the melt. A liquid undergoing equilibrium crystallization may react with an earlier-formed crystal to yield a new phase. A well-known example of equilibrium resorption occurs in the olivine-diopside-quartz ternary system (Fig. 28).

A basaltic melt of composition X in this system will cool until it hits the liquidus and then begin to precipitate olivine. Olivine will continue crystallizing and the melt composition will move directly away from the olivine endmember until it reaches the cotectic. This is a reaction boundary, and although the system is still in equilibrium, a reaction of olivine and melt must occur to precipitate enstatite; thereby the olivine phenocrysts are resorbed (Morse, 1980).

Resorption in the Bonanza volcanic units is probably due to a variety of reasons. Because all phenocryst phases in the rocks are resorbed to some extent, an equilibrium process is probably not responsible (Cox et al., 1979). Undoubtedly, changes in pressure and temperature as the magma rose to the surface caused some resorption. Also, the presence of xenocrysts is suggested by the two alkali feldspars, because one is a high temperature phase and the other is a low temperature phase. Magma mixing may also be responsible for some of the resorption, although two compositional populations of phenocrysts are not observed

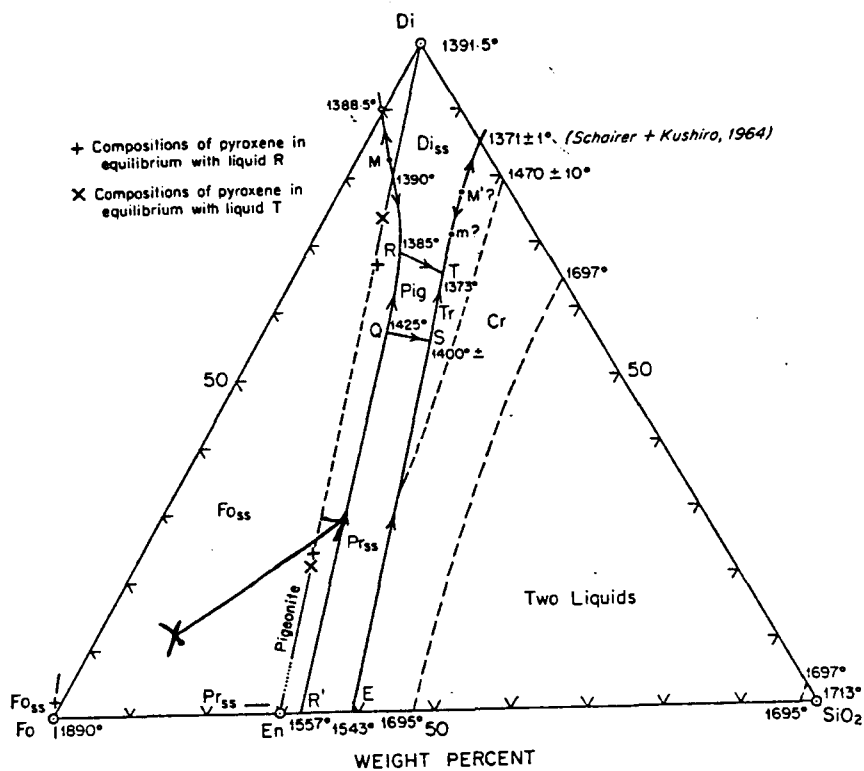


Fig. 28. Fo-Di-SiO₂ phase equilibria diagram. The crystallization path of composition X is discussed in the text (after Morse, 1980).

for most phases. Often mixing pulls the liquid composition off the liquidus, so that both endmember phenocryst compositions are resorbed, and a third generation of phenocrysts may precipitate upon cooling (Fig. 29) (Barton et al., 1982).

Zoning in feldspars

The variety of zoning displayed by feldspars in the Bonanza volcanic units is a common feature of calc-alkaline rocks, and reflects the complex interaction of numerous processes that culminated in the eruption of the Bonanza lavas and pyroclastics. Crystals with no compositional zoning occur when cooling is slow enough for the crystals to completely exchange cations with the melt, and total solid solution occurs. Unzoned crystals are also observed in cumulates, which were removed from the melt before further reaction could take place (Cox et al., 1979).

Normal zoning occurs when a magma cools too quickly for the cores of the crystals to exchange cations with the melt. As the melt cools and evolves, more sodic layers are successively added outward from the calcic core, effectively sealing the core off from further interaction with the liquid. Similarly, a calcic xenocryst dropped into a slightly more sodic melt will develop normal zoning if cooling proceeds rapidly enough to seal the core from interaction with the melt and thus prohibit re-

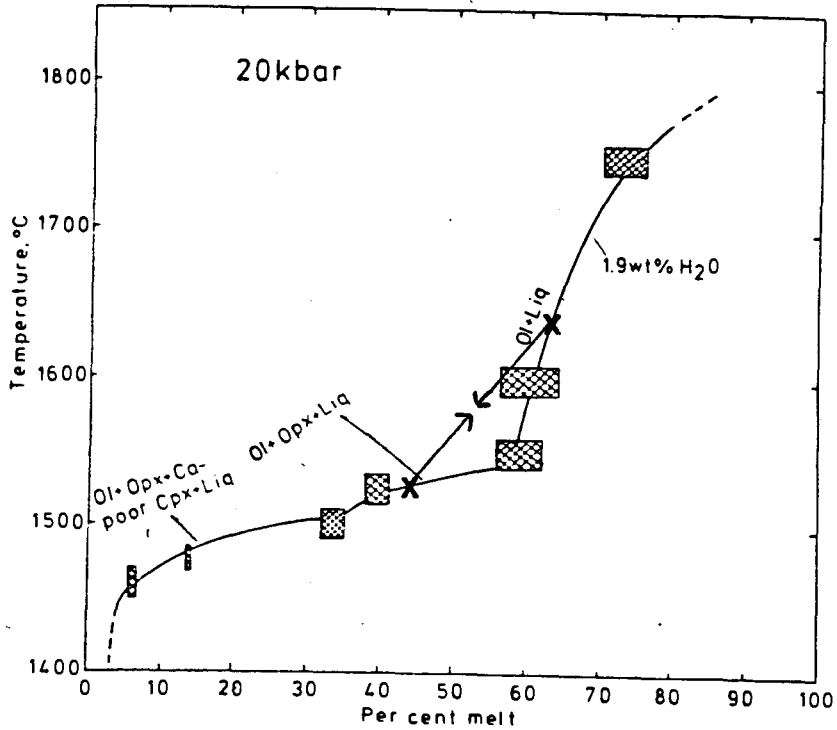


Fig. 29. Melting curve for MORB compositions. Cusps in the liquidus occur at changes in mineral assemblages. Arrows demonstrate how the mixing of magmas can pull the hybrid magma composition off the melting curve and into the liquid field, where phenocrysts from both endmember magmas will be resorbed (modified from Mysen and Kushiro, 1978).

equilibration from occurring. Such a xenocryst would be difficult to discern unless the difference in composition between the melt and the xenocryst was substantial (Cox et al., 1979).

Many of the same processes that cause resorption may also result in compositional zoning if the cooling rate of the magma is relatively rapid. For example, if a sodic xenocryst were picked up by a calcic magma, either resorption could occur, or reversed zoning could form if the magma cooled rapidly and calcic plagioclase layers grew around the crystal in time to isolate the core. Relatively rapid cooling during the ascent of a magma from depth could also result in reverse zoning instead of resorption, because as pressure decreases, the solidus-liquidus loop of plagioclase rotates downward (Fig. 30). Thus, with decreasing pressure, the liquid coexists with a plagioclase of a more anorthitic composition.

The accumulation of volatiles in a fractionating melt is yet another possible cause of reverse zoning, for the addition of water also rotates the plagioclase solidus-liquidus loop downward (Fig. 31), causing a wet melt to be in equilibrium with a more anorthitic plagioclase composition than a dry melt (Barton, personal communication, 1986).

The causes of oscillatory zoning are still controversial, but a theory first presented by Harloff

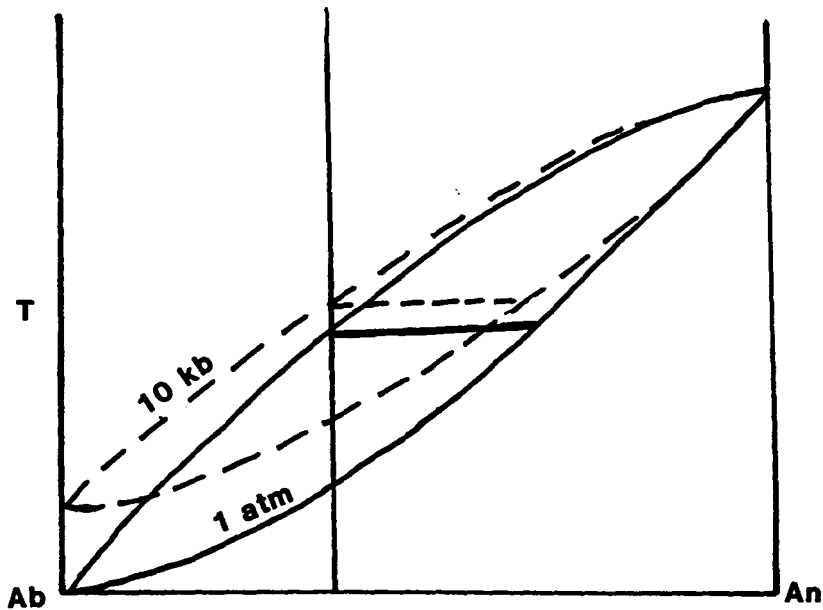


Fig. 30. X-T diagram for the Ab-An system showing the effects of pressure on the solidus-liquidus loop (after Barton, personal communication, 1986).

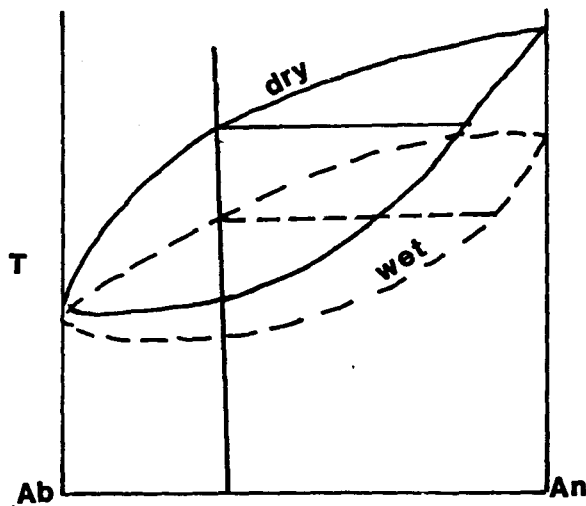


Fig. 31. X-T diagram for the Ab-An system showing the effects of water content on the solidus-liquidus loop (after Barton, personal communication, 1986).

(1927) suggests that this type of zoning occurs due to discrepancies between crystal growth rate and cation diffusion rate. Studies by Bowen (1913) show that crystallizing plagioclase is enriched in Ca and Al and depleted in Na and Si relative to the melt. Because supersaturation is the driving force of crystal growth, crystallization of plagioclase occurs only when the melt has become supersaturated with Ca and Al. At the beginning of crystallization, growth is so rapid that Ca and Al are taken into the crystal faster than the diffusion rate can restore these elements to the area surrounding the crystal, so that the outer crystal layers become increasingly An-depleted. Yet as the supersaturation of Ca and Al around the crystal decreases, crystal growth slows. The chemical gradient previously created during the rapid growth stage causes Ca and Al to be supplied to the depleted liquid area, and supersaturation can build up once again and renew crystal growth of An-rich material. Na diffuses much more rapidly than either Ca or Al, so that the Na diffusion rate is the controlling factor of crystal growth (Bottinga, et al., 1966).

Previous explanations for oscillatory zoning have proposed that convective overturn in a thermally zoned magma chamber or the eruptive venting of the magma chamber would lead to large variations in pressure, temperature and water content, thereby upsetting the existing plagioclase-

liquid equilibrium (Bottinga et al, 1966). Harloff (1927) argues that his diffusion theory is more reasonable because it explains the regular cyclic pattern of oscillatory zoning. The other processes would not be so consistently repetitive. Bottinga et al. (1966) provide supporting evidence for Harloff's theory by detecting measurable concentration gradients of elements near crystal-liquid interfaces.

Thus, the observed plagioclase zoning in the Bonanza volcanics may be the result of several different processes. The predominantly unzoned phenocrysts of samples 8 through 12 may have formed in a deep, slowly cooling part of the magma chamber, where cations had time to completely exchange with the melt. Zoned crystals probably formed in more rapidly-cooling, roofward zones of the chamber, where diffusion rates and changes in pressure affected the composition of the crystal. The reverse zoning noted in the anorthoclase xenocrysts most likely developed when they became included in the more anorthitic magma.

Oxidation Features

The lamellae of Ti-rich material observed within the magnetites of the Bonanza Tuff appear to be exsolution features, however, researchers agree that such features are not primary characteristics because the intergrowths cannot be homogenized without changing the bulk composition

(Buddington and Lindsley, 1964). Buddington and Lindsley suggest that, at the time of crystallization, titanomagnetites contain predominantly Fe_2TiO_4 (Usp) in solid solution, with only minor amounts of FeTiO_3 (Ilm), and that the observed ilmenite lamellae are actually caused by the subsolidus oxidation of ulvospinel. This oxidation occurs due to the thermal dissociation of water-rich fluids in the magma according to the reaction $\text{H}_2\text{O} = \text{H}_2 + 1/2(\text{O}_2)$. Hydrogen preferentially escapes from the magma due to its small atomic radius, creating oxidizing conditions in the liquid which convert much of the ulvospinel directly to magnetite (Fe_3O_4) and ilmenite according to the formula:



Ilmenite is relatively insoluble in spinel, and consequently it exsolves as lamellae in the host magnetite. Often in volcanic rocks, extreme oxidation produces excess Fe_2O_3 . Indeed, the opaques in sample 70 have a reddish color, and appear to have been totally oxidized to hematite.

Other oxidation features include the opaque rims around crystals of biotite, amphibole, and pyroxene. These rims probably formed during the magma eruption, as rapidly exsolving gases oxidized the minerals.

Secondary silicification

Secondary silicification can be recognized by the tendency of silica to cut across and often obscure primary textures such as pyroclastic shards. Such silicification may result from fumarolic activity or from alteration by hydrothermal fluids. Fumarolic activity occurs when gradual compaction of the vesicular pyroclastic fragments releases vapor from which silica minerals crystallize (Cox et al., 1979). In the Valley of Ten Thousand smokes in southern Alaska, fumarolic release of gases from the pyroclastic units continued for ten years after their eruption from Mt. Katmai (Leet et al., 1978).

Silicification of the intracaldera rocks at Bonanza probably resulted from alteration by silicic hydrothermal fluids that flowed through fractures formed during caldera collapse (see Chapter 3). Causes for the secondary silicification observed in the upper Bonanza Tuff samples will be discussed in Chapter 7.

CHAPTER 5

GEO THERMOMETRY AND GEOBAROMETRY

Two-feldspar geothermometer

The possibility of using the distribution of albite between two coexisting feldspars to determine the equilibration temperatures of silicic igneous and metamorphic rocks was first suggested by Barth in 1934. Since that time Barth's empirical method has been modified by numerous workers (Barth, 1951, 1956, 1962; Orville, 1962; Iiyama, 1966; Perchuck and Ryabchikov, 1968; Seck, 1971; Stormer, 1975; Powell and Powell, 1977; Ferry, 1978; Brown and Parsons, 1981; Stormer and Whitney, 1985) in attempts to better constrain the feldspar solvus and to apply thermodynamic calculations to feldspar reaction relationships. The methods of Stormer (1975) and Brown and Parsons (1981) will be discussed in the following paragraphs, with most of the information being taken from these two references.

Stormer's (1975) method

The feldspar thermometer of Barth and later workers is based on the thermodynamic constraint that, at

equilibrium, the chemical potential of albite in the alkali feldspar phase (AF) and in the plagioclase feldspar phase (PF) must be equal:

$$\mu_{ab,AF} = \mu_{ab,PF} \quad (1)$$

Chemical potential, μ , can be thought of as the energy available to drive a chemical reaction, with each component in a phase contributing to the chemical potential of that phase. Because chemical potentials of complex phases are difficult to calculate, the chemical potential of the phase of interest must be related to a known chemical potential. Usually pure phases are chosen for the known, or standard state, chemical potential, because values for many pure phases have been tabulated by Robie and Waldbaum (1968) and Helgeson et al. (1978). Pure albite was chosen for the standard state in the two-feldspar reaction:

$$\mu_{ab,AF} = \mu_{ab,AF}^* + RT \ln a_{ab}^{AF} \quad (2)$$

$$\mu_{ab,PF} = \mu_{ab,PF}^* + RT \ln a_{ab}^{PF} \quad (3)$$

Here μ^* is the standard state chemical potential, and $RT \ln a$ corrects for any differences between the standard state chemical potential and the chemical potential of the phase of interest. R is the gas constant, T is temperature ($^{\circ}K$),

and "a" is the activity of the albite component. Activity is a function of the composition of the phase of interest, and reflects the interaction (repulsion and attraction) of unlike components within that phase.

Substituting equations (2) and (3) into equation (1) and rearranging produces:

$$\mu_{ab,PF}^* - \mu_{ab,AF}^* = RT \ln \left(\frac{a_{ab}^{AF}}{a_{ab}^{PF}} \right) \quad (4)$$

Because the standard state chemical potentials are both for pure albite and therefore are the same, subtracting them reduces equation (4) to:

$$0 = RT \ln \left(\frac{a_{ab}^{AF}}{a_{ab}^{PF}} \right) \quad (5)$$

Therefore:

$$\frac{a_{ab}^{AF}}{a_{ab}^{PF}} = 1 \quad (6)$$

and

$$a_{ab}^{AF} = a_{ab}^{PF} \quad (7)$$

If all atoms in the solutions interacted identically, both solutions would be ideal and the activity

of a component would be equal to X , the mole fraction of that component. However, Na atoms do not behave the same as Ca and K atoms in the plagioclase and alkali feldspar phases due to differences in atomic radii, valence, and charge density. Therefore, these are real solutions and activity becomes a complex function of composition (Fig. 32) expressed by:

$$a_{ab}^{AF} = \gamma_{ab}^{AF} X_{ab}^{AF} \quad ; \quad a_{ab}^{PF} = \gamma_{ab}^{PF} X_{ab}^{PF} \quad (8)$$

where γ is the activity coefficient that expresses the deviation from ideality. Obviously, $\gamma = 1$ for ideal solutions.

Substituting equation (8) back into equation (7) yields:

$$\gamma_{ab}^{AF} X_{ab}^{AF} = \gamma_{ab}^{PF} X_{ab}^{PF} \quad (9)$$

Rearranging equation (9) and writing it in terms of the distribution coefficient, K_D , produces:

$$K_{D_{ab}} = \gamma_{ab}^{PF} / \gamma_{ab}^{AF} = X_{ab}^{AF} / X_{ab}^{PF} \quad (10)$$

Experiments by Bowen (1928, p. 176) and Orville

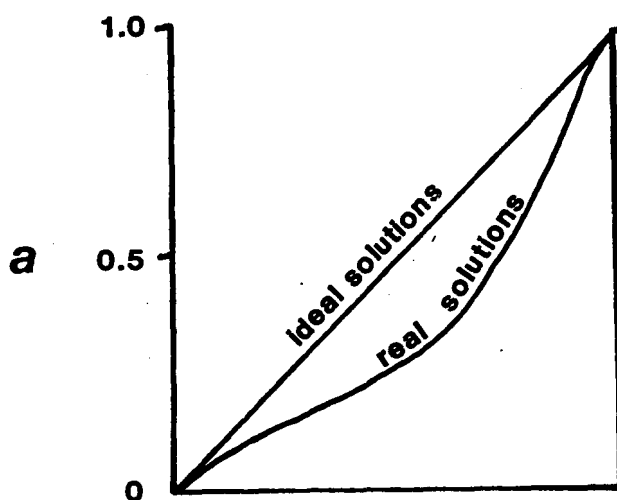


Fig. 32. Comparison of activity-composition relationships for real and ideal solutions (after Barton, personal communication, 1986).

(1972) indicate that the plagioclase series can be considered a nearly ideal solution at high temperatures over the composition range Ab_{100} to approximately Ab_{45} . However, the peristerite and other solvis (Fig. 33) prove that this ideality does not extend to low temperatures. Because nearly all plagioclase feldspars that coexist naturally with alkali feldspars are within the compositional range of Ab_{100} to Ab_{45} , it may be assumed that $\gamma_{ab,PF}$ has a value near one at high temperatures and at the pressures of most interest. Equation (10) then becomes:

$$K_{D_{ab}} = 1 / \gamma_{ab}^{AF} \quad (11)$$

To fully describe the activity coefficient for albite in alkali feldspar, Stormer selects the equation derived by Thompson and Waldbaum (1969a, 1969b) in the form of Margules parameters:

$$w_G^{ab} = 6326.7 + 0.0925P - 4.6321T \quad (12)$$

$$w_G^{Qr} = 7671.8 + 0.1121P - 3.8565T \quad (13)$$

Margules parameters, w_G , are equations that indicate the contribution of each component to the solution's deviation

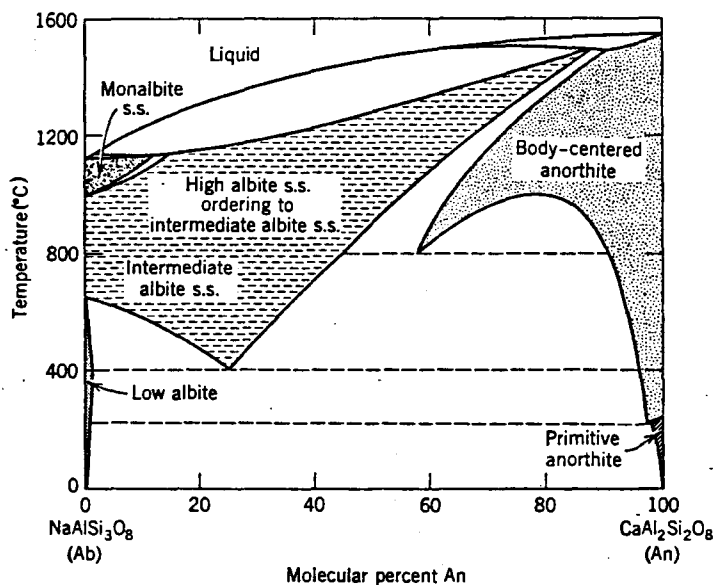


Fig. 33. Phase diagram for the Ab-An system showing regions of unmixing (after Hurlbut and Klein, 1977).

from ideality, and are obtained by mathematically fitting curves to experimental calorimetric and x-ray data. W_G depends on pressure and temperature, but not on composition (Nordstrom and Munoz, 1985).

The Margules parameters of Thompson and Waldbaum (1969) were developed from experimental work on binary plagioclase and alkali feldspar systems because the binary solvus is fairly well constrained at high temperatures. However, natural feldspars are actually ternary systems, with plagioclase feldspar containing small amounts of the potassium component and alkali feldspar containing minor amounts of the anorthite component. The models of both Barth and Stormer assume that the amounts are so small that the potassium and anorthite components have no effect on the plagioclase feldspar and the alkali feldspar, respectively. The work of Lewis and Randall (1961, ch. 34) supports this assumption by demonstrating that, as a component in a ternary system becomes very dilute, the activity coefficients of the remaining two major components will approach the values of the activity coefficients in the binary system. Therefore:

$$\gamma_{(ab, \text{ternary system})} = \gamma_{(ab, \text{binary system})} \quad (14)$$

and the binary Margules parameters of Thompson and Waldbaum

are indeed appropriate.

Using this approach, Stormer derived a formula for temperature as a function of composition of the coexisting feldspar pairs. First, Stormer took Thompson's (1967) equation which describes the activity coefficient in terms of Margules parameters:

$$RT \ln \gamma_{ab}^{AF} = \left(2W_G^{Ab} - W_G^{Or} \right) \left(X_{ab}^{Pf} \right) + 2 \left(W_G^{Or} - W_G^{Ab} \right) \left(X_{ab}^{PF} \right)^3 \quad (15)$$

and simplified it to:

$$\ln \gamma_{ab}^{AF} = \left(1/RT \right) \left[\left(1 - X_{ab}^{AF} \right)^2 \left[W_G^{Ab} - 2X_{ab}^{AF} \left(W_G^{Or} - W_G^{Ab} \right) \right] \right] \quad (16)$$

He then combined it with the natural logarithmic form of equation (11):

$$\ln K_{D_{ab}} = \ln \left(1/\gamma_{ab}^{AF} \right) = -\ln \gamma_{ab}^{AF} = - \left(1/RT \right) \left[\left(1 - X_{ab}^{AF} \right)^2 \left[W_G^{Ab} - 2X_{ab}^{AF} \left(W_G^{Or} - W_G^{Ab} \right) \right] \right] \quad (17)$$

By substituting equations (12) and (13) for W_G and solving for T, Stormer produced the final geothermometry equation:

$$\begin{aligned}
T \left(^\circ \text{K} \right) = & \left\{ 6326.7 - 9963.2 \left(X_{ab}^{AF} \right) + 943.3 \left(X_{ab}^{AF} \right)^2 + \right. \\
& 2690.2 \left(X_{ab}^{AF} \right)^3 + \left[0.0925 - 0.1458 \left(X_{ab}^{AF} \right) + 0.0141 \left(X_{ab}^{AF} \right)^2 + \right. \\
& \left. \left. 0.0392 \left(X_{ab}^{AF} \right)^3 \right] P \right\} / \left[4.6321 - 10.815 \left(X_{ab}^{AF} \right) + \right. \\
& \left. 7.7345 \left(X_{ab}^{AF} \right)^2 - 1.5512 \left(X_{ab}^{AF} \right)^3 - 1.9872 \ln \left(X_{ab}^{AF} / X_{ab}^{PF} \right) \right]
\end{aligned}
\tag{18}$$

Stormer was the first to note that T is a function of P as well as a function of the mole fraction of albite in the coexisting feldspar phases.

Brown and Parson's (1981) method

Brown and Parsons (1981) pointed out the need to be sure that the feldspar pairs used for calculations are in equilibrium. Otherwise, the previously presented thermodynamic basis for the thermometer does not apply, and the resulting temperatures are meaningless.

Brown and Parsons also emphasized the great effect that Al-Si framework order has on the feldspar geothermometer. Indeed, the temperatures calculated from completely ordered and completely disordered feldspar pairs can vary as much as 150°C. Researchers are still uncertain as to which state of order is the most realistic to use for calculations of natural feldspars in igneous rocks; however, disorder seems to be the likely assumption because experimental data show that synthetic feldspars begin growing in a highly disordered state and later become

ordered (MacKenzie, 1957). Stormer's (1975) thermometer assumed Al-Si disorder.

To improve the accuracy of Stormer's thermometer, Brown and Parsons revised the Margules parameters for feldspar activity, using the most recent experimental data defining the binary solvus. Substitution of these new parameters:

$$w_G^{Ab} = 2890 + 0.079P - 0.58T \quad (19)$$

$$w_G^{Or} = 6100 + 0.168P - 2.29T \quad (20)$$

into Stormer's (1975) equation yields the revised temperature equation (Barton personal communication, 1986):

$$T^{\circ}K = \left\{ 2890 + 640 \left[X_{ab}^{AF} \right] - 9950 \left[X_{ab}^{AF} \right]^2 + 6420 \left[X_{ab}^{AF} \right]^3 + \left[0.02 \left[X_{ab}^{AF} \right] = 0.079 - 0.277 \left[X_{ab}^{AF} \right]^2 + 0.178 \left[X_{ab}^{AF} \right]^3 \right] P \right\} / \left\{ 0.58 - 4.0 \left[X_{ab}^{AF} \right]^2 + 3.42 \left[X_{ab}^{AF} \right]^3 - 1.9872 \ln \left[\left[X_{ab}^{AF} \right] / \left[X_{ab}^{PF} \right] \right] \right\}$$

However, Brown and Parsons questioned whether the temperatures calculated in this way would be very accurate, because the revised parameters still describe the properties of a binary system. Brown and Parson's foremost criticism of earlier geothermometers was that it is inaccurate to assume that ternary feldspars can be

adequately treated as two binary systems.

To ignore the effects of K and Ca in plagioclase and alkali feldspar, respectively, the solubility of the minor component must be nearly the same at all compositions in the binary system. However, as shown by Seck's (1971) ternary experimental data, the amount of An changes greatly with the Ab:Or ratio in alkali feldspars. Thus, Seck (1971) showed that the minor components cannot be ignored and that the feldspars should be treated as a ternary system. Stormer's assumption that the effect of the minor components is negligible is only true in the presence of less than two to three percent of these components; however, at such a composition and at an average magma temperature of 750°C, only one phase of feldspar would exist and so the thermometer could not be used.

Brown and Parsons and Stormer and Whitney (1985) agree that the most accurate two-feldspar thermometer available at this time is a graphical version based on ternary experimental data by Seck (1971) and presented by Brown and Parsons (1981, p.372) (Fig. 34). Unfortunately, Seck's data was not of sufficient quantity to adequately define the ternary solvus at high temperatures. Therefore, ternary Margules parameters cannot be calculated from Seck's work to derive a ternary feldspar geothermometry formula at this time.

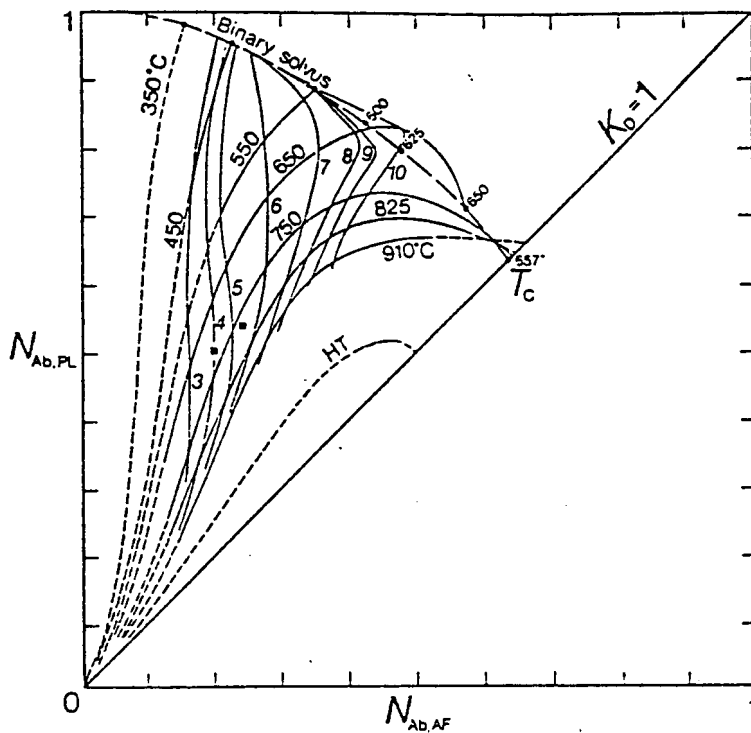


Fig. 34. Graphical two-feldspar thermometer based on the experimental data of Seck (1971) (after Brown and Parsons, 1981, p. 372).

Accuracy of the two-feldspar geothermometer

Despite concern that the two-feldspar thermometers may be based on incorrect assumptions (i.e. that ternary feldspars can be treated as two binary systems), they do seem to give reasonable results. Stormer and Whitney (1985) believe that Stormer's (1975) geothermometer is probably accurate within 30 to 50°C for intermediate feldspar compositions, but is unsuitable for plagioclase crystals with very high Na, K, or An contents.

Seck's (1971) graphical thermometer gives temperatures that are more reliable; it is accurate within ± 20 to 30°C for compositions of less than 40 mol percent albite in sanidine and less than 50 mol percent albite in plagioclase (Stormer and Whitney, 1985).

Brown and Parson's (1981) thermometer also gives results that seem to be roughly correct. Stormer and Whitney (1985) calculated the temperature of metamorphism for some granulites in an area where independent mineral control gave temperature and pressure estimates of 750-800°C at four to eight kilobars. Using Brown and Parson's (1981) feldspar geothermometer, they calculated feldspar temperatures of 770°C at six kilobars pressure. Bohlen and Essene (1977) also found good agreement between two-feldspar and Fe-Ti oxide temperatures for granulites in the Adirondack Mountains at an independently estimated pressure of eight kilobars.

Application to the Bonanza volcanics

The two feldspar thermometer is applicable for only a small number of the Bonanza samples, because only coexisting feldspars in samples #14 and 18 were analyzed. Feldspar pairs to be used as thermometers were first tested according to the guidelines of Brown and Parsons (1981, p. 374) to make sure that they were in equilibrium. None of the extremely albitic feldspars were in equilibrium with sanidine, supplying further proof of their xenocrystal origin. Compositions of the equilibrium feldspar pairs were then used to calculate the temperatures reported in Table 1. Feldspar pair number two of sample #14 probably gives the most reliable temperature estimate, because the orientation of the tie-lines between this pair most closely matches the orientation of Seck's (1971) experimentally-determined equilibrium tie-lines. The graphical thermometer based on Seck's experimental work (Brown and Parsons, 1981) could not be employed because the temperatures of the Bonanza magma exceed those for which the thermometer is appropriate.

Because the position of the feldspar solvus is pressure-dependent, an independent estimate of temperature is needed in addition to the two feldspar data to pinpoint the pressure of equilibration. Unfortunately, neither the widely-used two pyroxene thermometer (Lindsley, 1964; Wood

Table 1. Temperatures of feldspar equilibration with magma for samples from the lower and upper Bonanza Tuff. Temperatures were obtained using the two-feldspar thermometer of Brown and Parson's (1981).

Sample #14 - Tbl

Pressure (kb)	Feldspar pair #1 Temp. (C)	Feldspar pair #2 Temp. (C)	Feldspar pair #3 Temp. (C)
1	1029	973	1087
2	1047	991	1105
3	1065	1009	1123
4	1083	1027	1141
5	1101	1045	1159
6	1119	1063	1177
7	1137	1081	1195
8	1155	1099	1213
9	1173	1117	1231
10	1191	1135	1249

Sample #18 - Tbu

Pressure (kb)	Feldspar pair #1 Temp. (C)	Feldspar pair #2 Temp. (C)	Feldspar pair #3 Temp. (C)
1	1115	1048	1025
2	1133	1066	1043
3	1151	1084	1061
4	1169	1102	1079
5	1187	1120	1097
6	1205	1138	1115
7	1223	1156	1133
8	1241	1174	1151
9	1259	1192	1169
10	1277	1210	1187

and Banno, 1973; Wells, 1977) nor the two oxide thermometer/barometer (Buddington and Lindsley, 1964; Spencer and Lindsley, 1981) can be applied to the Bonanza units because they contain only one pyroxene phase and only one type of oxide. Exsolution lamellae of ilmenite are present in the grains of titanomagnetite, but these lamellae cannot be used for pre-eruption magma thermometry because they formed by subsolidus oxidation. Therefore, alternative methods must be employed.

Biotite thermometer

I.S.E. Carmichael formulated an empirical biotite thermometer (Luhr et al., 1984, p. 93) from which an independent magma temperature can be estimated. Carmichael hypothesized that in silicic volcanics, the Ti/Fe^{2+} ratio of biotites is largely a function of temperature. By examining biotites from rocks with known Fe-Ti oxide temperatures, Carmichael was able to relate the Ti/Fe^{2+} ratio in biotites and the temperature of formation by this equation:

$$T(^{\circ}K) = 838 / (1.0337 - Ti/Fe^{2+}) \quad (22)$$

The accuracy of this thermometer and its general applicability are difficult to determine; however,

Carmichael applied the thermometer to pyroclastic deposits of the El Chichon Volcano in Chiapas, Mexico, and obtained a temperature that was equivalent (within the range of analytical error) to the temperature determined by stable isotopes. The chemistry of the El Chichon pyroclastics is similar to that of the Bonanza tuffs, so that application of this thermometer to the Bonanza units seems reasonable.

Application

In order to get an accurate temperature of the pre-eruption magma, only biotites that are in equilibrium with the liquid should be analyzed. However, equilibrium with the Bonanza liquid is not easily discerned. G.P. Walker (1972) conducted a study of several pyroclastic flows, and in every case found that ignimbrites have a greater phenocryst/glass ratio than pumices from the same sample. Walker concluded that much of the fine glass is lost from an ash flow during the eruptive process, both in the column above the source vent and from the top of the moving flow. This winnowed glass is often deposited as fine ash in association with the flow, although sometimes as far as 2000 km away (Sparks and Walker, 1977).

The net result of this eruptive winnowing process is that elements that are preferentially concentrated in the melt (SiO_2 , Na_2O , K_2O , and incompatible trace elements) are lost during the eruption and deposition of the major

part of the flow. In fact, Sparks and Walker (1977) estimate that as much as 25 to 50 percent of the original magma is lost as fine vitric material, with a mean minimum loss of 35 percent. Thus, the whole-rock composition no longer is equal to the original liquid composition; it is much less evolved than the actual original magma. For this reason, only biotites that were in equilibrium with the whole-rock composition or a more evolved liquid were used for temperature calculations. To fit this criterion, the equilibrium relationships of biotite and liquid were calculated according to the relationship of the mole fraction of Mg in the biotite (x_{Mg}^{bi}) to the mole fraction of Mg in the whole-rock ($x_{Mg}^{W/R}$) given by Barton and Wyers (1986). Biotites that were in equilibrium with a less evolved liquid gave ridiculously high temperatures. These more mafic biotites are perhaps present due to magma mixing.

Assuming that the Bonanza biotites contain no Fe^{3+} , the temperatures shown in Table 2 are obtained. The absence of ferric iron is a reasonable assumption, because biotites generally have an FeO/Fe_2O_3 ratio of 20/1 (Deer et al., 1978, p.199). Even if ferric iron is present, the thermometer will still provide useful information by giving a minimum temperature for equilibration of biotite with the magma. Note that temperatures decrease with increasing stratigraphic height. This thermal zonation is consistent

Table 2. Temperatures of biotite equilibration with magma for representative samples from the lower and upper Bonanza Tuff, obtained using Carmichael's biotite thermometer.

Sample #	point #	Ti/Fe (afu)	T(K)	T(C)
18	5	.3174	1170	897
	6	.2169	1026	753
	7	.2258	1037	764
	8	.2426	1059	786
14	9	.3705	1264	990
	10	.3909	1303	1031
	11	.2996	1282	1009
9	17	.5062	1589	1315
	18	.5296	1662	1389
	19	.5078	1594	1320

with the mineralogic evidence of magmas becoming more evolved upsection, but it is the opposite of what one would expect for an eruption from a zoned magma chamber (Hildreth, 1981). Also, note that the temperatures obtained for sample #9 seem unreasonably high compared to the measured eruption temperatures of 1050 to 1100°C for magmas of intermediate composition (Gill, 1981). It appears that the biotite thermometer becomes less reliable for less evolved magma compositions.

Biotite temperatures for sample #14 were averaged to obtain a mean temperature of 1010°C. This value was then compared to the feldspar temperatures for the same sample (Fig. 35), revealing that the magma chamber equilibrated at a pressure of approximately 3.1 kb, or at an equivalent depth of 9.3 km. This depth is fairly shallow compared to the estimated 24 km depth of the Fish Canyon Tuff magma chamber (Stormer and Whitney, 1985) and the total crustal thickness in this region of approximately 50 km (Plouff and Pakiser, 1972). Biotite temperatures for sample #18 were too low to compare to the corresponding feldspar temperatures, perhaps indicating that the biotites in this sample are not in equilibrium with the feldspars.

Determination of water content

Kudo and Weill (1970) developed a plagioclase-liquid thermometer based on more than 90 experimental analyses of

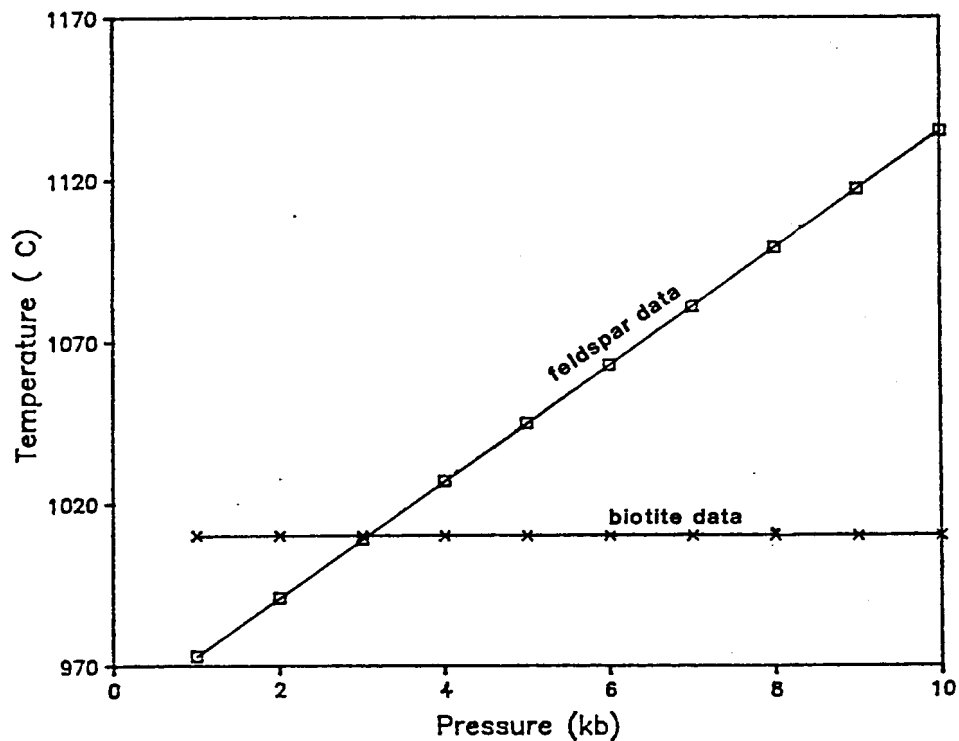


Fig. 35. Comparison of the biotite temperature compared to the pressure-dependent feldspar temperature obtained for lower Bonanza Tuff sample #14. The intersection point at 3.1 kb indicates the pressure at which these minerals equilibrated with the magma.

natural granites. If the composition of plagioclase-liquid equilibrium pairs are known, temperatures can be determined by solving an empirical formula. Water dissolved in the melt lowers both the solidus and the liquidus of the Ab-An system (see Fig. 31), so that there are different formulae for different water pressures. Consequently, if the compositions of the equilibrium pairs and the temperature of the magma are known, the water content of the magma can be determined.

Glass compositions can be considered together with the rims of the plagioclase crystals to calculate the equilibrium conditions for the final magma after some crystallization has occurred, or plagioclase cores can be compared to the whole-rock composition to find the equilibrium conditions of the magma as plagioclase crystallization began. Unfortunately, glass compositions were not analyzed during this study; it is likely that even if the glass had been analyzed, the results would have been erroneous due to alteration (see discussion in Chapter 7). Whole-rock compositions of the ash flows were analyzed, although winnowing probably resulted in whole-rock compositions that are more An-rich than the original magma. None-the-less, these whole-rock compositions can be used to at least determine a minimum water content for the Bonanza units.

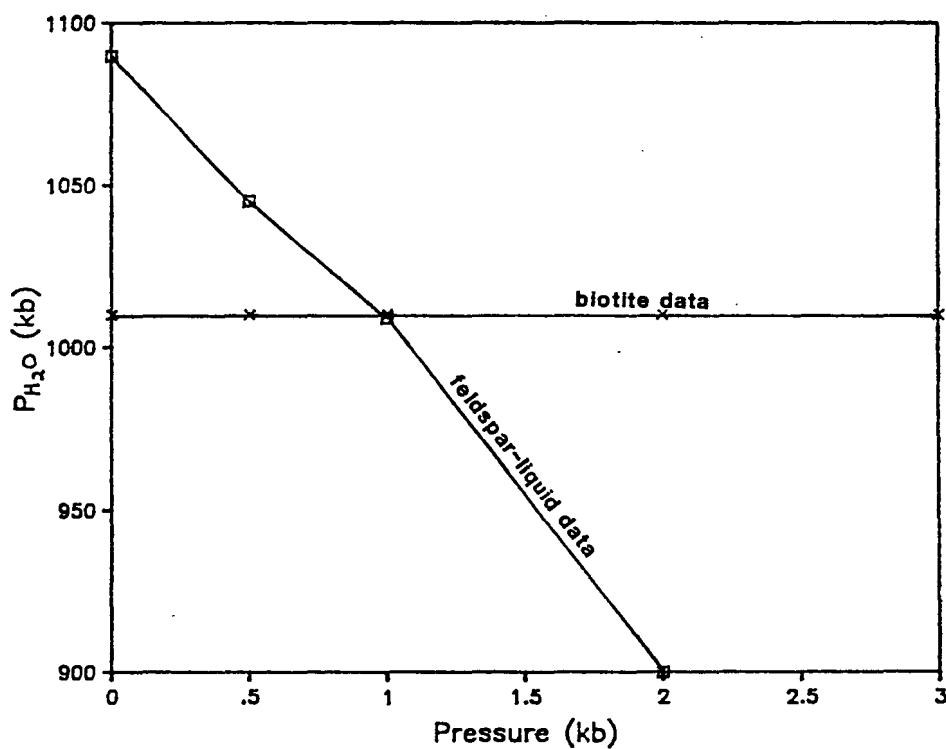


Fig. 36. Comparison of the biotite temperature to the P_{H_2O} -dependent feldspar temperature obtained for lower Bonanza Tuff sample #14. The intersection point at .09 kb indicates the minimum water pressure at which the minerals equilibrated with the magma.

Results of the Kudo and Weill thermometer are presented in Figure 36. The resulting minimum water pressure is approximately 0.9 kb at the calculated biotite temperature. The pressures obtained by this method compared to the total pressures derived from the two-feldspar thermometer suggest that water pressure is less than total pressure, and therefore the magma was water-undersaturated. Fluorine also existed as a vapor phase (probably as HF), as is evidenced by the high fluorine content of the biotite phenocrysts.

CHAPTER 6
WHOLE-ROCK CHEMISTRY

Introduction

The twenty samples that were examined petrographically were also analyzed for whole-rock major and trace elements using x-ray fluorescence (XRF) by J.P.P. Huijsmans at the State University of Utrecht, The Netherlands. The techniques and estimates of analytical uncertainty are given by Huijsmans (1985). Results of the whole-rock major element analyses are presented in Table 3. Concentrations have been normalized to 100 and calculated on a water-free basis. CIPW norms are given in Table 4. Fe^{3+} contents for the calculation of the norms were determined assuming an $\text{Fe}_2\text{O}_3/\text{FeO}$ ratio of 0.20.

Major element chemistry

The whole-rock analyses are plotted on an AFM diagram in Fig. 37. According to Irvine and Baragar's classification (1971, Fig. 2), the Bonanza volcanics are calc-alkaline and show the characteristic lack of iron-enrichment. Silica oversaturation is indicated by normative quartz and hypersthene (see Table 4), except for sample #18 (Tbu from Findley Ridge) which is not hypersthene normative, but

Table 3. Whole-rock major element chemistry for the Bonanza volcanic units.

MAJORS

sample #	SiO2	TiO2	Al2O3	FeO	MnO	MgO	CaO	Na2O	K2O	P2O5
Findley Ridge										
19	65.20	.70	16.27	3.92	.11	.74	3.93	3.79	5.15	.19
18	62.33	.39	14.67	1.89	.06	.40	10.45	3.94	5.81	.06
16	64.12	.76	17.57	4.31	.07	.82	3.20	3.61	5.34	.20
14	62.80	.77	17.97	4.03	.08	1.08	3.21	4.15	5.66	.24
13	63.93	.82	17.56	4.22	.07	.75	3.31	3.83	5.29	.22
12	67.06	.70	16.54	3.20	.06	.79	2.23	3.65	5.64	.12
11	67.22	.69	15.56	3.11	.07	.76	3.13	3.69	5.62	.14
10	61.33	.76	18.20	4.02	.06	.99	5.37	3.80	4.76	.26
9	62.28	.77	18.18	4.07	.09	1.57	4.49	3.46	4.47	.17
8	64.30	.82	17.58	4.21	.06	.77	4.00	3.85	4.23	.18
Dry Gulch										
34	61.19	.88	17.04	5.46	.10	2.44	4.59	4.00	4.04	.25
29	76.67	.18	11.88	1.06	.07	.30	1.14	3.64	5.04	.02
71	79.68	.17	10.86	1.00	.05	.03	.40	3.20	4.61	.00
70	63.90	.78	18.01	3.54	.04	.85	2.60	3.71	5.92	.26
28	63.62	.76	17.47	4.00	.06	1.02	3.10	3.79	5.46	.28
30	77.02	.22	12.16	1.18	.07	.07	.70	3.55	5.02	.00
Elkhorn Gulch										
42	70.89	.48	14.58	2.74	.09	.77	1.98	2.40	5.51	.06
46	70.39	.48	14.45	2.92	.11	.83	1.85	2.91	5.66	.07
49	63.84	.78	17.58	4.38	.14	1.34	2.63	3.37	5.19	.26
75	52.85	1.57	17.57	8.31	.18	3.01	8.82	2.56	3.70	.51

Table 4. CIPW norms for the Bonanza volcanics.

Sample #	Qtz	Or	Ab	An	Di	Hy	Ht	Ilm	Ap	Cor	Wo
34.00	7.90	23.85	33.81	16.59	3.75	10.28	1.57	1.67	.59	---	---
19.00	13.79	30.41	32.04	12.16	5.18	3.52	1.13	1.33	.45	---	---
18.00	3.43	34.32	33.33	5.18	5.92	---	.55	.74	.14	---	16.39
16.00	13.25	31.61	30.59	14.59	---	6.29	1.25	1.45	.47	.51	---
14.00	7.37	33.43	35.09	13.68	.57	6.69	1.16	1.46	.56	---	---
13.00	11.78	31.24	32.38	14.97	---	6.31	1.22	1.56	.52	.04	---
12.00	17.13	33.32	30.87	10.27	---	5.22	.92	1.33	.28	.66	---
11.00	16.49	33.20	31.21	9.29	4.48	2.80	.89	1.31	.33	---	---
10.00	8.23	28.24	32.27	18.61	5.41	4.02	1.16	1.45	.62	---	---
9.00	11.68	26.52	29.34	20.95	.25	8.18	1.18	1.47	.40	---	---
8.00	14.58	24.98	32.55	18.18	.41	6.12	1.21	1.56	.43	---	---
75.00	1.02	22.03	21.83	25.71	12.50	10.30	2.42	3.00	1.22	---	---

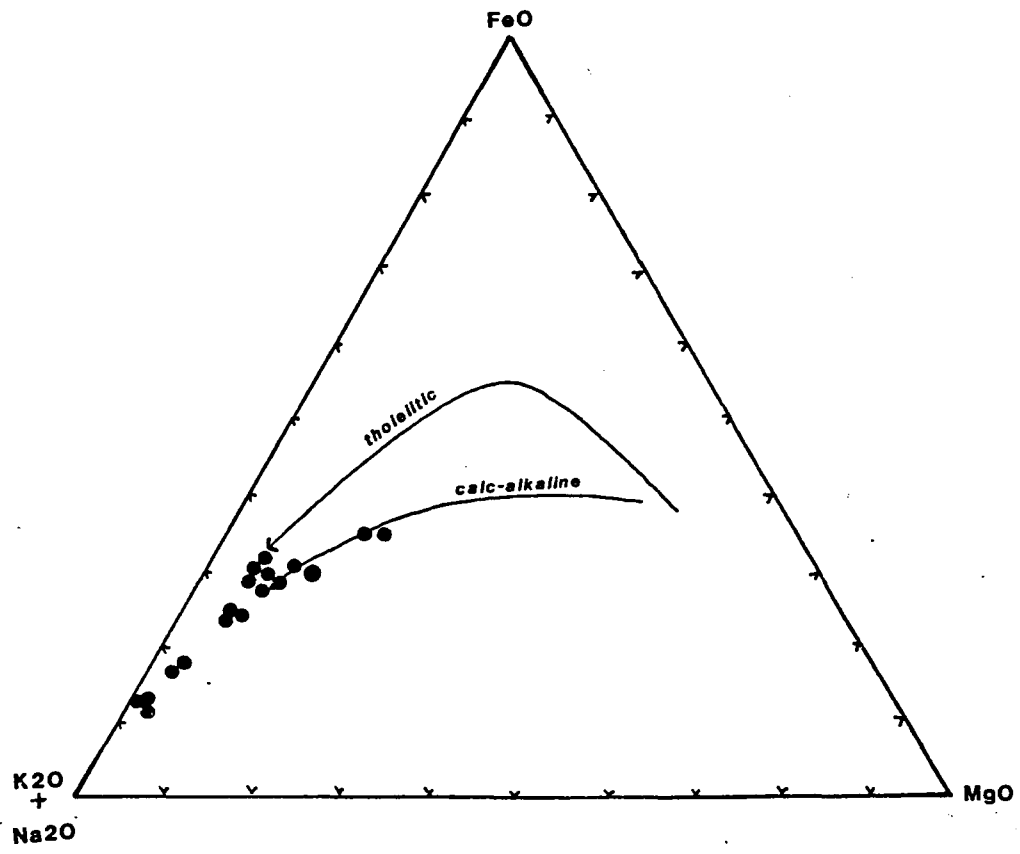


Fig. 37. AFM diagram of major element chemistry. Typical tholeiitic and calc-alkaline trends are indicated

contains normative wollastonite. Several samples contain normative corundum and hence are peraluminous.

Alteration

Samples #29 and #30 of Table 3 are not considered in further detail, as they show noticeable secondary silicification of the groundmass when viewed in thin section. Samples #42, 46, and 71 also have anomalously high silica contents compared with other samples, and the greenish color and abundance of chlorite in the first two samples (Tb1 from within the caldera) indicate hydrothermal alteration. Sample #18 has an unusually high CaO content, as might be expected (n.b. normative wollastonite), and petrographic examination of sample #18 reveals that the rock matrix has been somewhat altered to clay. Montmorillonite and beidellite commonly form through alteration of tuffs and volcanic ash (Deer, et al., 1978), and the presence of these clays would explain the observed high CaO content, although the sample is not particularly Al_2O_3 -rich. Samples #49 (Tb1) and #75 (Ra) are not anomalous chemically, but the highly altered appearance of #75 in thin section and the evidence of hydrothermal alteration in #49 (see Chapter 4) suggest that the chemistry of these two units may have been affected by post-depositional processes and thus should be interpreted with caution.

K₂O contents compared

Because the Bonanza rocks plot near the alkali endmember on the AFM diagram (Fig. 37), Figure 38 is used to compare the K₂O and SiO₂ contents of the Bonanza units with the averaged compositions of sialic volcanics from island arcs and orogenic continental margins of various geographic regions (compiled by Ewart, 1979). The Bonanza units have markedly higher K₂O contents than most subduction-associated volcanics, including the volcanics of the western U.S. and western South America.

Instead, the Bonanza volcanics are more similar chemically to the potash trachyte series. If one considers the dashed part of the Bonanza series data that corresponds with units which are suspected to be altered, both the Bonanza rocks and the potash trachytes have K₂O contents that peak and then decline with greater SiO₂ content. Finally, the potassium content of the volcanics in the U.S increases inland from the western belt through the eastern belt towards the Bonanza region. This variation of potassium content with geography is a well-documented phenomenon thought to be related to subduction, and is corellated to the increasing depth to the Benioff zone with increasing distance from the trench (Dickinson, 1968, 1970).

Variation diagrams

Major element data plotted as Harker variation diagrams are seen in Figure 39. Samples that appear to have undergone

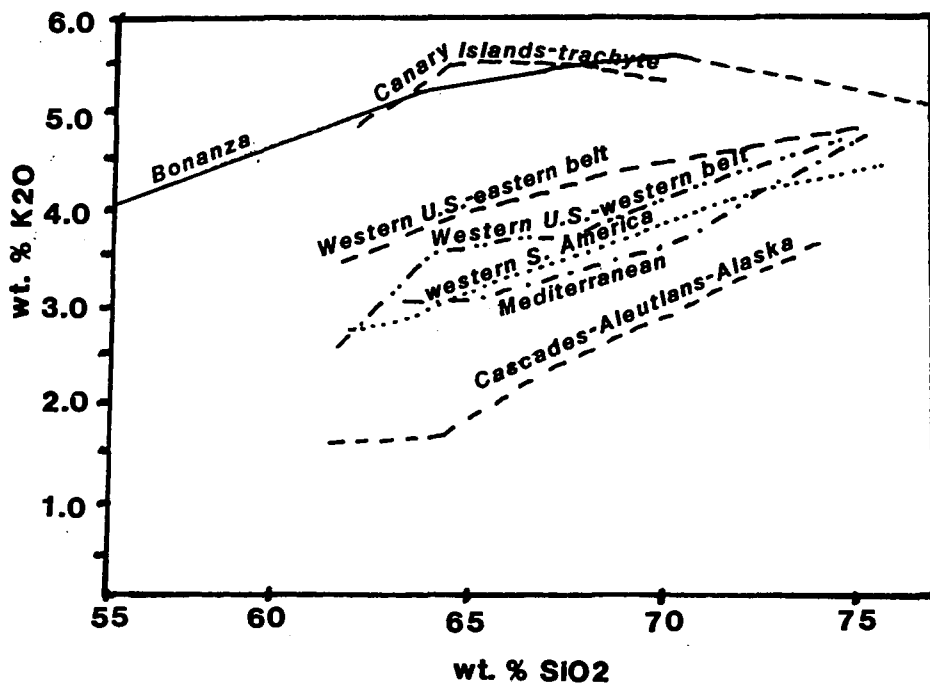


Fig. 38. Variation diagram comparing the K₂O and SiO₂ contents of the Bonanza units to average data for silicic volcanic suites from various geographic regions (modified from Ewart, 1979).

secondary silicification have been omitted. Although sample 18 does appear to be anomalous for most elements, it is included because its chemistry will be discussed in later sections. Scatter in the other data points may be due to:

- 1) The phyric nature of the units, so that the samples do not represent strictly a liquid-line-of-descent;
- 2) The presence of lithic inclusions within the tuffs so that whole-rock chemistry varies with the proportions of lithic fragments;
- 3) Different amounts of winnowing of vitric materials during the eruptive process;
- 4) Cyclic fractionation and magma mixing processes which do not occur in exactly the same way every time;
- 5) Alteration of the samples by meteoric or hydrothermal fluids.

The trends observed on the Harker variation diagrams are typical for chemical changes caused by fractional crystallization processes. CaO and MgO contents both decrease with increasing SiO₂ until 64 wt. % SiO₂, and then level out at 3.0 and .75 wt. percent, respectively. FeO and TiO₂ are constant until 64 wt. % SiO₂, and then begin to decrease. Al₂O₃, Na₂O, and P₂O₅ all tend to decrease with increasing silica, while K₂O, although widely scattered, seems to increase on average with increasing silica. MnO also seems to show a lot of scatter, but the dispersion of data for this element is really over less than 0.1 wt. percent so that the scatter is not significant. Note that sample #75 (Ra) is quite different in chemistry from the

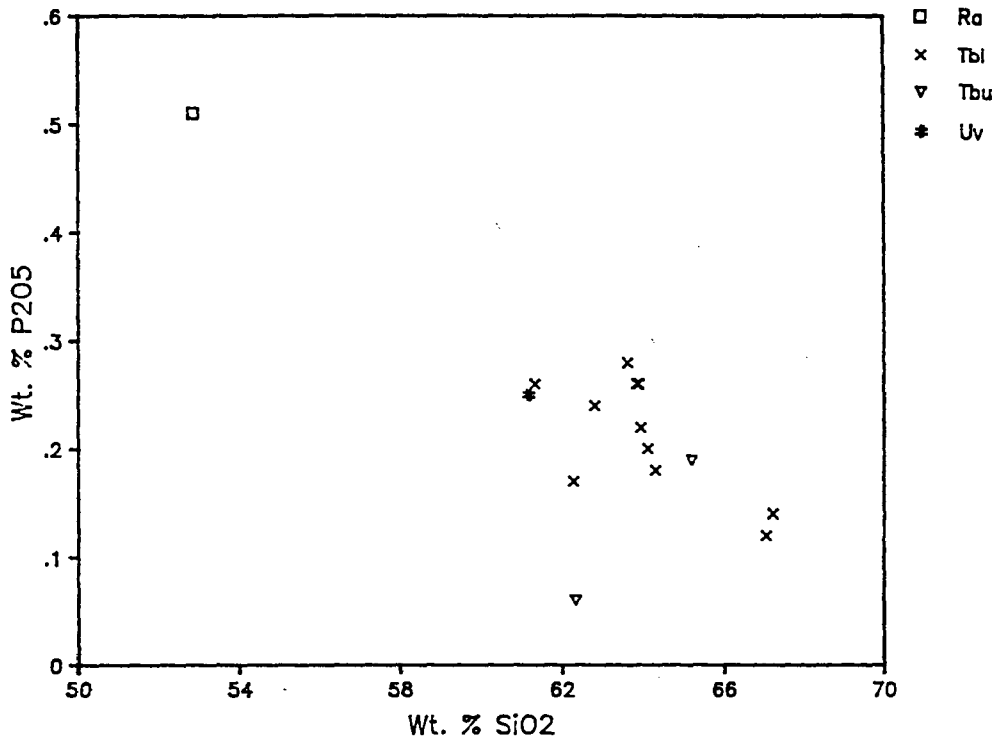
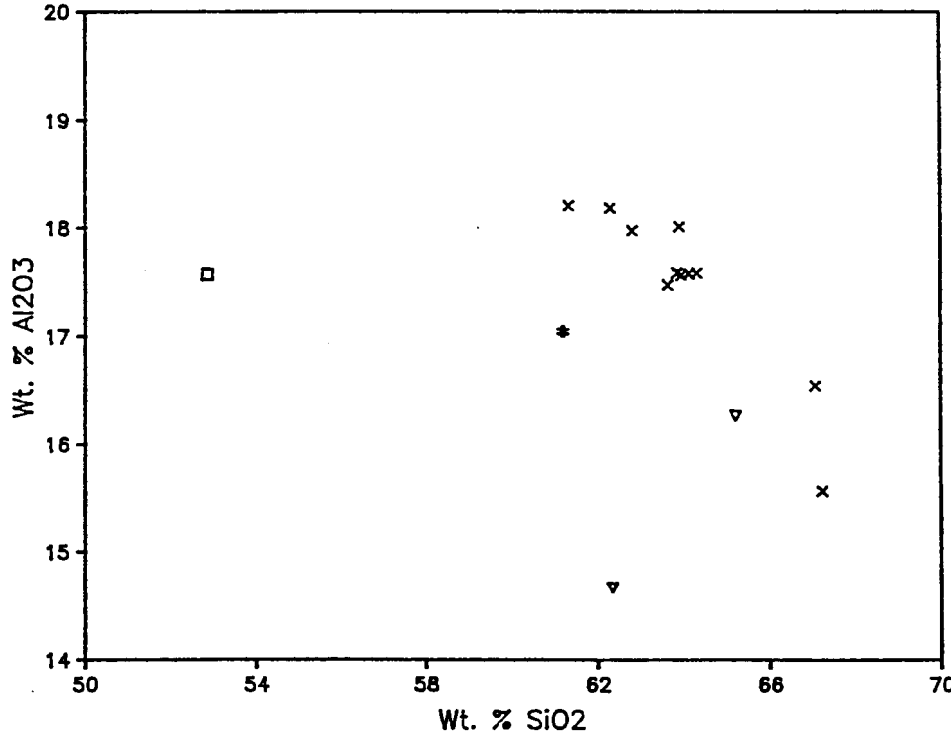
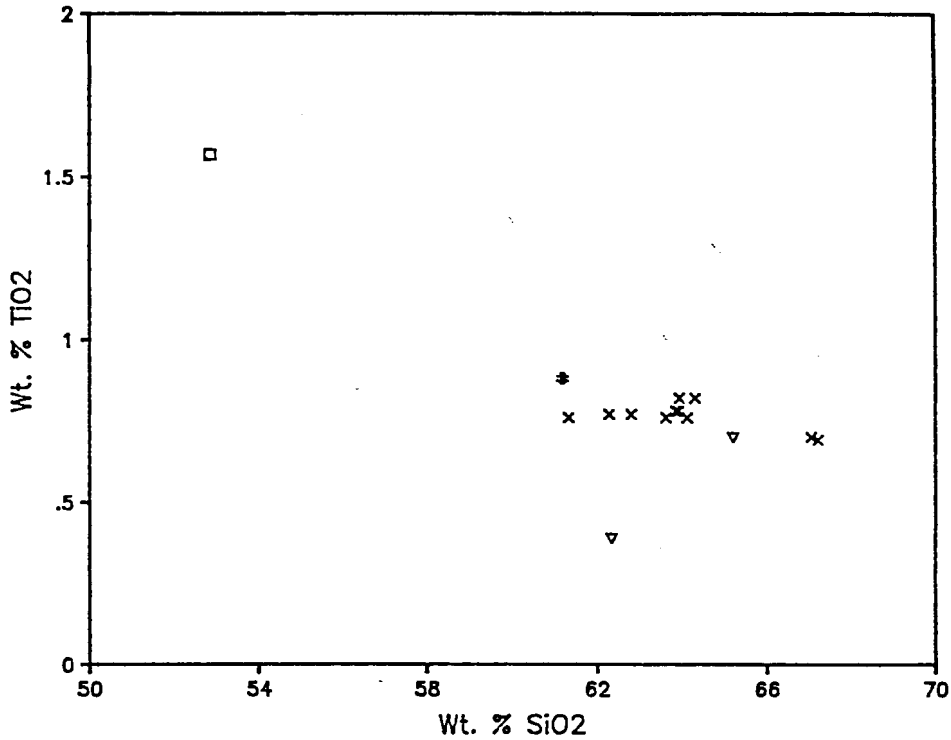
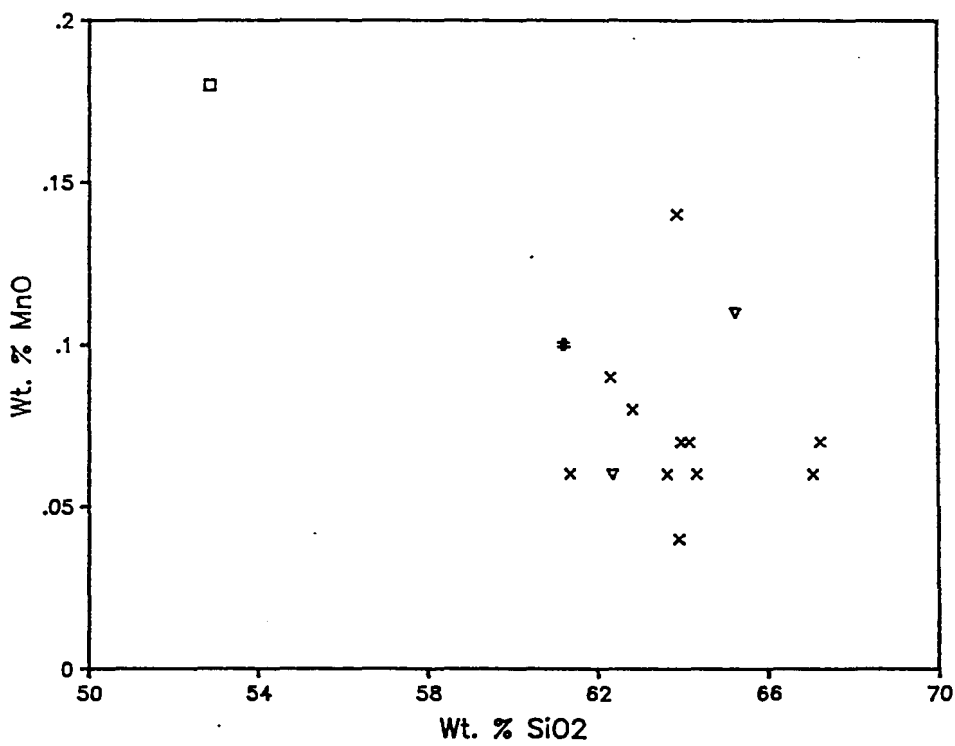
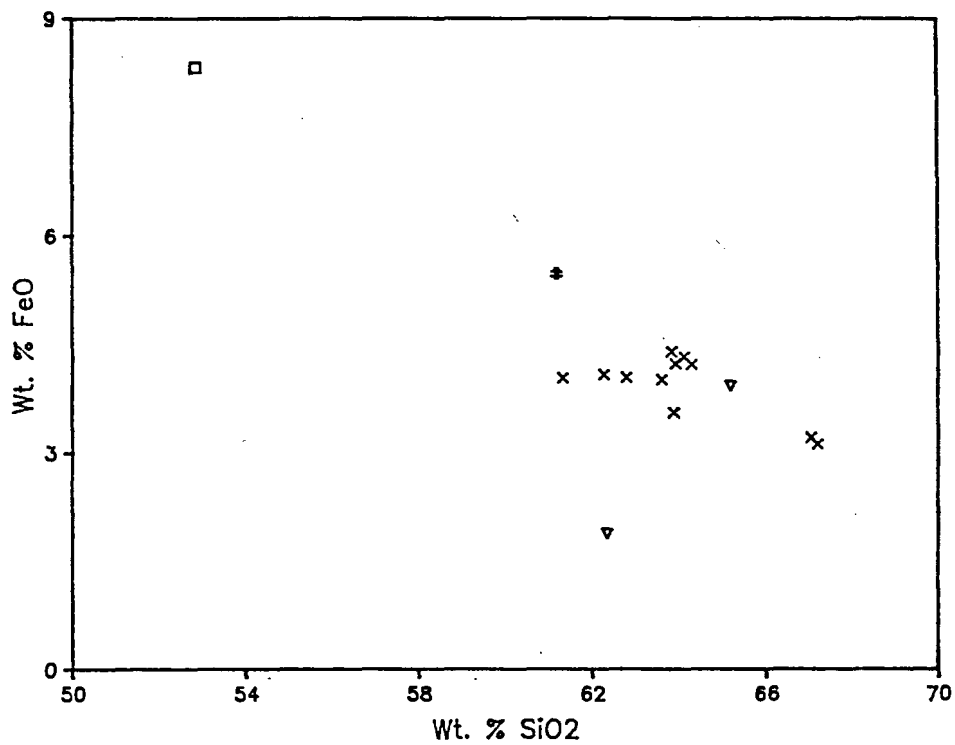
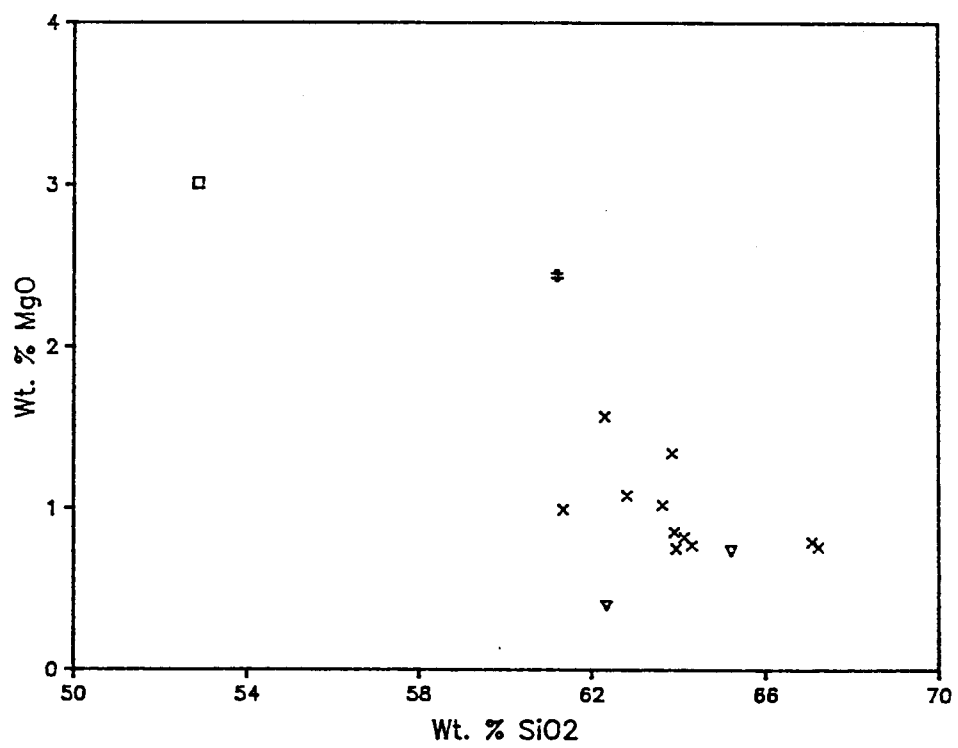
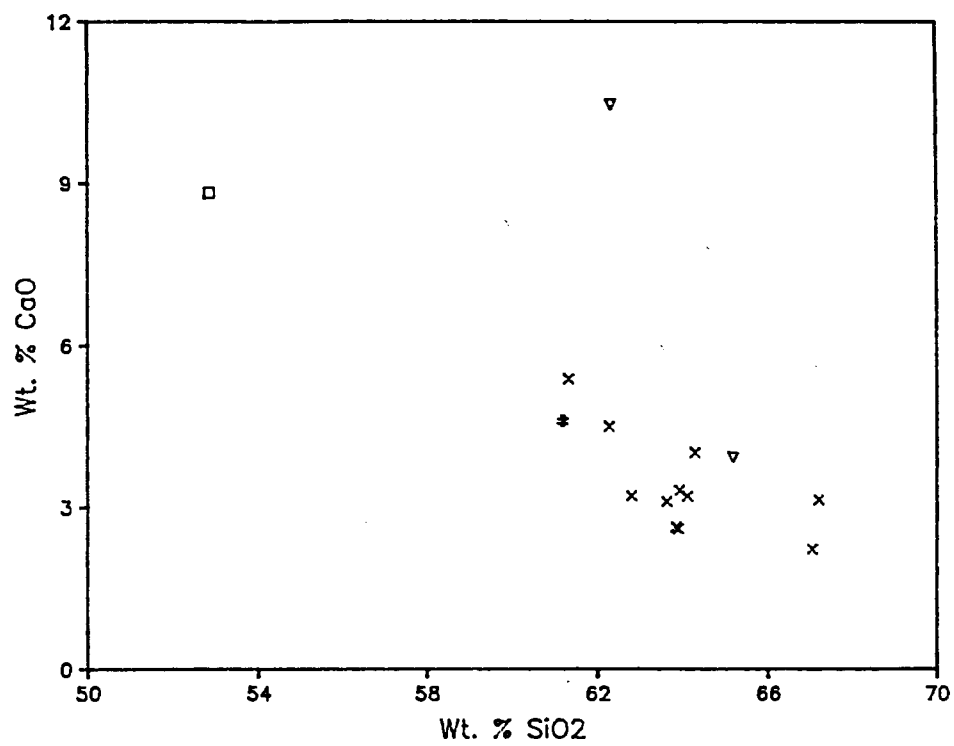
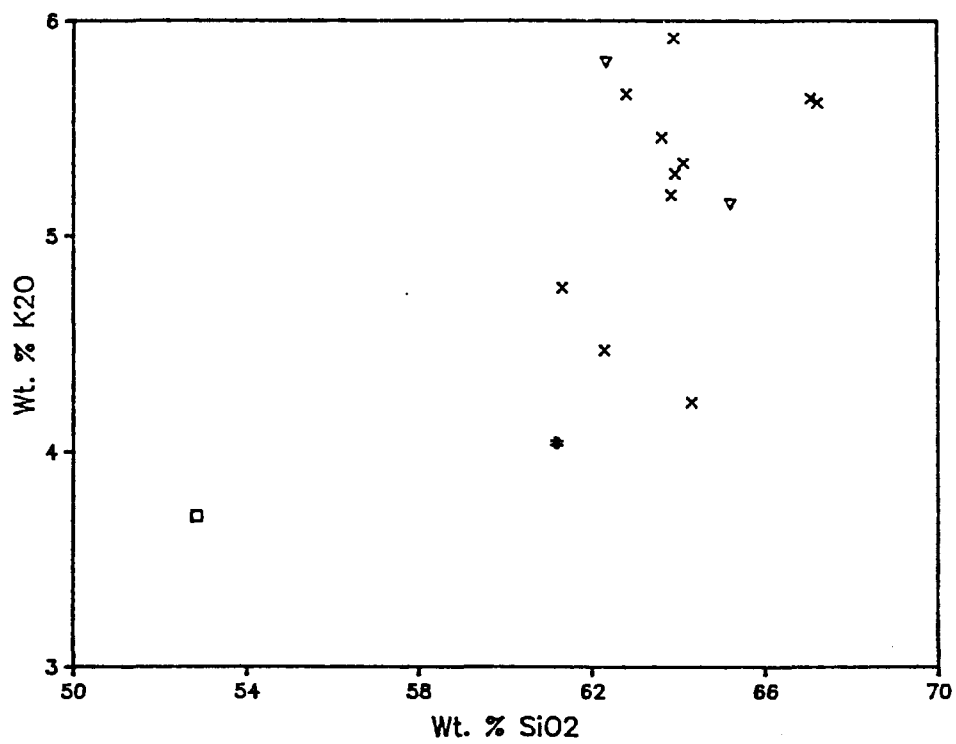
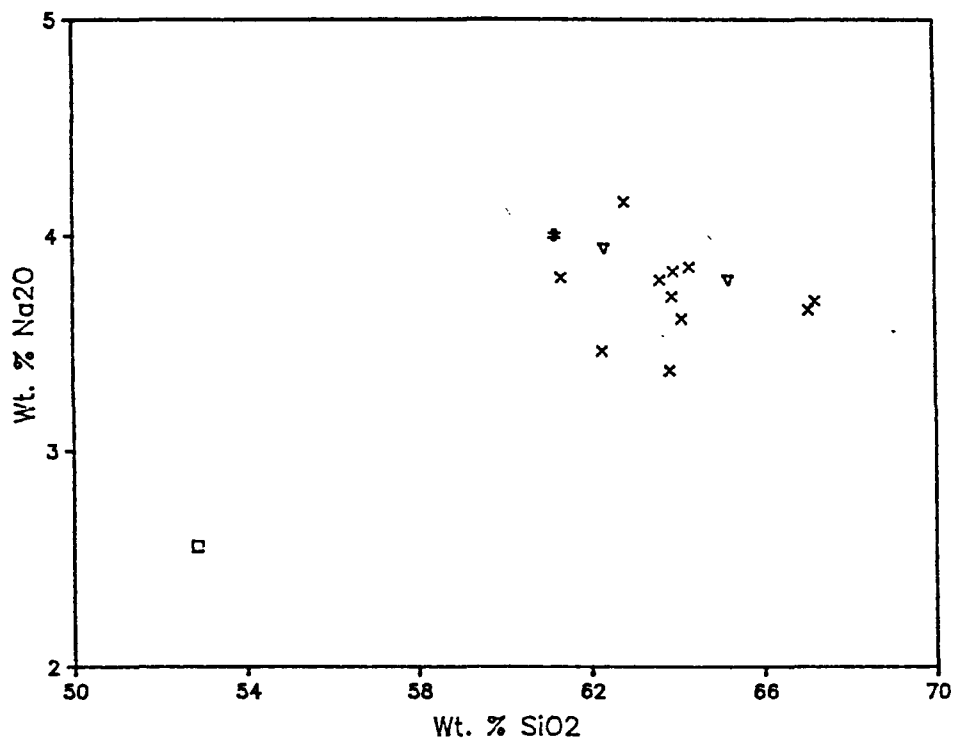


Fig. 39. Harker variation diagrams of major element chemistry data for the Bonanza volcanic rocks.









pyroclastic units, but it does follow the general chemical trend of the tuffs.

Fractional crystallization involving removal of the observed phases (plagioclase, titanomagnetite, sanidine, augite, biotite, apatite, and zircon) can qualitatively explain the observed trends, with proportions of the crystallizing minerals changing when the magma reached a composition of 64 wt. % SiO_2 . Such a change in the proportions of minerals precipitating would not necessarily be reflected by the few unfractionated phenocrysts that are retained in the liquid. Although being incorporated by crystallizing sanidine and biotite, K_2O increases in concentration in the melt because bulk distribution coefficients for this element is less than one.

Trace element chemistry

Trace elements are important in petrogenetic studies because they have an even greater tendency than major elements to be fractionated preferentially into either liquid or solid phases (Cox et al., 1979). The drawback of using trace elements for genetic interpretation is that many of these elements are also more mobile than major elements during alteration.

The trace element abundances for the Bonanza volcanic units are presented in Table 5, where they are compared to the compositions of other subduction-related calc-alkaline

Table 5. Trace element chemistry of the Bonanza volcanic units compared to trace element abundances of orogenic silicic volcanics from various geographic regions (modified from Ewart, 1979).

	Andes	eastern belt of western U.S.	Caribbean	western belt of western U.S.	Mediterranean	Cascades-Alaska -Aleutians	Bonanza
Rb	101-173	93-163	37-52	127-199	69-138	39-125	100-227
Ba	570-798	1330-1680	242-352	1324-1700	484-1032	493-716	403-1607
Sr	214-582	339-1000	283-416	455-1070	204-486	361-954	62-746
Zr	79-178	248-330	106-117	176-245	129-205	160-188	220-411
Zn	95-122	68-95	48-66	43-79	51-69	63-122	30-73
La	--	77-110	--	79-125	19-56	15-25	48-88
Y	6-7	25-31	22-26	18-29	23-41	32-61	28-37
Cu	16-33	13-25	40-46	10-34	19-43	17-32	16-36
Ni	12-49	5-36	30-40	8-32	6-14	4-34	0
Co	8-12	3-13	--	8-27	5-13	4-16	0-9
Cr	22-58	4-61	96-130	15-94	6-17	5-44	0
Mb	--	16-19	4-6	17-24	21-24	5-6.5	24-40
Pb	--	24-34	--	19-29	6.2-7.0	5.5-15	20-26

volcanics. Ba, Nb, Pb, La, Rb, and Zr, elements that are closely correlated with K, are noticeably higher in the high-K suites of Bonanza and the western U.S. (Ewart, 1979), with the Bonanza units containing especially high amounts of Nb (24-40 ppm) and Zr (220-411 ppm). Bonanza volcanics are also noticeably depleted in the compatible elements Ni, Co, and Cr compared to other volcanics in the western U.S.. Sr contents are high in both the Bonanza and the western U.S. rocks.

The variation of trace elements with SiO₂ content is illustrated in Figure 40, with trace elements again showing trends which typically reflect fractional crystallization. Highly compatible elements such as Cu, and Co are rapidly depleted with increasing removal of crystals from the melt and corresponding increasing SiO₂. Co often substitutes for ferrous iron, and therefore could easily be incorporated into fractionating biotite, augite, or magnetite (Cox, et al., 1979). Ta, which is present only in minor amounts, is often incorporated into zircon, titanomagnetite, and/or ilmenite (Mahood and Hildreth, 1982).

Sr and Zn are also behave as compatible elements in the Bonanza units, but decrease less rapidly with increasing silica content. Zn substitutes for Fe²⁺ in various mineral phases, and Sr substitutes for Ca in plagioclase, apatite, and sphene.

Y and Pb both maintain fairly constant values of approximately 31 ppm and 25 ppm respectively. U seems to

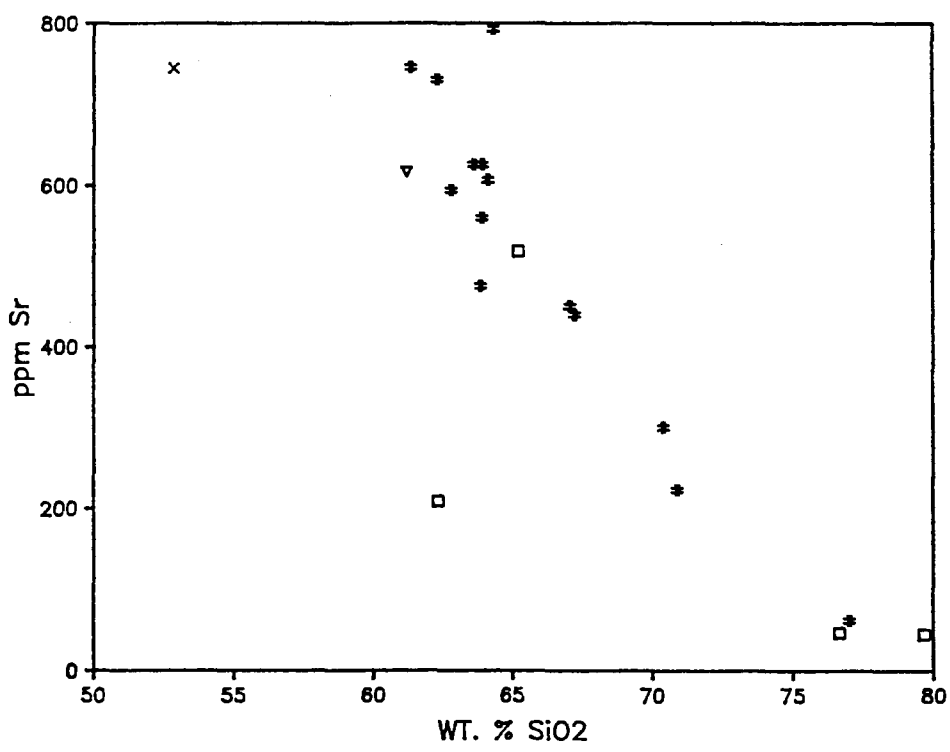
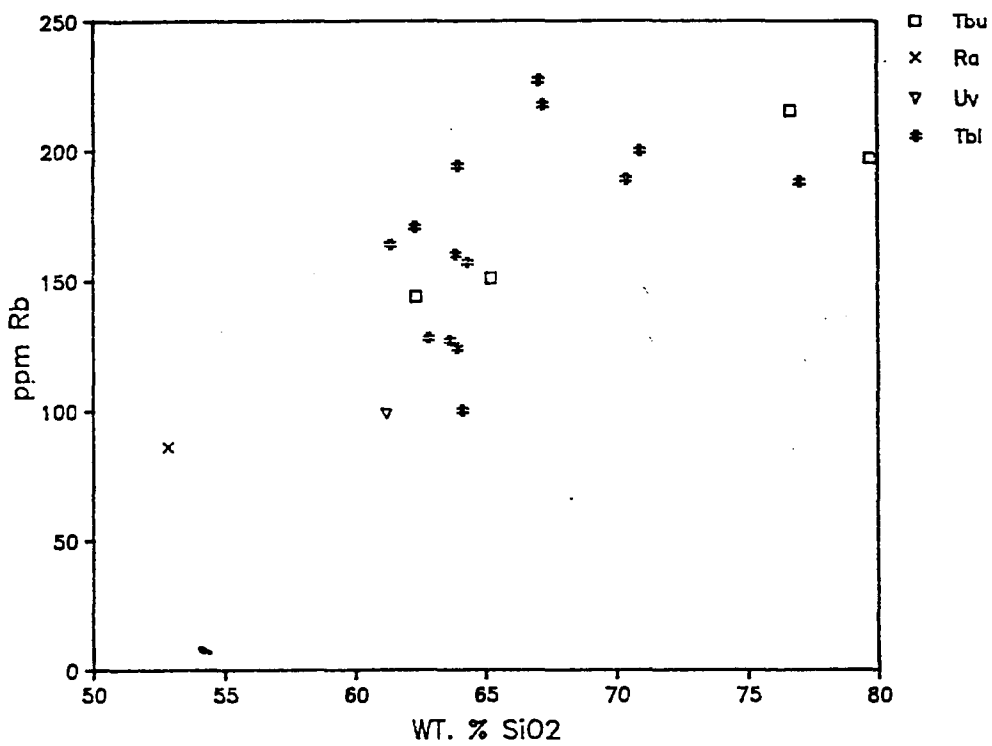
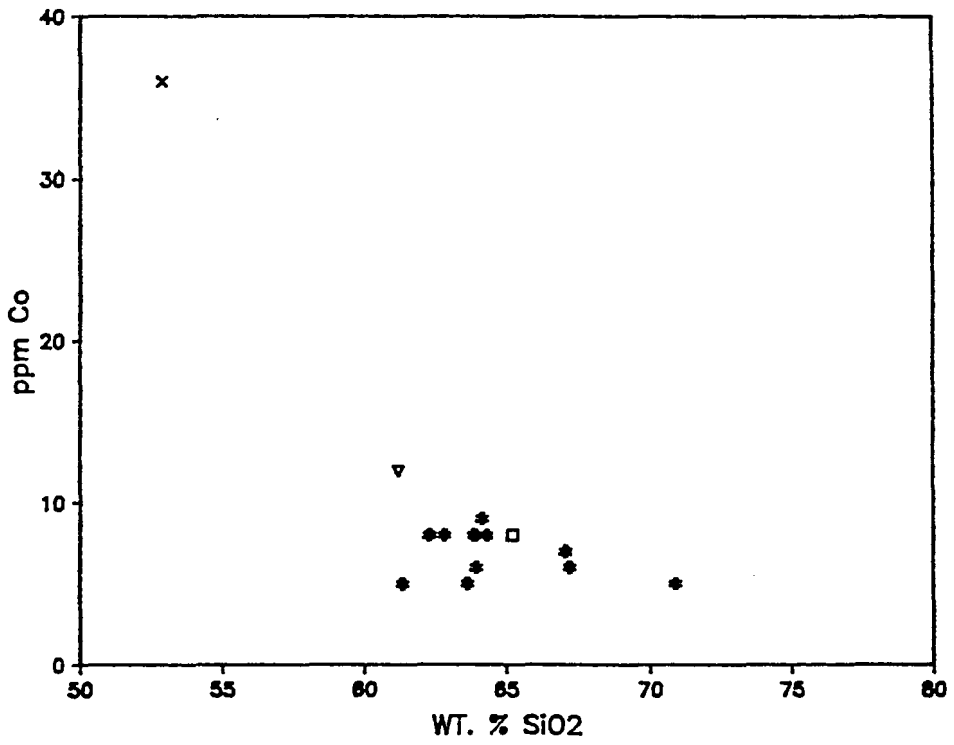
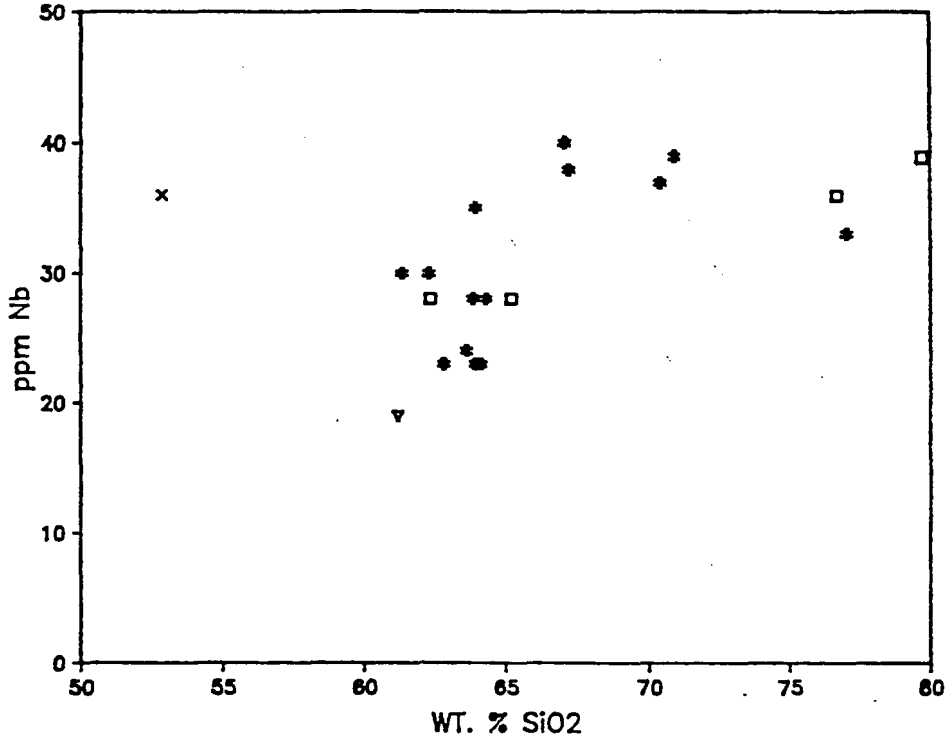
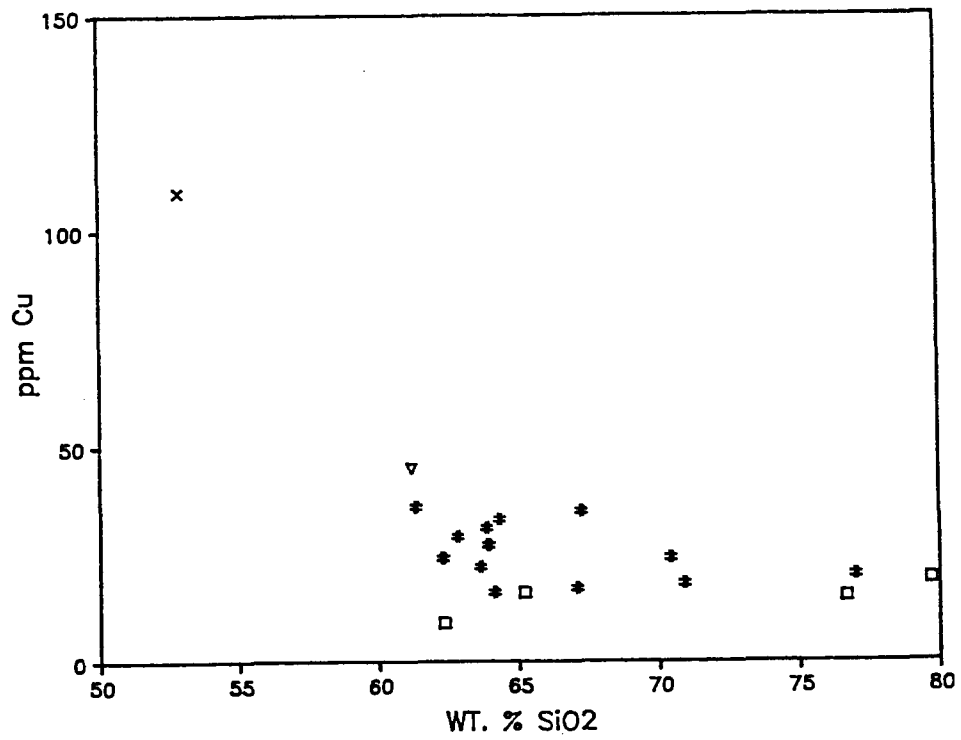
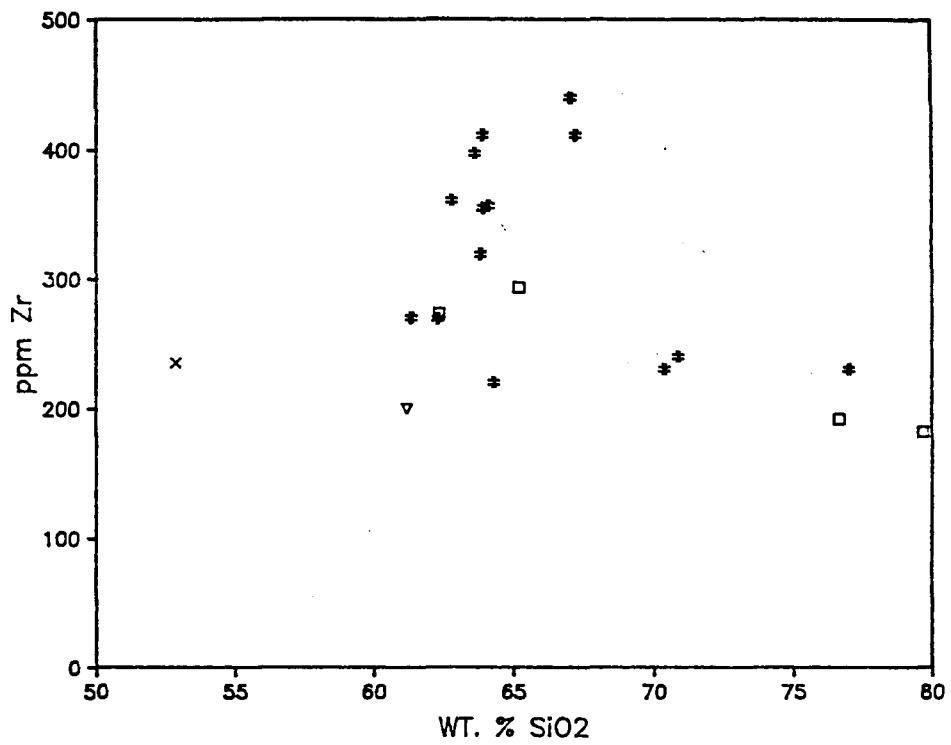
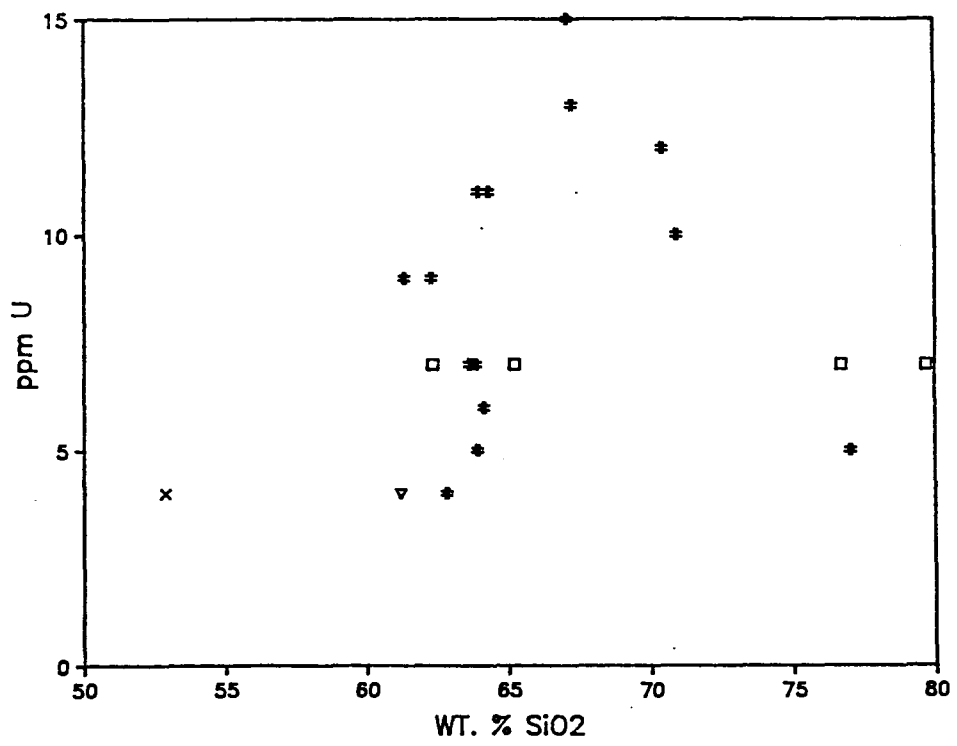
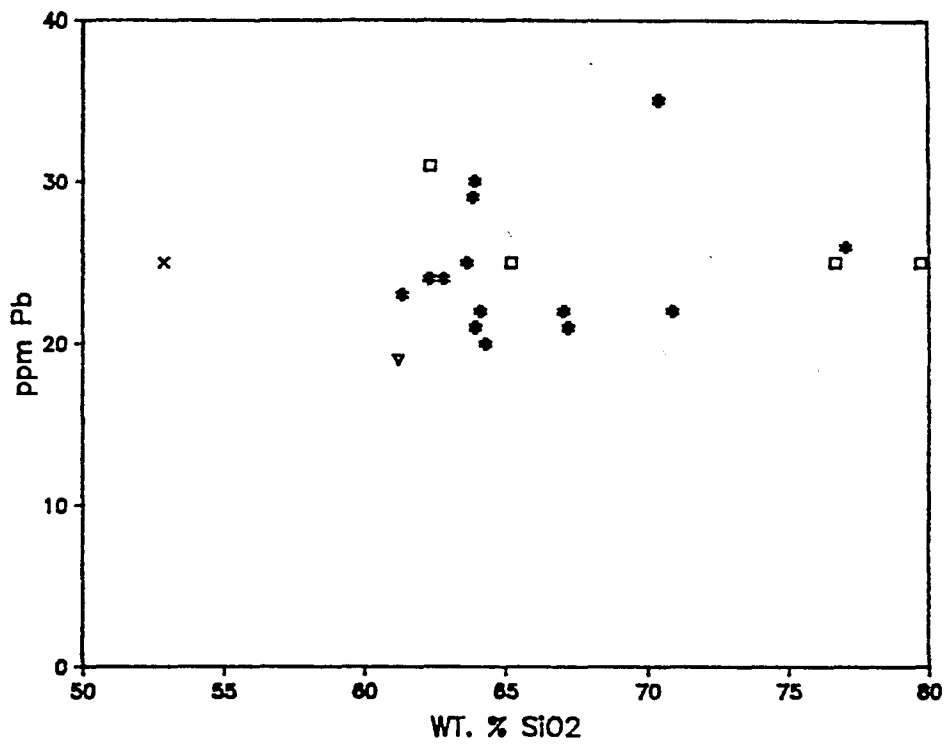
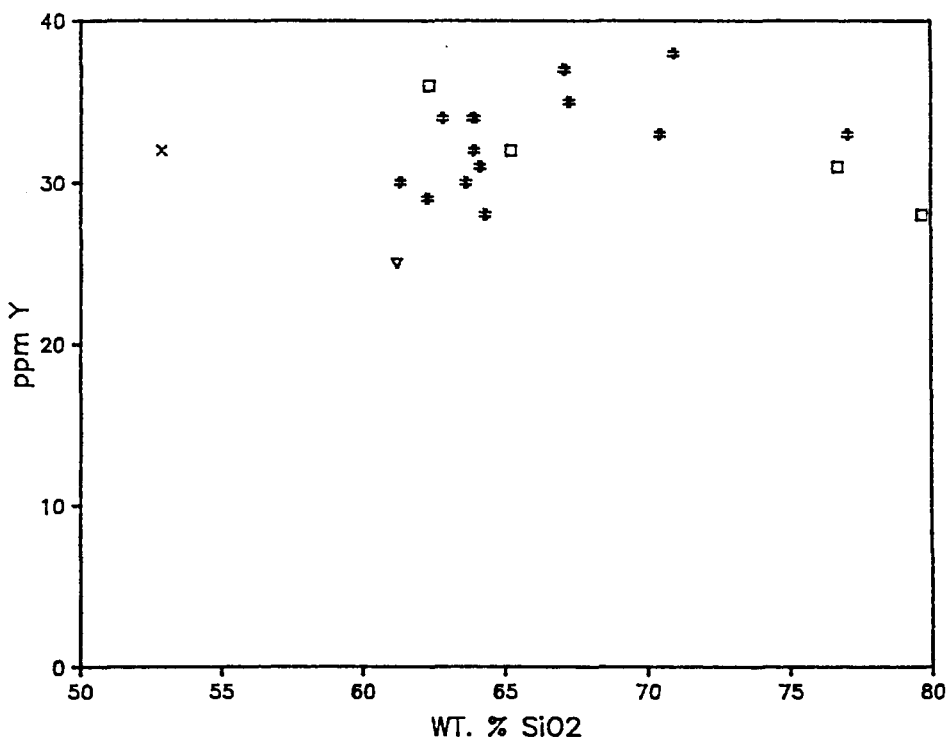
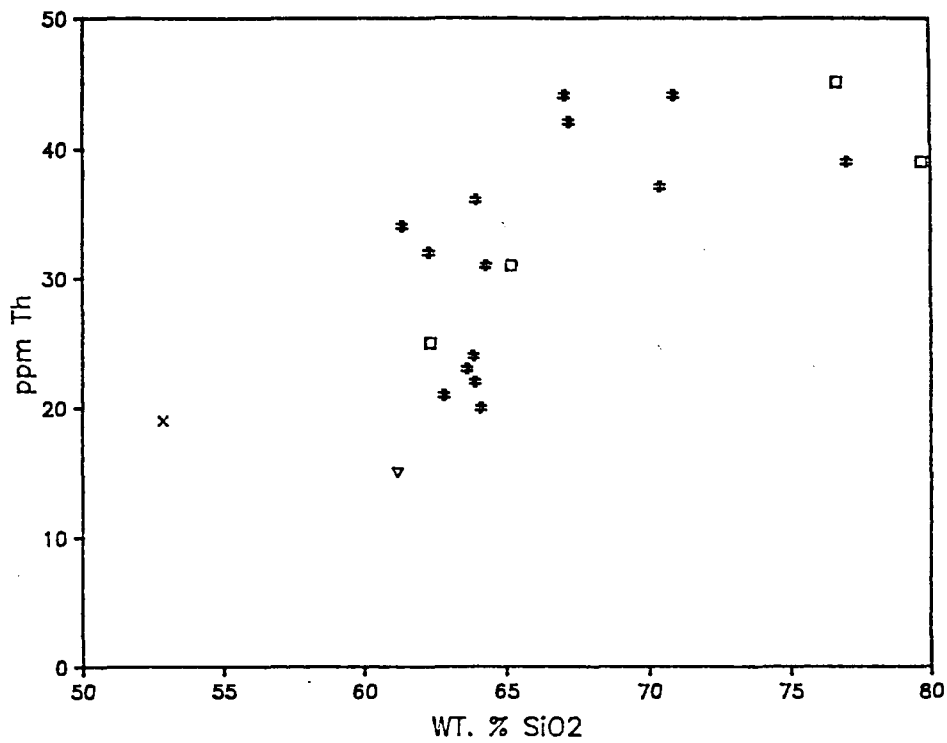


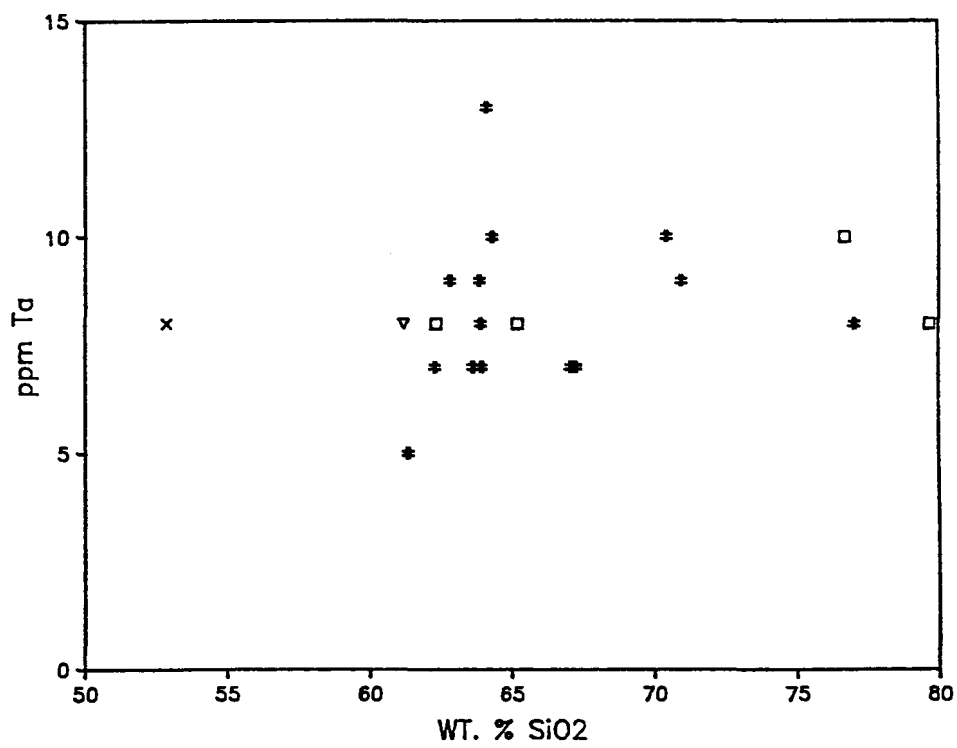
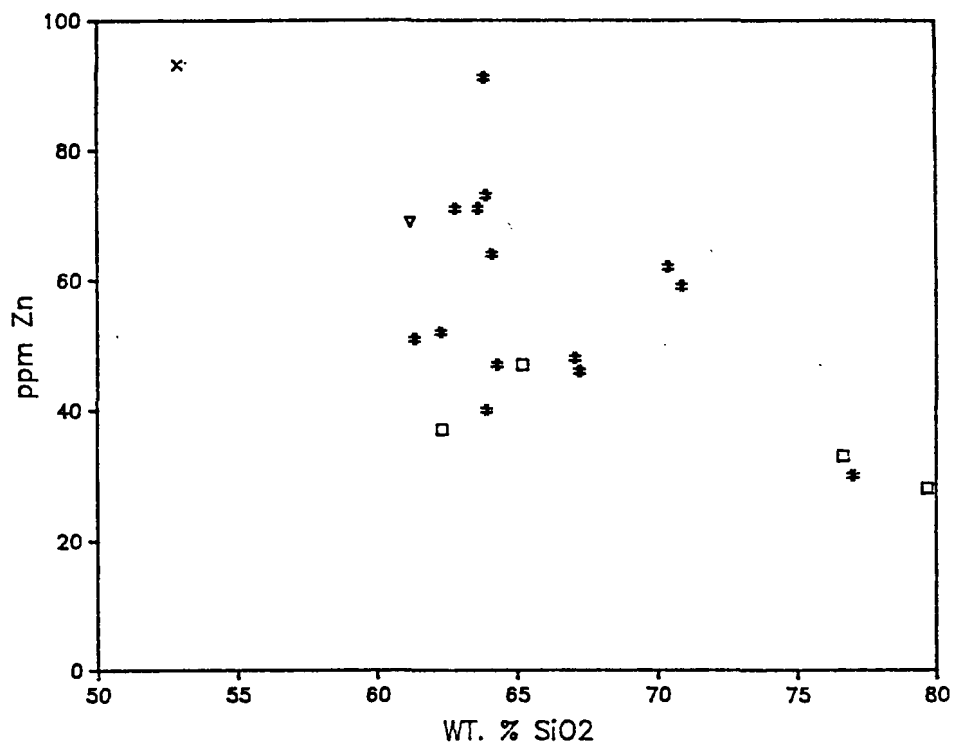
Fig. 40. Harker variation diagrams of trace element chemistry data for the Bonanza volcanic rocks.











peak at a concentration of 15 ppm at 68 wt. % SiO_2 , and then decreases. This decrease in U could be due to incorporation in a minor phase (zircon or apatite) which began crystallizing later in the magmatic history (Mahood and Hildreth, 1982). The plot involving Zr shows large amounts of scatter, but show an overall negative correlation with SiO_2 , perhaps caused by incorporation into fractionating zircon, biotite, or sanidine.

Finally, the highly incompatible elements Th, Rb, and Nb all increase with increasing silica, and then level out after 68 wt. % SiO_2 . Incompatible elements are ones which, due to their large ion size, are not readily incorporated into solids and are therefore partitioned into the melt. The variation diagrams of Figure 41 better illustrate the relationships of the incompatible elements. Here the incompatibles are plotted against ppm Th. The fact that a line drawn through the Rb and Nb data does not intersect the origin of the chart may indicate that both Rb and Nb have higher distribution coefficients ($K^{S/L}$) than Th. This would suggest that these two elements were behaving slightly compatibly, and were perhaps being incorporated into fractionating sanidine or biotite. An alternative explanation for the observed Rb and Nb trends is that these elements behaved slightly differently than Th during alteration processes.

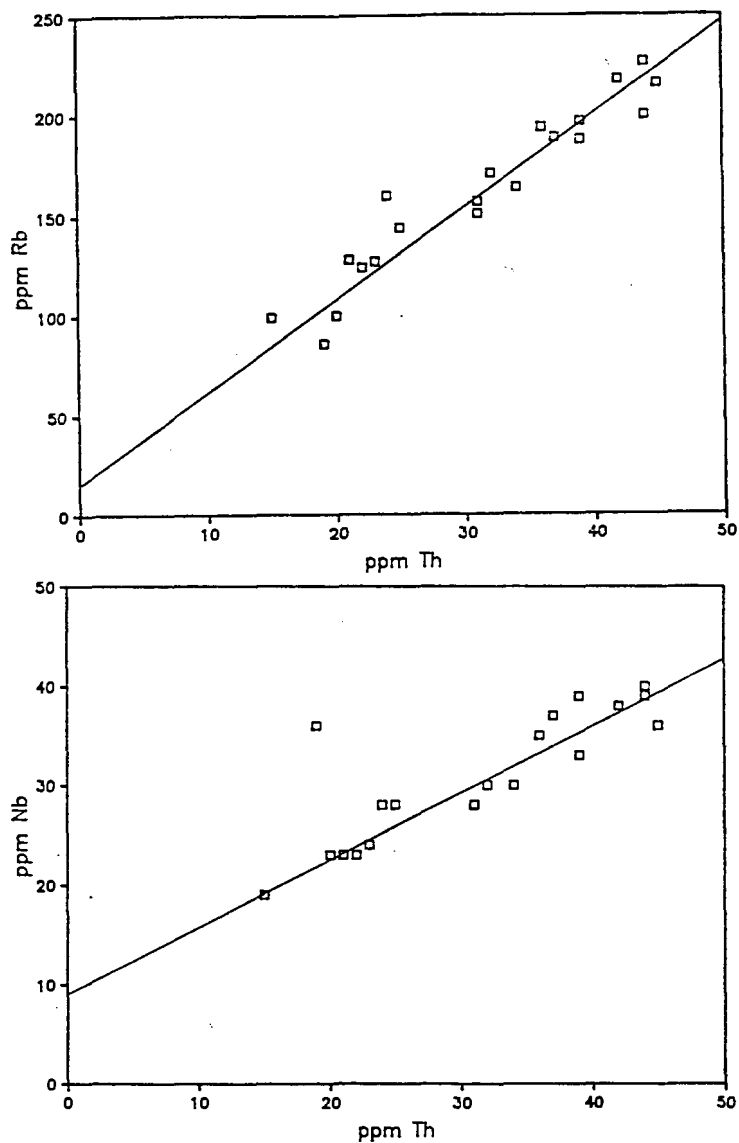


Fig. 41. Variation diagrams of incompatible trace elements plotted versus ppm Th. The fact that a line drawn through the data does not intersect the origin of the chart indicates that both Rb and Nb have higher distribution coefficients than Th, or that these two elements behave differently than Th during alteration.

Compositional trends with time

Although so far the trends observed on Harker diagrams seem to indicate that the Bonanza volcanics were derived by fractional crystallization, problems with this interpretation arise when changes in chemistry with time (represented by stratigraphic height) are considered. Plots of the mineralogy and mineral chemistry (Figs. 15 through 25 indicate that the Bonanza magma was becoming more evolved with stratigraphic height. The presence of sanidine and the hydrous minerals sphene and hornblende in the uppermost samples suggest that concentrations of K_2O , H_2O , and probably SiO_2 in the melt were increasing with time. The fact that biotites become more Fe-rich and plagioclase crystals grow more sodic upsection supports this interpretation.

One would therefore expect the most siliceous units on the Harker diagrams (samples #11 and 12) to contain phenocrysts of sanidine and hydrous minerals, and to occur near the top of the stratigraphic section. However, this is not the case; the uppermost stratigraphic units do not plot as the most evolved units on the Harker diagrams.

Examples of lavas that show a lack of correlation between degree of evolution and stratigraphic height are quite common, and include the Aden volcano in South Yemen (Cox et al., 1979) and Santorini (Huijsmans, 1985). In these cases, instead of representing a single liquid-line-of-descent caused by one parent magma continually

differentiating, the chemical trends on Harker diagrams represent several overlapping, but generally similar lines-of-descent. Overlapping lines of descent can be caused by periodic injection of mafic magma into a chamber in which fractional crystallization occurs continuously, with eruptions sporadically bringing samples of the magma to the surface. Such processes should produce cyclic trends when plotted versus time or stratigraphic height, with the trend repeating itself each time new magma is injected into the chamber (Fig. 42).

Multiple injection combined with fractional crystallization does not appear to explain the Bonanza whole-rock chemical data, because cyclic trends are not observed when major oxides are plotted against stratigraphic height (Fig. 43). Except for sample #18, TiO_2 , FeO , Na_2O , P_2O_5 , MnO , and MgO in the tuff samples all vary by less than one wt. percent, and show no evidence of the magma becoming more evolved with time. The only elements that show any trends are K_2O , Al_2O_3 , and SiO_2 . K_2O varies over approximately 2 wt. percent, and correlates fairly well with mineralogy. K_2O increases with stratigraphic height in samples #8 through #11, then remains fairly constant until sanidine phenocrysts appear. K_2O content then decreases in samples # 18 through 19, which is the trend that would be expected if sanidine were fractionating. The chemical response is not exactly what one would predict, however, because sanidine phenocrysts

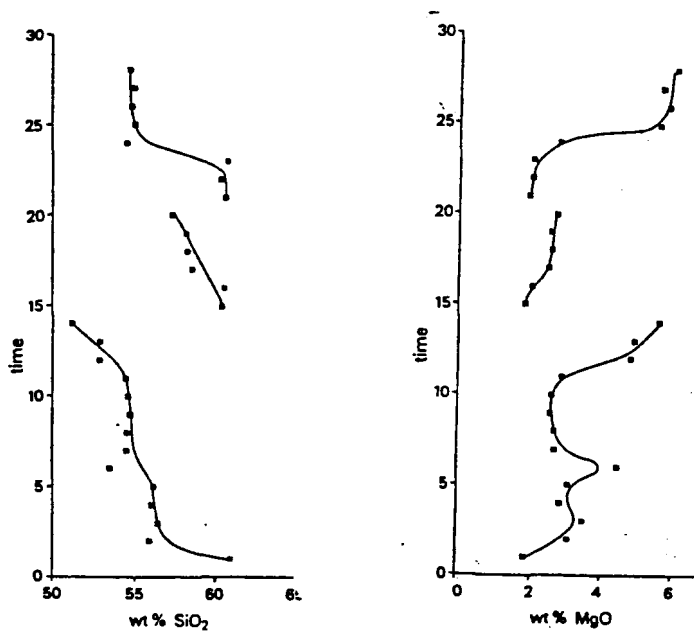


Fig. 42. Plots of major element compositions of Santorini lavas versus stratigraphic height. Cyclic trends are caused by periodic injection of mafic magma into a chamber in which fractional crystallization is occurring continuously (after Huijsmans, 1985).

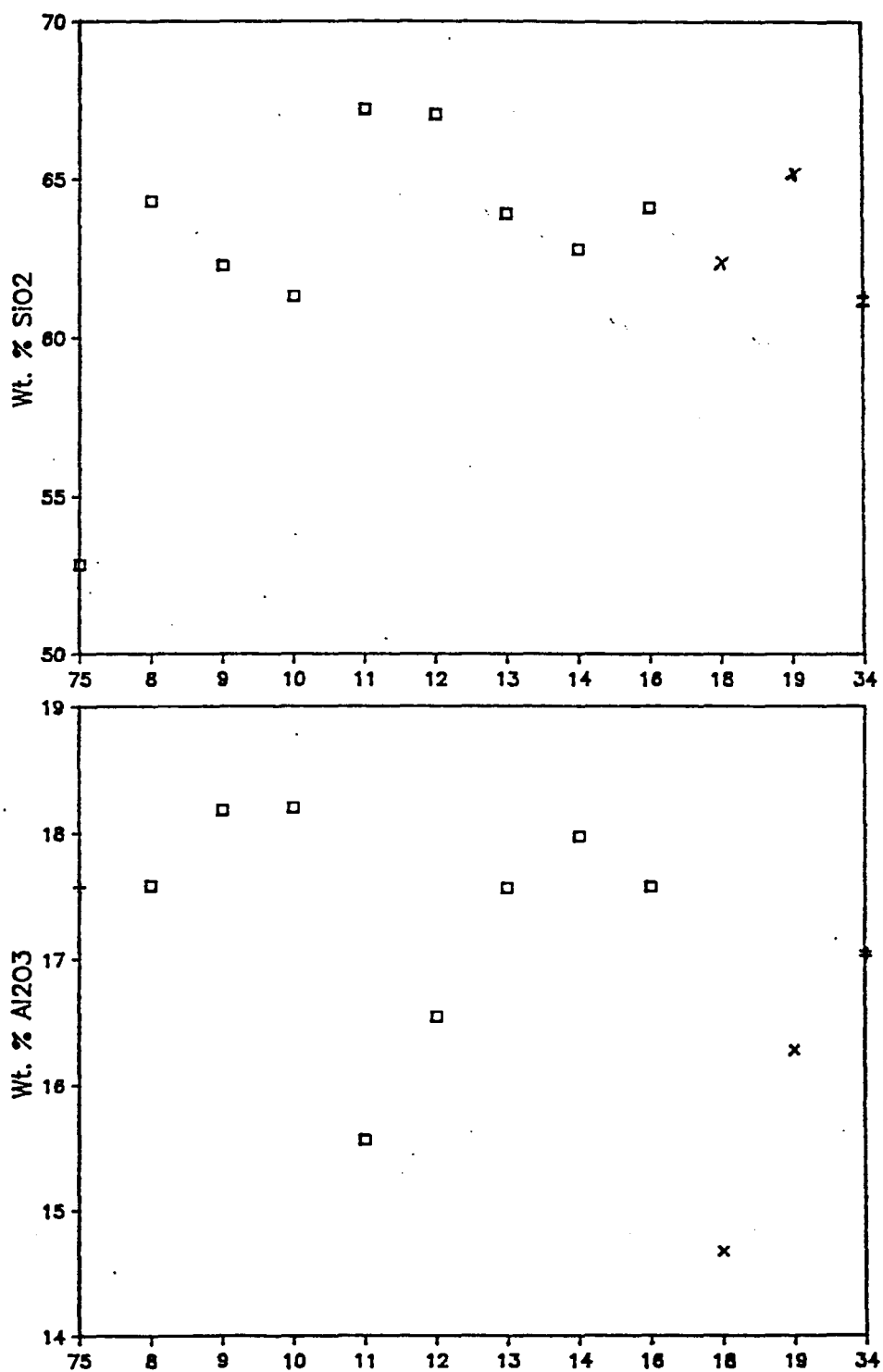
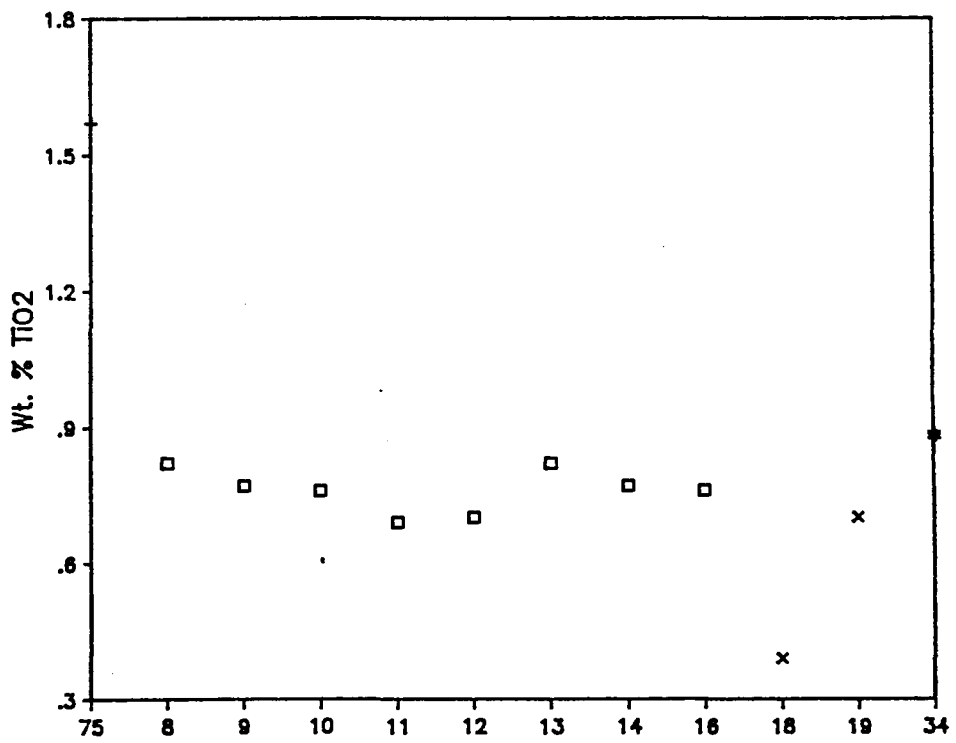
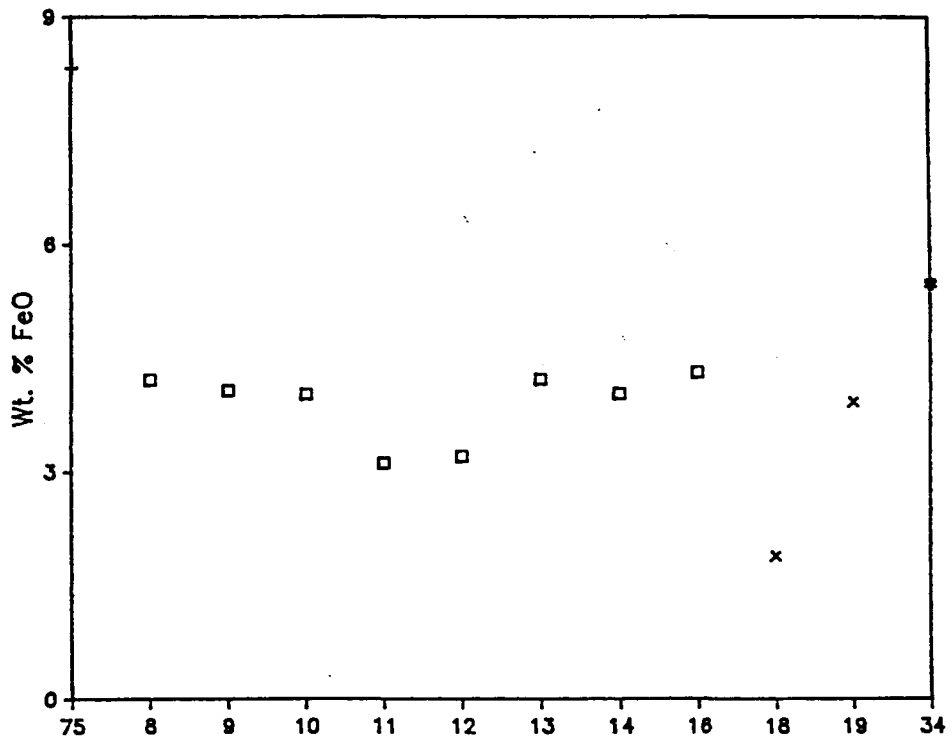
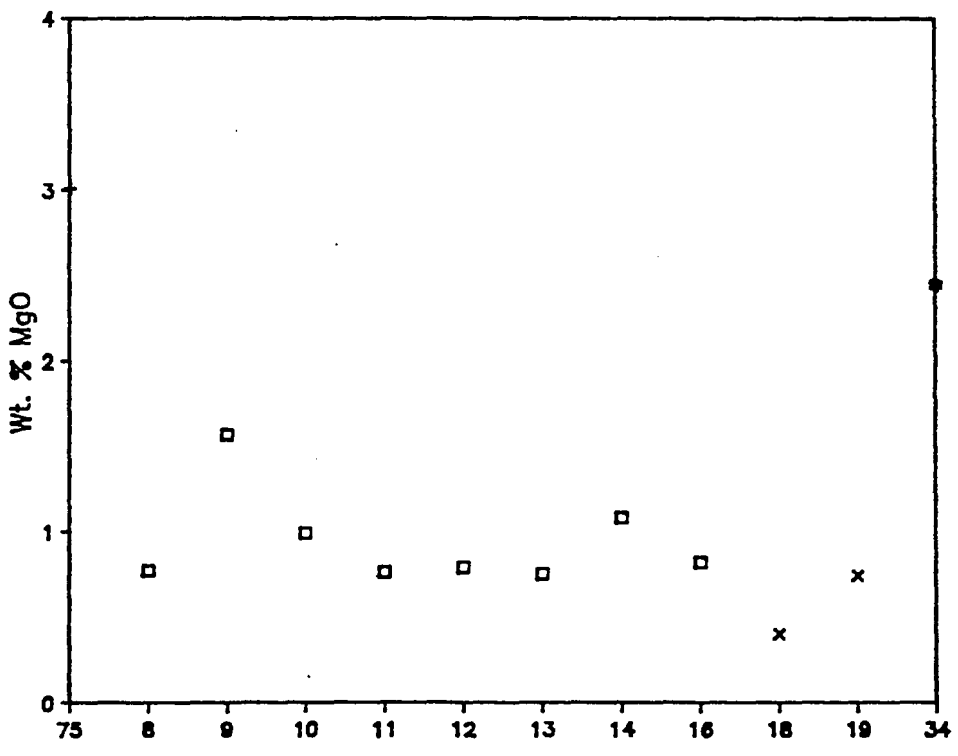
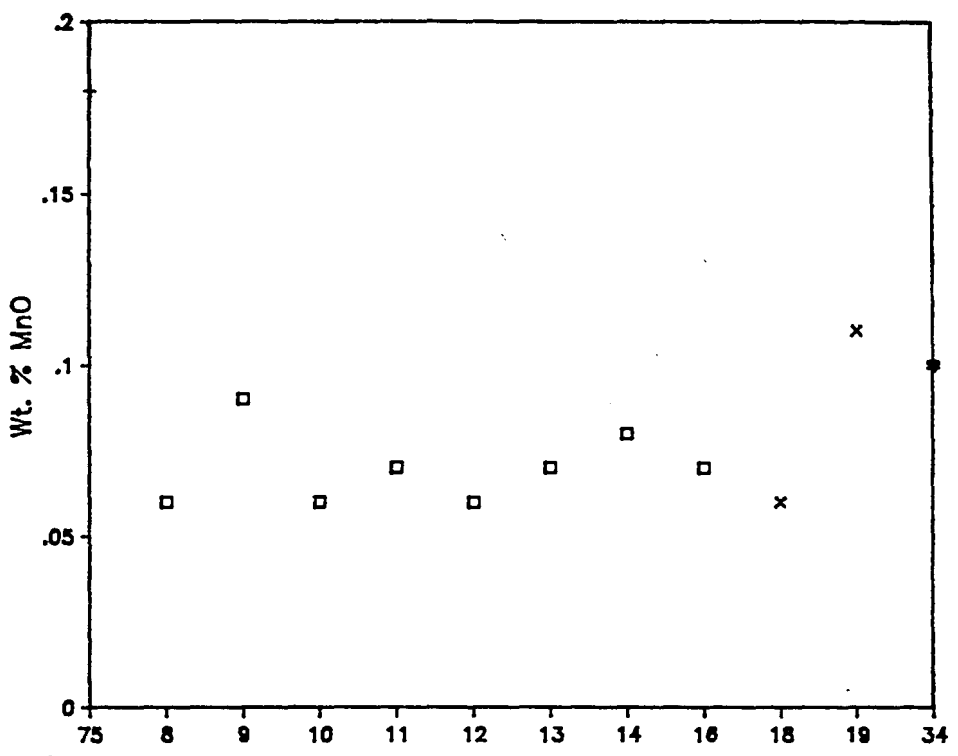
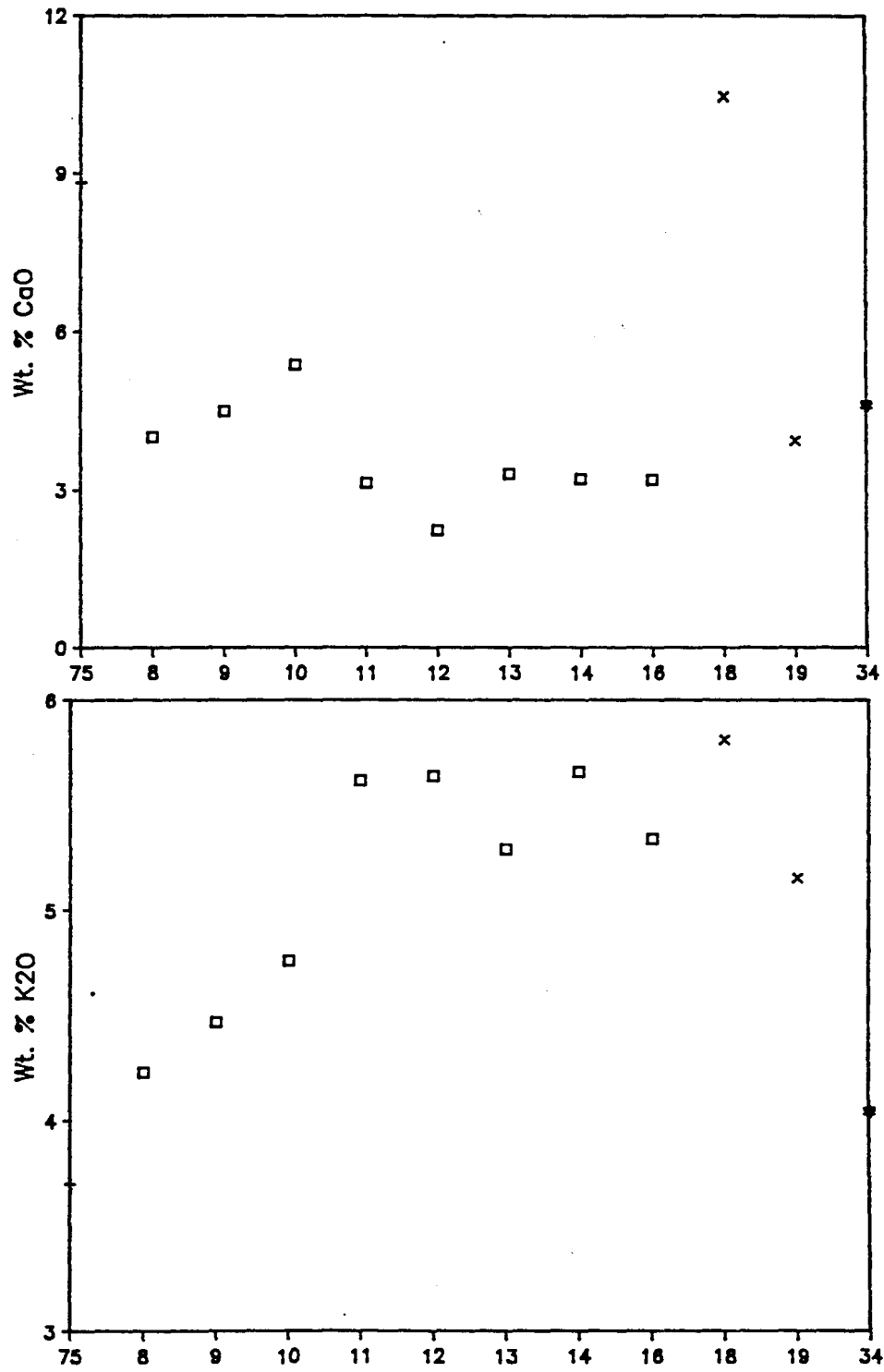
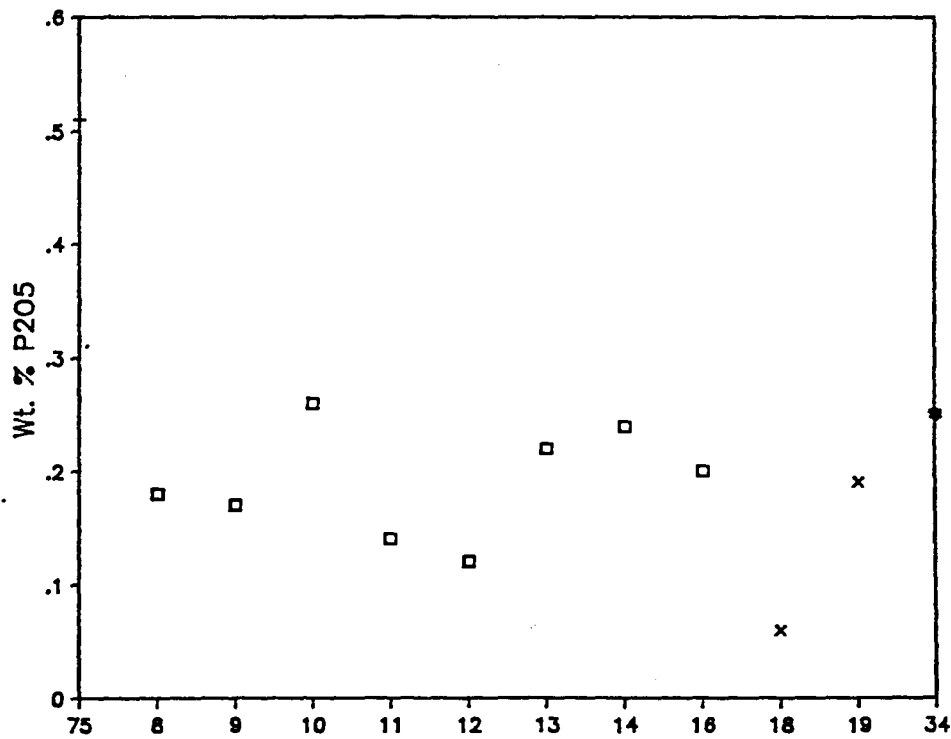
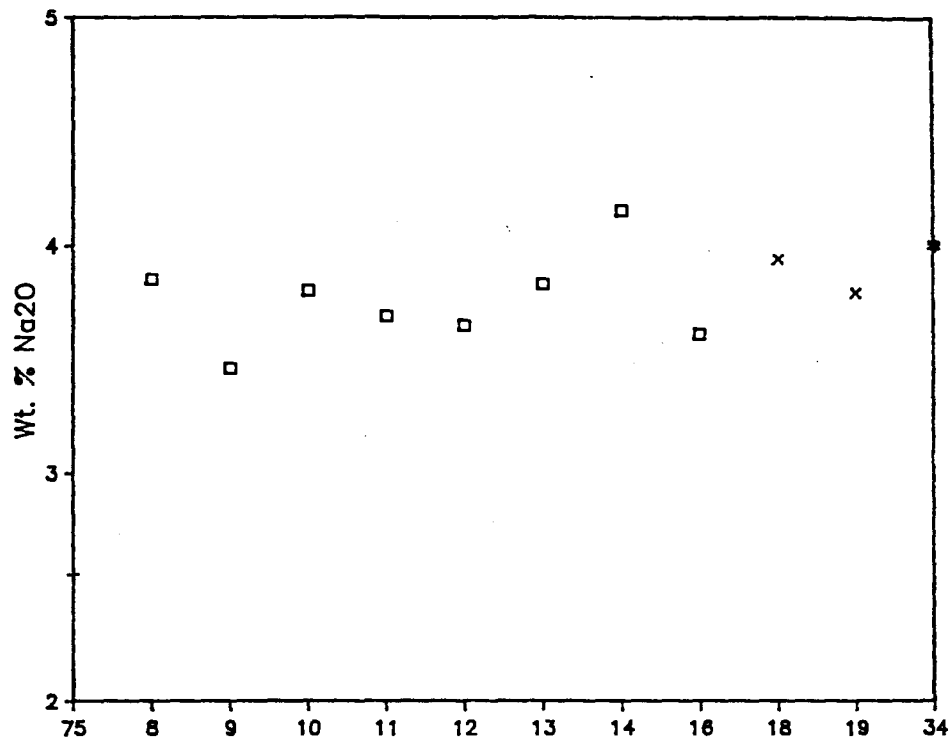


Fig. 43. Plots of major element compositions of Bonanza volcanics versus stratigraphic height.









first appear in sample #14, i.e. at a lower level than that at which K_2O contents first began to decrease. The presence of biotite as well as sanidine could, however, buffer K_2O contents and might explain the observed trends.

SiO_2 and Al_2O_3 , conversely, show very unusual trends with height, and appear to represent three cycles of progressively decreasing SiO_2 content and simultaneously increasing Al_2O_3 . The three cycles do not correspond to Marrs' flow boundaries (Fig. 12) and do not correspond to changes in mineralogy because new phases enter only in samples #14 and #18 (Fig. 15). In addition, it is very unusual for Al_2O_3 to show such large variations (3 wt. percent) while almost all other elements maintain relatively constant concentrations.

Trace elements show greater variation than major elements when plotted against stratigraphic height (Fig. 44), but these trends cannot be explained by fractional crystallization any better than those of the major elements. Note that the incompatible elements Rb, Th, Nb, and Y all tend to basically mimic the behavior of SiO_2 .

Isotope chemistry

Varga and Smith (1984) analyzed rocks of the Bonanza area for Sr isotope data, and calculated the initial $^{87}Sr/^{86}Sr$ values that are reported in Table 6. For the

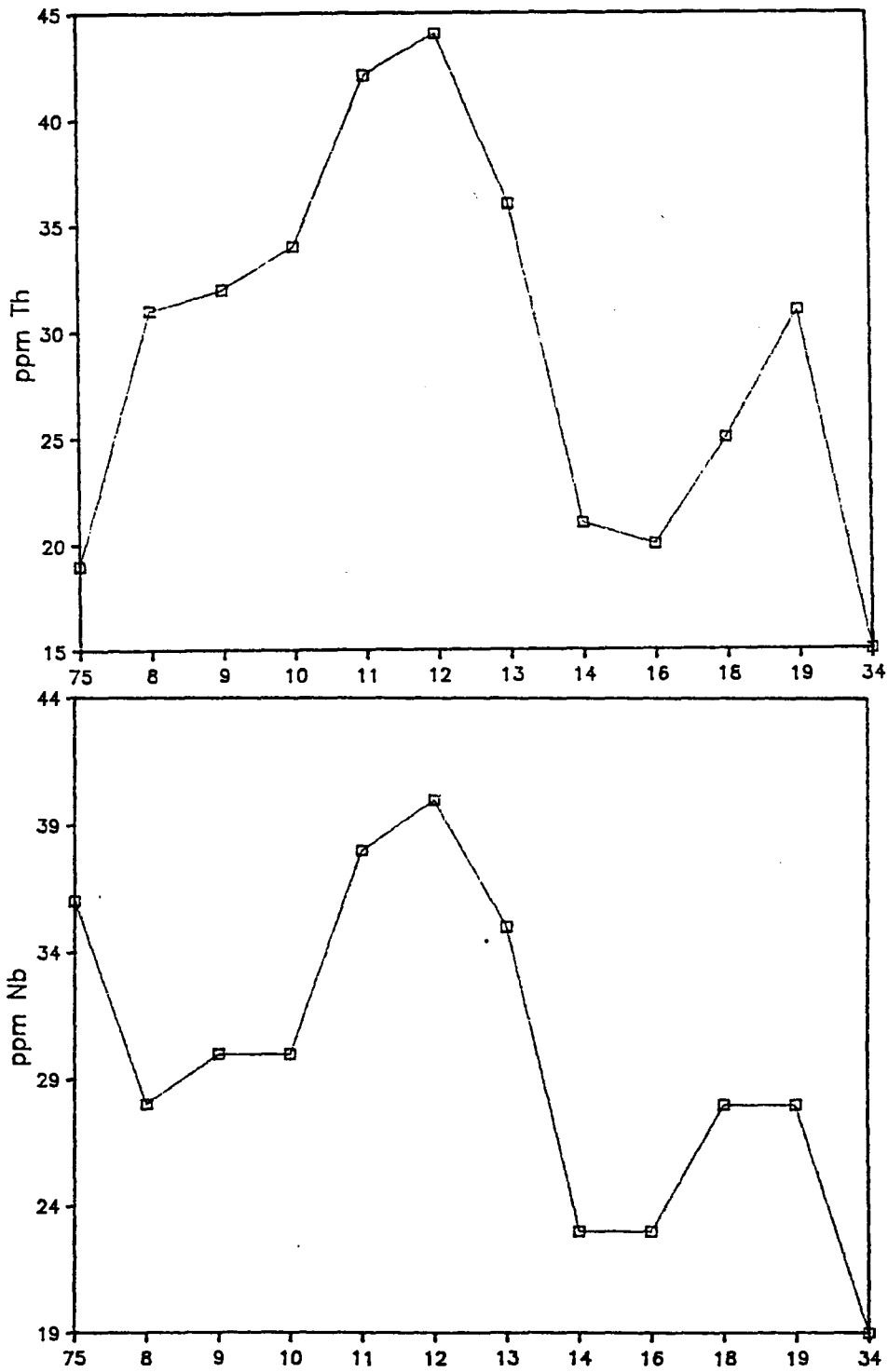
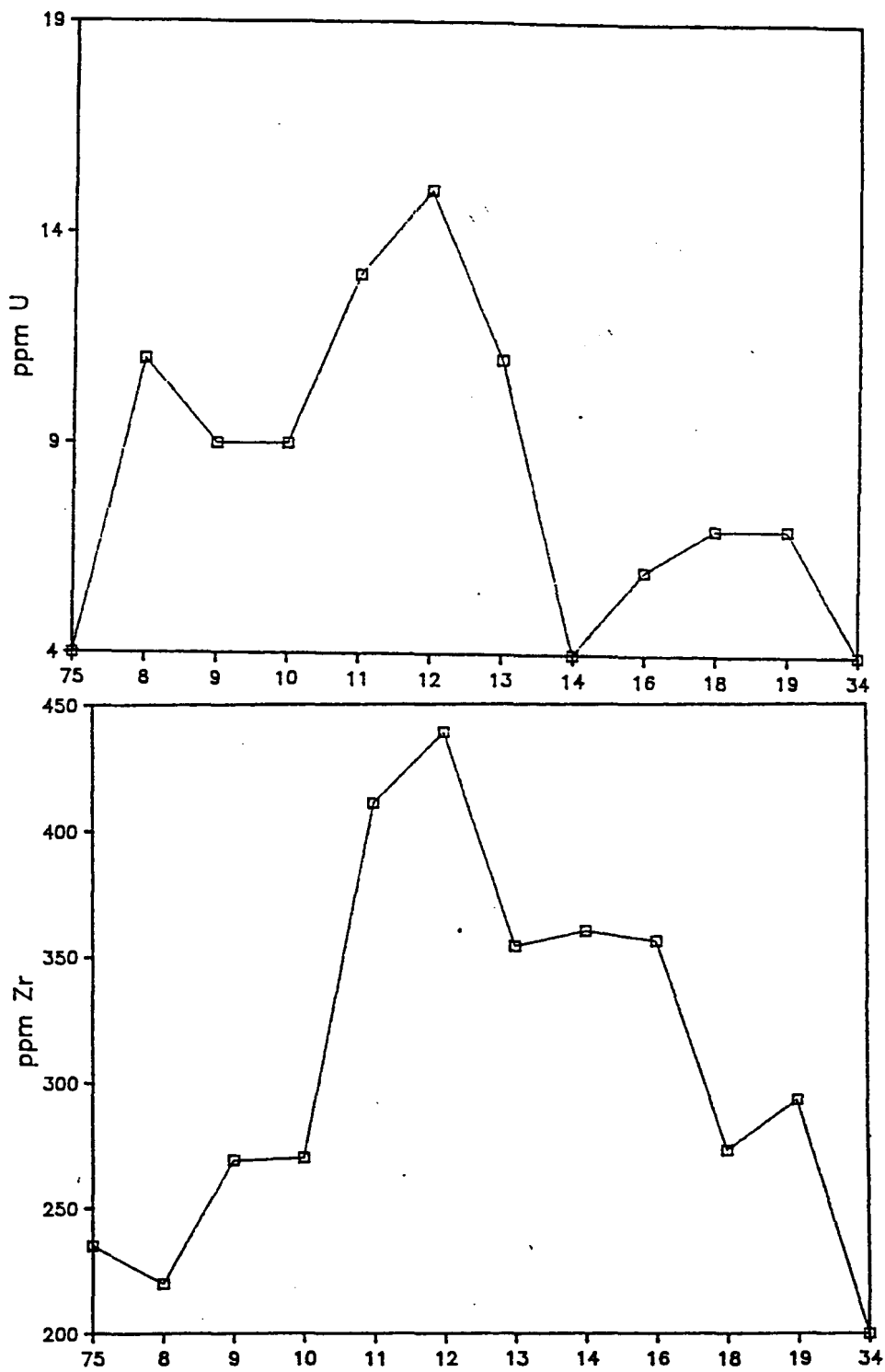
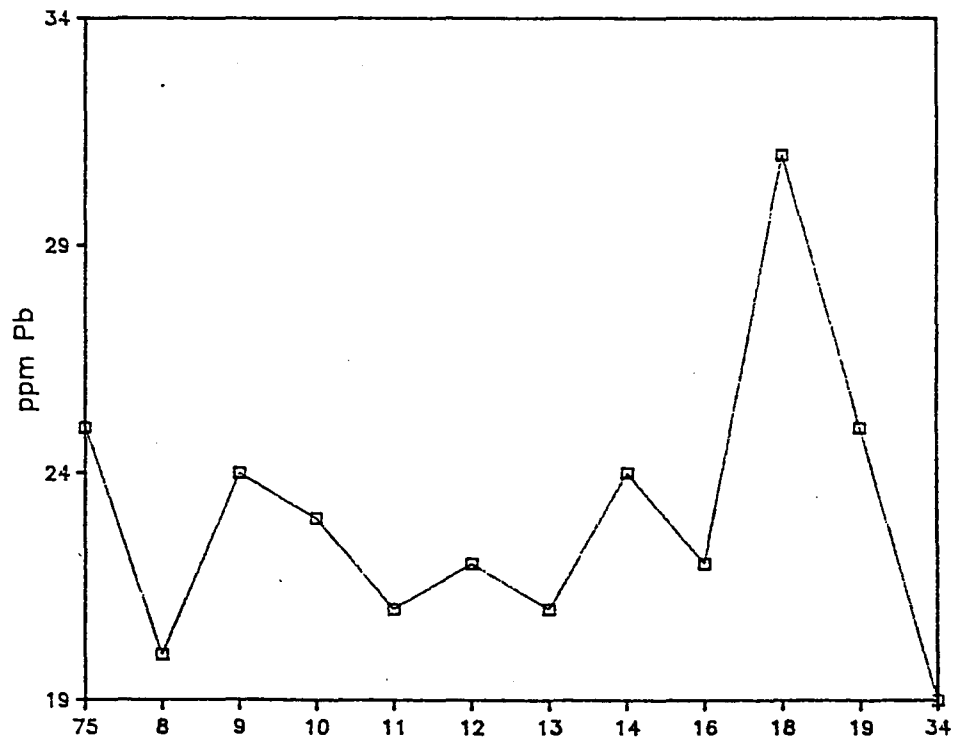
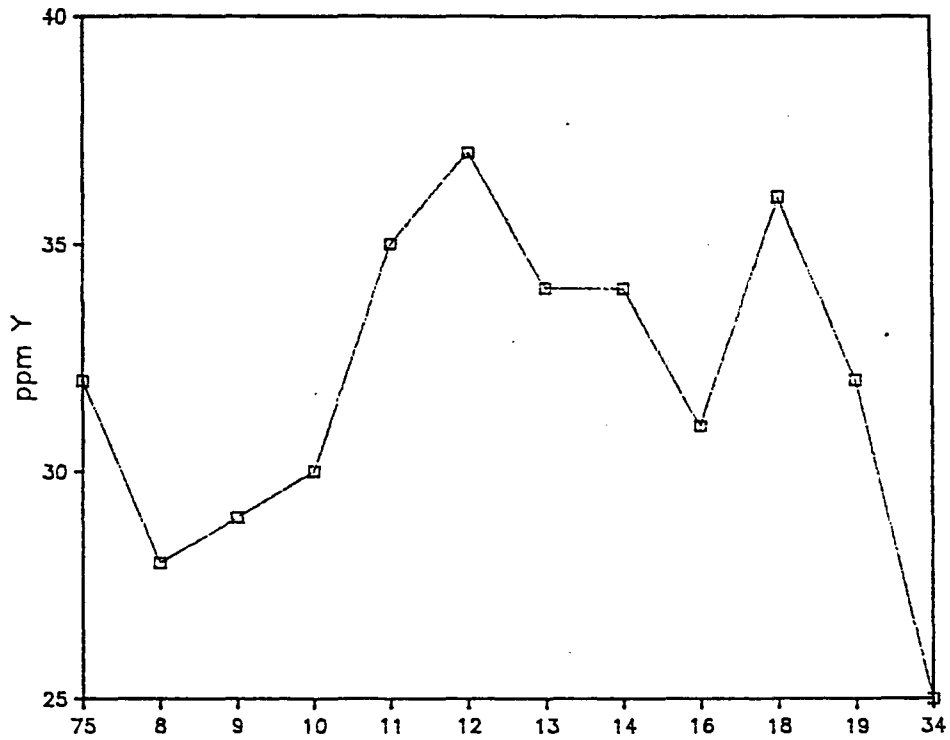
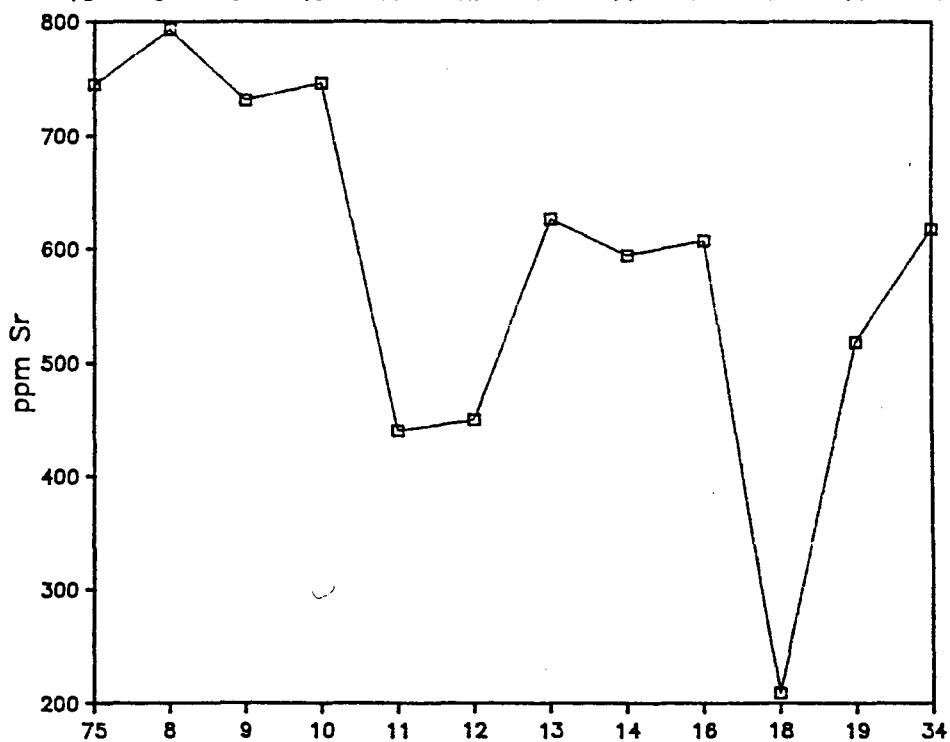
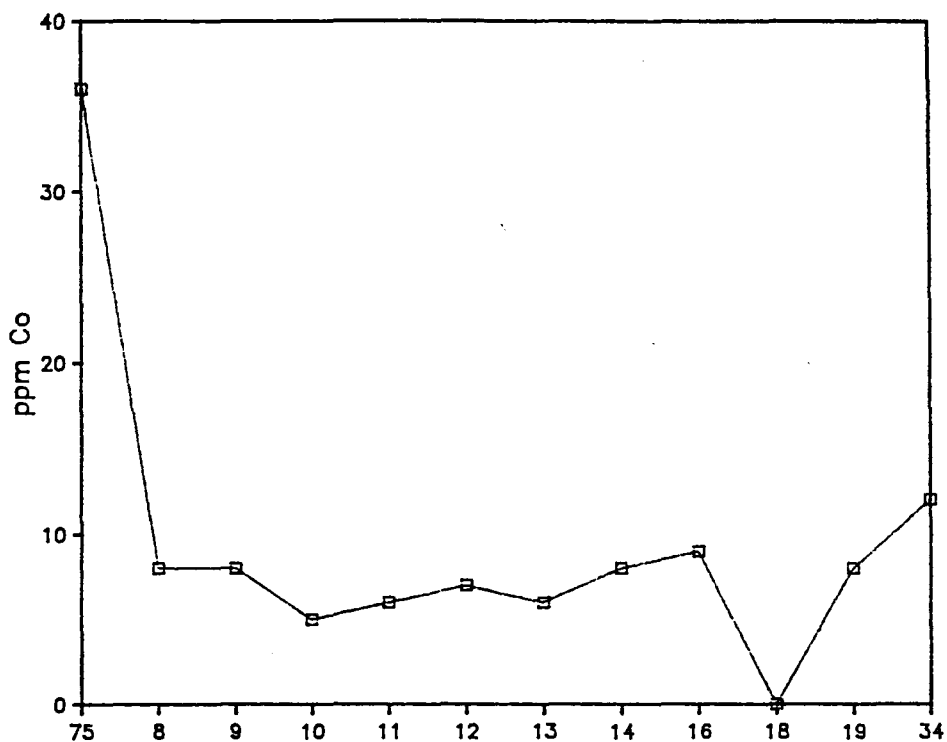
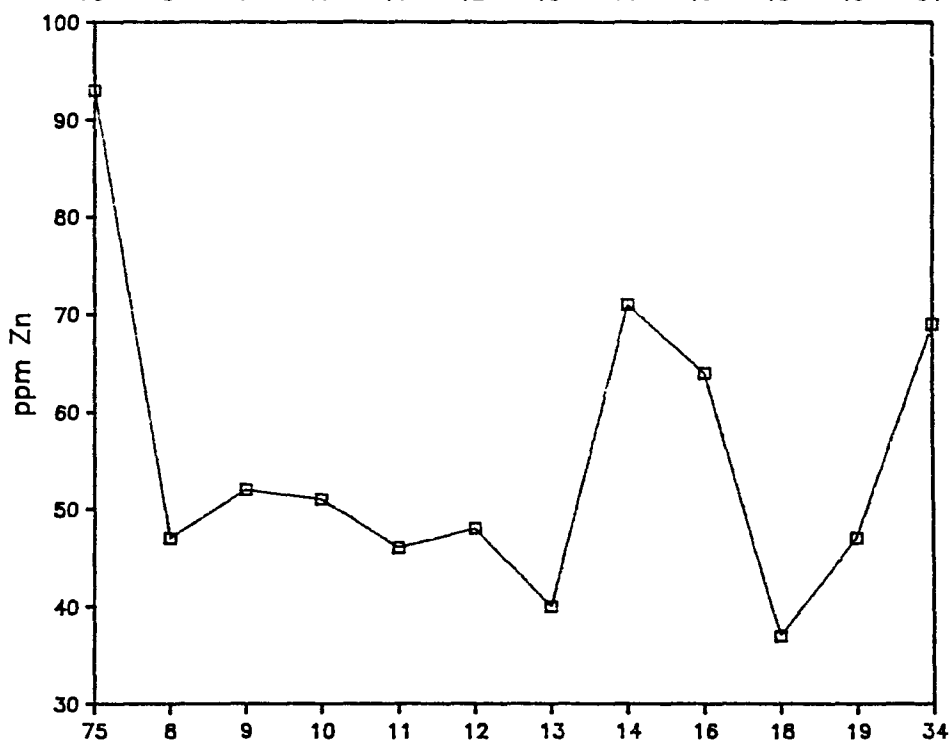
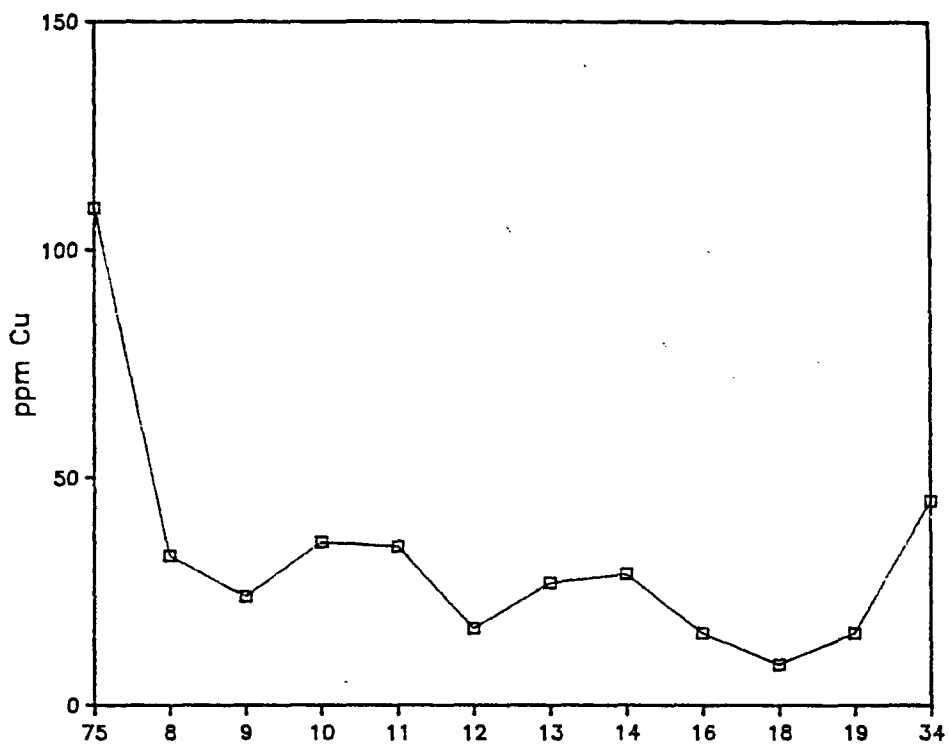


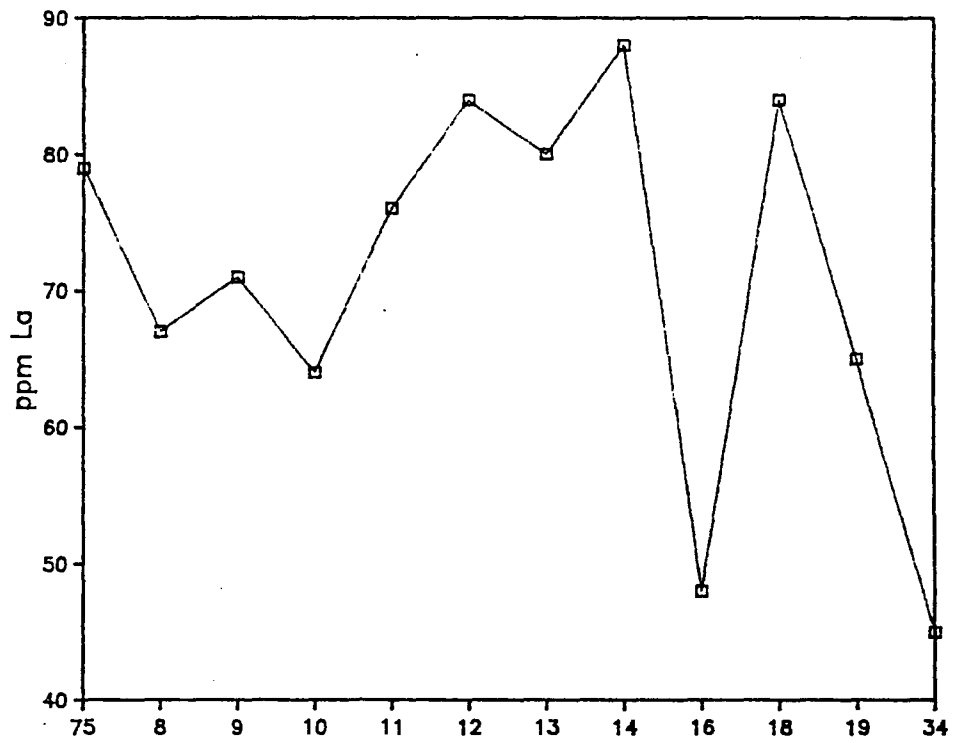
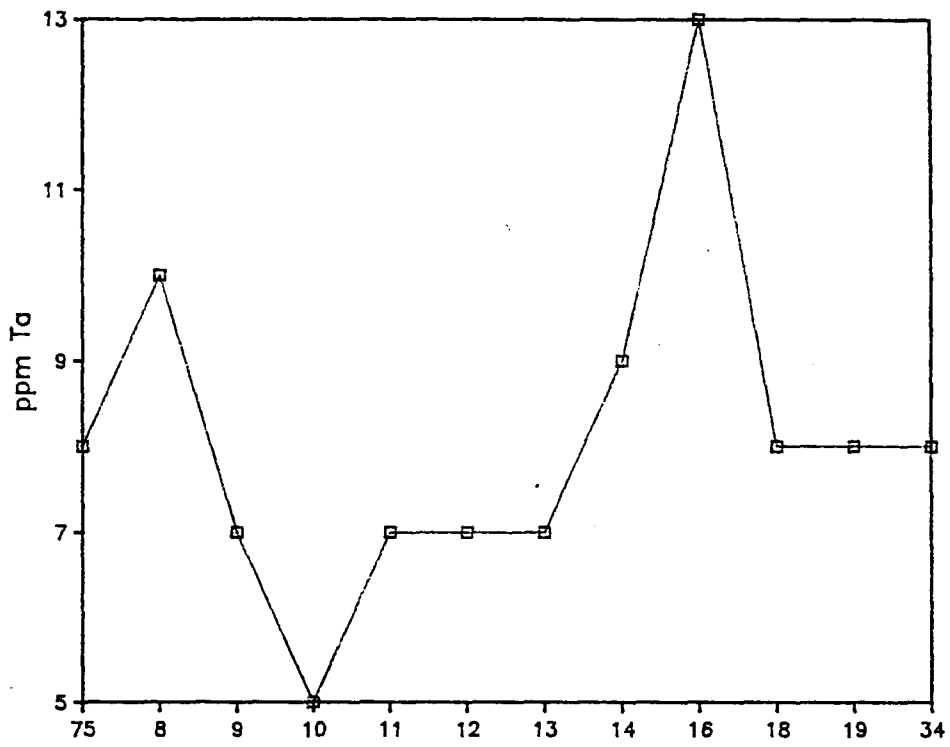
Fig. 44. Plots of trace element compositions of Bonanza volcanics versus stratigraphic height.

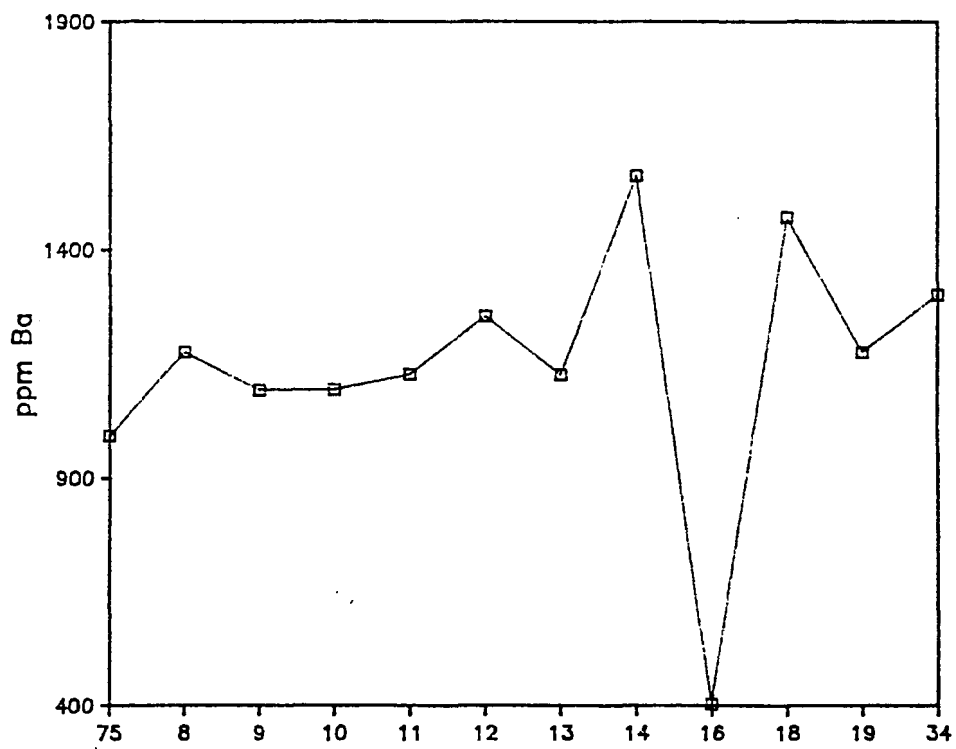
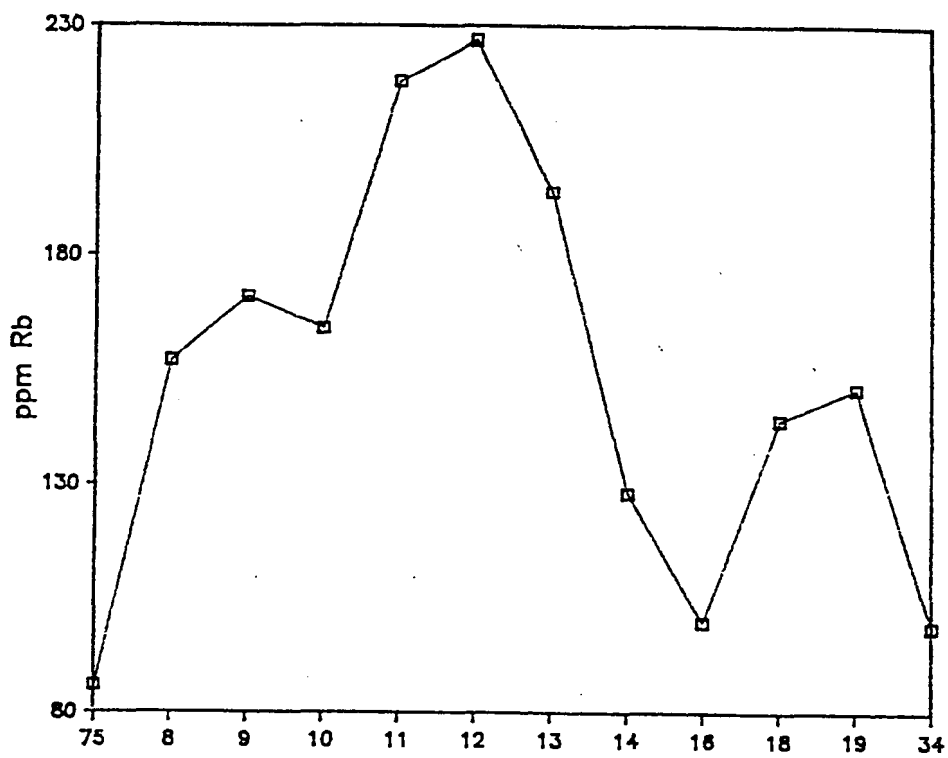












Suspected missing pages 154-155.

Table 6. $^{87}\text{Sr}/^{86}\text{Sr}$ values for rocks of the Bonanza area (after Varga and Smith, 1984).

Unit Analyzed	Sample Type	Age, Ma	Element Contents, ppm			$^{87}\text{Sr}/^{86}\text{Sr}$	
			Rb	Sr	Measured*	Initial	
Rawley Andesite	WR	~38	153.7	530.9	0.70638 (4)	0.70612	
	WR		66.9	918.9	0.70540 (1)	0.70529	
Bonanza Tuff, lower dacite	WR†	~36	134.4	619.5	0.70719 (3)	0.70688	
	WR‡		176.7	780.2	0.70618 (3)	0.70585	
Bonanza Tuff, upper rhyolite	S	~36	119.0	65.5	0.71113 (3)	0.70850	
Upper andesite sequence	WR	~35	111.5	642.9	0.70561 (3)	0.70536	

* Number in parentheses is 2σ in fifth decimal place.

† Flow 5 of Findley Ridge measured section

‡ Flow 1 of Findley Ridge measured section

WR, whole rock; S, sanidine.

Rawley Andesite alone, Varga and Smith obtained initial ratios ranging from 0.70529 to 0.70612 compared to the less radiogenic values of 0.70542 to 0.70560 for the Conjechos volcanics (Lipman, et al., 1978). For andesitic lava flows and the Tbl together, values ranging from 0.70529 to 0.70688 were obtained, compared to the range of 0.7048 to 0.7075 for the intermediate rocks of the larger San Juan field (Lipman, et al., 1978). Lipman also considered other rocks of the western U.S., and concluded that most mafic units have lower Sr values whereas the silicic units are generally more radiogenic than the flows of the San Juans. Indeed, Cenozoic rhyolites of the western U.S. frequently have initial Sr ratios as high as 0.710 to 0.715.

CHAPTER 7

DISCUSSION

Introduction

Several questions concerning unusual features of the Bonanza volcanics have been raised in this study, and merit further discussion:

- 1) Why did the Bonanza Tuff erupt five million years earlier than any other pyroclastic deposit in the San Juan volcanic field?
- 2) Why does the Bonanza Tuff contain virtually no Plinian airfall component?
- 3) Why do changes in chemistry of the Bonanza units not correspond to changes in mineralogy? Are these actual chemical trends that existed in the magma chamber, or have they been induced by eruptive or post-depositional processes?
- 4) Why do rocks of the Bonanza area have unusually high K_2O contents?
- 5) Does the Tbu have an anomalous chemistry because it is derived from a separate magma chamber, as has been suggested by Marrs (1973) and Varga and Smith (1984)?
- 6) Why does the mineral chemistry become more evolved with height instead of more mafic, as is expected for eruptions from a zoned magma chamber?

These questions will be considered in the following paragraphs.

1. Early eruption of the Bonanza Tuff

None of the data collected in this study provide insight into the mechanism(s) controlling the early eruption of the Bonanza Tuff. Varga and Smith (1984) believe that this anomalous timing is related to the location of the Bonanza caldera along the western edge of the Rio Grande rift system. Although most researchers believe that rifting began in the Miocene (5-22.5 mya), Tweto (1979) found subsurface evidence in the San Luis Valley that extensional faulting occurred in this area more than 28 mya (mid-Oligocene). Perhaps faulting was also active in the early Oligocene, beginning after the eruption of the Rawley Andesite and the Conjehos volcanics. This faulting may have caused a sudden release of pressure that precipitated movement of silicic magma from the main San Juan batholith to a chamber at shallow crustal levels. Continued faulting may have triggered the exsolution of volatiles from the melt and caused the early eruption of the Bonanza Tuff.

2. Lack of Plinian airfall

The lack of Plinian airfall deposits at Bonanza is in striking contrast to the large volumes of airfall pumice and ash preceding the ignimbrite eruptions at Vallez Caldera, New Mexico, Komagatake, Japan (Kozu, 1934), Crater Lake, Oregon (Williams, 1942), Soufriere, St.

Vincent (Hay, 1959), Mayon Volcano, Philippines (Moore and Melson, 1969), Ngauruhoe Volcano, New Zealand (Nairn and Self, 1978), and Santorini, Greece (Heiken and McCoy, 1984). At these localities, ash flows are attributed to the gravitational collapse of the eruption column. Wilson et al. (1978) calculated that the maximum height of an eruption column is proportional to the eruption rate, so that gravitational collapse of the column occurs as the eruption rate decreases. Eruption rate, in turn, decreases as the radius of the source vent increases, or as the content of exsolved water decreases (Wilson et al., 1980).

Evidence of a Plinian airfall component to the Bonanza Tuff occurs only in a restricted area at Windy Point (Fig. 12), near the proposed source vent for the tuff. Perhaps this paucity of airfall deposits indicates that the Bonanza ash flows were triggered by a mechanism other than column collapse. A lack of explosive exsolution of volatile components could have caused a "boiling over" of ash flows (similar to immediate column collapse) as has been observed at Mt. Lamington, Papua (Taylor, 1958), Cotopaxi, Ecuador (Wolf, 1878), and at least one of the eruptive events of Mt. Pelee in 1902 (Anderson and Flett, 1903). The high fluorine contents of the biotites in the Bonanza Tuff add plausibility to this suggestion. Fluorine is more soluble in magma than water,

and so would exsolve at lower pressures than H₂O (Fisher and Schminke, 1984). Just as a hand gun has a shorter range than a rifle, gases that exsolve nearer the surface do not provide as much upward propulsion to an erupting lava as those that exsolve deeper in the eruptive system.

3. Chemistry vs. mineralogy

It was noted in Chapter 6 that the most evolved samples of the Bonanza volcanics on the basis of mineralogy do not plot at the most siliceous end of the Harker diagrams, but instead are scattered throughout the overall trend. Similarly, although minerals become more evolved with stratigraphic height (i.e. more Fe- and Na-rich, etc.), whole-rock chemistry shows no systematic trend with time. Because the minerals show a consistent change in composition with stratigraphic height, it must be assumed that the phenocryst phases preserve the actual chemical zonation of the pre-eruptive magma chamber, and that the glass or whole-rock chemistry has somehow deviated from the original composition. This is not a surprising conclusion, because glass certainly is much more susceptible to alteration than phenocrysts.

a. Magmatic Processes

It is unlikely that a late-stage magmatic process would alter only the liquid (and therefore whole-rock)

composition of a zoned magma and preserve the existing phenocryst compositions. If a process such as mixing or assimilation occurred late in the history of a zoned magma chamber, one would expect to see rims of different compositions on the existing phenocrysts. However, none of the mineral phases exhibit optically or chemically distinguishable zonation except the feldspar phenocrysts, and zonation of the latter was probably caused by diffusion processes, as explained in Chapter 4. Certainly no large-scale convection has occurred, otherwise the stratigraphic trends exhibited by the phenocryst phases would not have been preserved. As described by Rice (1981), some double diffusive convection may have occurred, but this cannot explain the observed chemical trends. Late-stage underplating of the chamber by a mafic magma could cause upward migration of volatiles with concurrent transfer of volatile elements (e.g., K, Na, F, Cl, etc.) and thus alter the existing liquid compositions. However, this process would be expected to result in thermal and chemical gradients, and hence would only modify any pre-existing stratigraphic zonation -- not destroy it. Thus, pre-eruptive processes can be eliminated as a likely cause for the existing chemical trends of the Bonanza units.

b. Lithic Accumulation

The syn-eruptive processes of lithic accumulation and winnowing should also be explored. Lithic clasts picked up from the source vent or from deposits over-ridden by the ash flows are not uniformly distributed throughout the Bonanza Tuff samples. Because of their greater density, lithics are preferentially located near source vents and at the bottom of pyroclastic flows (Walker, 1972; Marrs, 1973). Also, eruptions in which new vents are opened or in which old vents are shifted contain a greater percentage of lithic fragments. Abnormal concentrations of lithics in a particular sample could significantly change the whole-rock chemistry.

To test the effects of lithic accumulation on the chemistry of the Bonanza volcanics, the volumetric percent of lithics has been plotted versus stratigraphic height in Figure 45. Samples #10 and 13 contain a relatively large number of lithic fragments, and perhaps mark a shifting or widening of the source vent. These two samples, however, do not display anomalous chemical compositions and this fact thereby eliminates the process of lithic accumulation as the major cause for the lack of correlation between whole-rock chemical variations and mineralogical variations.

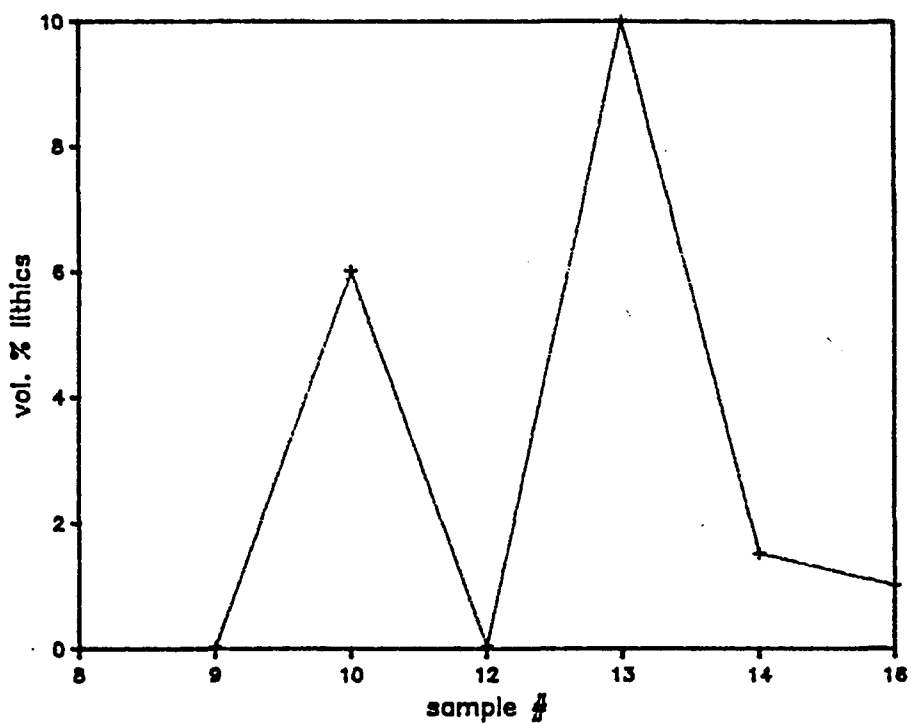


Fig. 45. Plot of volume percent lithics in the Bonanza Tuff ash flows versus stratigraphic height.

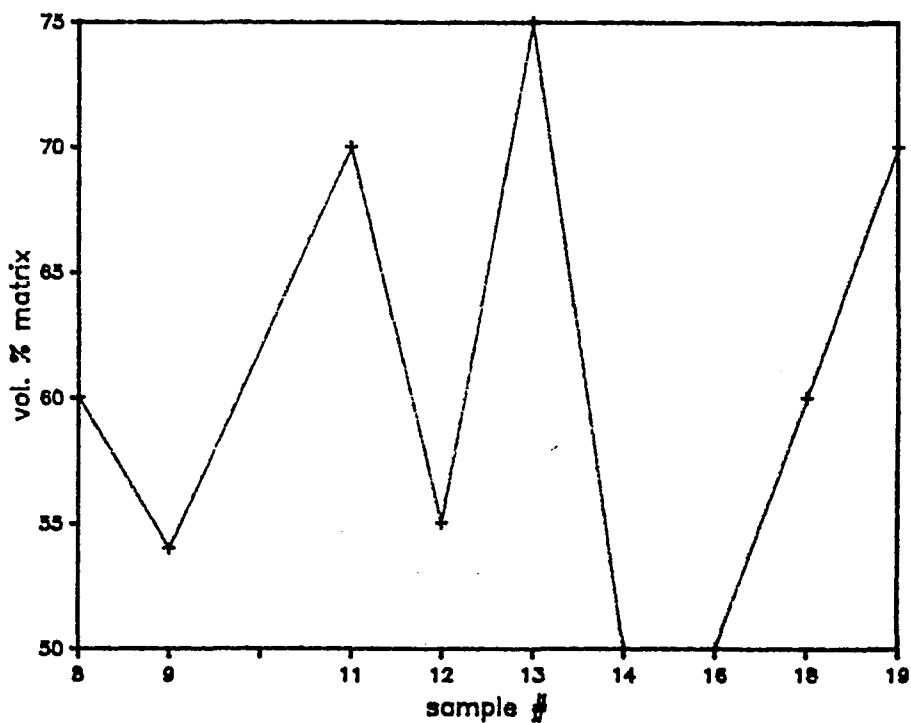


Fig. 46. Plot of volume percent matrix in the Bonanza Tuff ash flows versus stratigraphic height.

c. Eolian Winnowing

Eolian winnowing of vitric fines is another possible process by which whole-rock chemistry could have been modified (see Chapter 5). Every eye-witness account of historic ash-flow eruptions has reported billowing clouds of ash trailing above the dense gravity flows, so that winnowing of ash has certainly occurred in the Bonanza pyroclastic flows as well. To gauge the impact of winnowing on the Bonanza whole-rock chemistry, the volume percent of matrix in each sample has been plotted versus stratigraphic height (Fig. 46). Theoretically, samples with greater percent matrix have undergone less winnowing and should correspond to compositions richer in the "vitric components" (SiO_2 , K_2O , Na_2O , and incompatible trace elements). In reality, however, only the large increase in percent matrix between samples 9 and 11 consistently corresponds to an increase in vitric components, and matrix-poor samples 14 and 16 (especially 16) frequently are the least enriched in vitric components. The elements with trends that correspond least to fluxuations in percent matrix are SiO_2 and K_2O .

The lack of complete correspondence between percent matrix and vitric component content, however, does not mean that winnowing was not significant during eruption of the Bonanza ash flows. First, in this study the effects of welding cannot be separated from the effect of

winnowing. Greater degrees of welding in a flow will produce a greater concentration of phenocrysts in a given volume, and thus a sample from this flow will seem to have undergone greater degrees of winnowing. Second, the effects of alteration have probably overprinted the relative depletion or enrichment of elements caused by winnowing. For example, the secondary silicification of samples 29 and 71 causes relative depletion of all other elements in the rocks, as can be seen in Table 3.

4. High K₂O

A second unusual feature of the Bonanza chemistry is the unusually high K₂O content of the rocks, as demonstrated in Figure 40. Studies by Larsen and Cross (1956) and Varga and Smith (1984) report comparable K₂O values for the Bonanza units, indicating that this is a real characteristic of the rocks and not one induced during sample selection or by analytical techniques. K₂O content is not a result of winnowing during the eruptive process, either, because winnowing would tend to decrease K₂O content. Thus, the observed enrichment of K₂O is either a result of pre-eruptive magmatic processes or of post-depositional conditions.

a. Magmatic Processes

Magmatic processes which can concentrate K_2O in a melt include crustal melting, assimilation, large degrees of fractional crystallization, or small degrees of mantle melting. Crustal melting is an unlikely source for the Bonanza magmas because the partial melting of granite would produce equal amounts of quartz, orthoclase, and plagioclase liquids (Stewart, 1979). An average granite has a K_2O content of 4.07 wt. percent (Cox, et al., 1979), so that even the complete melting of a granitic crust (orthoclase is the last mineral to melt) would not form a magma with the composition of average Bonanza Tuff (K_2O content of 5.20 wt. percent). Indeed, a source rock composed predominantly of K-feldspar would have to be melted to produce this value (Stewart, 1979). Furthermore, the low $^{87}Sr/^{86}Sr$ values of the Bonanza volcanics (Varga and Smith, 1984) preclude large-scale interaction with crustal rocks. These arguments also discount assimilation as a cause for high K_2O .

Large degrees of fractional crystallization and/or small degrees of mantle melting have both been cited as possible processes for the formation of high-K rocks, such as the trachytes examined by Ewart (1982). However, whereas the K_2O contents produced by these processes may be similar to those at Bonanza, other resulting chemical characteristics are quite different. For example,

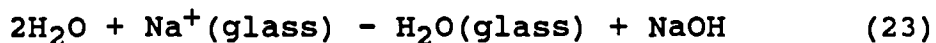
trachytes generally have K_2O/Na_2O ratios approximately equal to one and SiO_2 contents of 61 wt. percent compared to the composition of Bonanza's Rawley Andesite (K_2O/Na_2O ratio of 1.45 and SiO_2 content of 52.8 wt. percent). Thus, the formation of Bonanza compositions by fractional crystallization or mantle melting would require unusual conditions, or an initially high-K/low Na source. In addition, whereas K_2O contents of the Bonanza volcanics are unusually high, the concentrations of incompatible trace elements are relatively low. Fractional crystallization or partial melting would tend to concentrate all of these elements in comparable proportions. Therefore, neither of these processes can be responsible for the observed chemical features of the Bonanza rocks.

Finally, underplating of silicic magma in the chamber by basalt could lead to the transfer of K_2O by volatiles migrating roofward to areas of lower pressure. This process could only produce the K_2O contents observed at Bonanza in a magma chamber sited at the unlikely depth of 30 km, however, because vapor is less potassic than natural granite at vapor pressures less than ten kilobars (Stewart, 1979). A vapor much more potassic than granite would be required to create the average Bonanza Tuff K_2O content of 5.20 wt. percent.

b. Alteration

The most plausible explanation for the high K₂O content of the Bonanza rocks is that they have been altered by cation exchange with meteoric water. Varga and Smith (1984) report high O¹⁸ values for the Bonanza rocks, suggesting that they equilibrated at values lower than magmatic temperatures, and therefore have undergone hydrothermal alteration and/or weathering.

Fisher and Schmincke (1984) report that K-enrichment is the second stage of post-depositional alteration of volcanic glass, occurring after hydration of the glass and before the formation of secondary minerals such as clays and zeolites. This type of alteration occurs because Na⁺ and K⁺ are susceptible to exchange with the H⁺ ions in groundwater. Na⁺ is often leached from the rocks according to the reaction:



(Fisher and Schmincke, 1984). The leached Na₂O may then be replaced by K₂O, causing the high K₂O contents observed in many volcanic glasses (Sparks and Walker, 1977). Cases of K₂O substituting for other cations in industrial glasses have been cited by Stanworth (1950, p. 117, 151).

Other elements in glasses are also affected by groundwater leaching. Lipman (1965) compared the chemical

composition of glassy and crystalline volcanic rocks from the western U.S., and observed that the glasses were lower in SiO_2 and Na_2O than the crystalline rocks, and that immobile Al_2O_3 was relatively enriched. Lipman then sampled groundwater from the volcanic terrains, and noticed that the water was very low in Al_2O_3 , but high in SiO_2 and Na_2O . Sparks and Walker (1977) estimate that two to four times as much SiO_2 than Na_2O is leached from glasses. Minor leaching of F_2 , Cl_2 , CO_2 (Fisher and Schmincke, 1984), Li (Zielinski et al., 1976), and Ca, and the addition of Mg and Sr (Noble, 1970) have also been reported. U and Fe are fairly immobile, but Fe becomes strongly oxidized with groundwater interaction (Noble, 1970; Fisher and Schmincke, 1984).

The Bonanza units exhibit great scatter of K_2O and Na_2O data, which is consistent with post-depositional alteration processes. In addition, the complementary trends of SiO_2 and Al_2O_3 suggest that these variations are the result of relative depletion of Al_2O_3 in samples that have undergone secondary silicification, and relative enrichment of Al_2O_3 in samples from which SiO_2 has been leached during weathering. Because SiO_2 and Al_2O_3 compose approximately 80 percent of each sample by weight, the trends of elements other than Al_2O_3 are not noticeably affected by enrichment or depletion of silica (Lipman, 1965).

In his study, Lipman (1965) noticed that rocks that have greater porosity (ie. poorer welding or smaller shard size) also have greater K_2O/Na_2O ratios due to greater interaction with water. The Bonanza tuffs show no such correlation; however, the tuffs do have dramatically higher alkali ratios than the more dense Rawley Andesite and Upper volcanic lavas. In addition, there is a positive correlation between alkali ratio and the water contents of the Bonanza units analyzed by Varga and Smith (1984), suggesting that K_2O content is related to hydration of the volcanic glass (Fig. 47).

5. Chemistry of the Tbu

Previous workers have classified the Tbu as a separate unit from the Tbl based on petrologic differences such as a greater sanidine/plagioclase ratio, a deficiency in biotite crystals (Marrs, 1979), and the presence of quartz phenocrysts in the Tbu (Varga and Smith, 1984). In addition, the greater silica contents of the Tbu caused it to be classified as a rhyolitic ash flow (in contrast to the dacitic Tbl flows). Based on these differences, Varga and Smith (1984) decided that the Tbu was cogenetic with the Tbl, but not comagmatic. Because the petrographic and chemical data obtained during this study do not support previous interpretations of the relationship of the Tbu to the Tbl, hypotheses for the origin of the Tbu should be

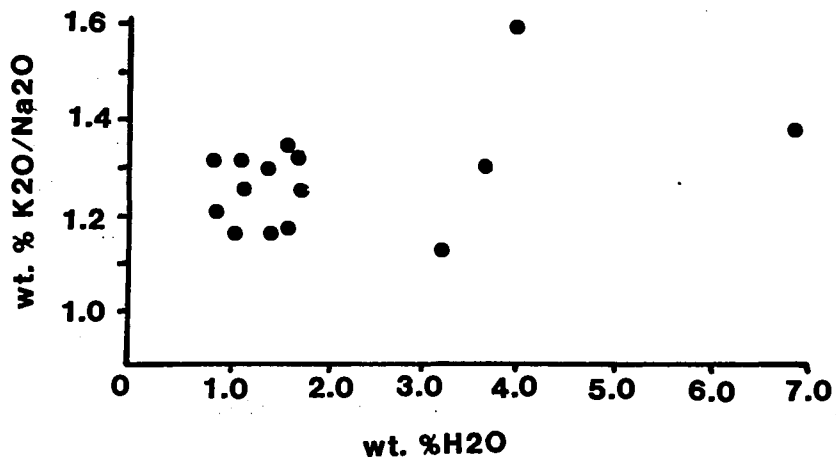


Fig. 47. Plot of K_2O/Na_2O ratio of the Bonanza Tuff samples analyzed by Varga and Smith (1984) versus wt. percent H_2O .

re-examined.

Although the samples of Tbu examined in the present study do not contain quartz phenocrysts, they do have matrices composed largely of secondary quartz, which presumably shifts the whole-rock chemical composition into the rhyolitic range. The Tbu samples studied also show greater sanidine/plagioclase ratios and fewer mafic minerals than the underlying Tbl flows, confirming the petrographic description of Marrs (1979). What the previous workers do not mention is the secondary nature of the silicification in these rhyolitic rocks, or the presence of an overlying ash flow (sample #19) with the same mineralogy as the Tbu, but with a chemistry very similar to that of the Tbl.

The fact that the Tbu (samples 18, 29, and 71) has the same mineralogy as the overlying flow and mineral chemistries that are largely consistent with the overall variations observed in the Bonanza region suggests that the Tbu is indeed comagmatic with the Tbl, and that the drastically different whole-rock chemistry of the Tbu is due to high degrees of alteration. Secondary silicification is evident in Tbu samples 29 and 71, and is perhaps related to the first, ore-barren phase of hydrothermal fluids that circulated within the caldera. High O^{18} values (Varga and Smith, 1984) support the hypothesis that the Tbu has been highly altered.

One question that might be raised is how the Tbu came to be so silicified, when it is sandwiched between unsilicified units. Perhaps the flow of silicifying fluids occurred only in this unit because of its poor welding and associated high porosity, or perhaps flow was fracture-controlled, as is indicated by the spatial variability of the silicification. The silicification also could have been caused by the escape of gases as the tuff compacted, but this explanation implies that the Tbu was more volatile-rich than the other flows, including the overlying flow.

6. Mineral chemistry trends

It is evident from the previous discussion that the glass and whole-rock chemistry of the Bonanza units are not equivalent to the original liquid compositions, and therefore cannot be used to characterize the pre-eruption magma chamber. Instead, the mineral phases offer the only key to conditions within the magma chamber. It is upon examination of the mineral chemistries that the most unique feature of the Bonanza volcanics is revealed. The mineral chemistry of the Bonanza flows becomes more evolved with stratigraphic height, the opposite trend reported for eruptions from almost all zoned chambers (Smith, 1979).

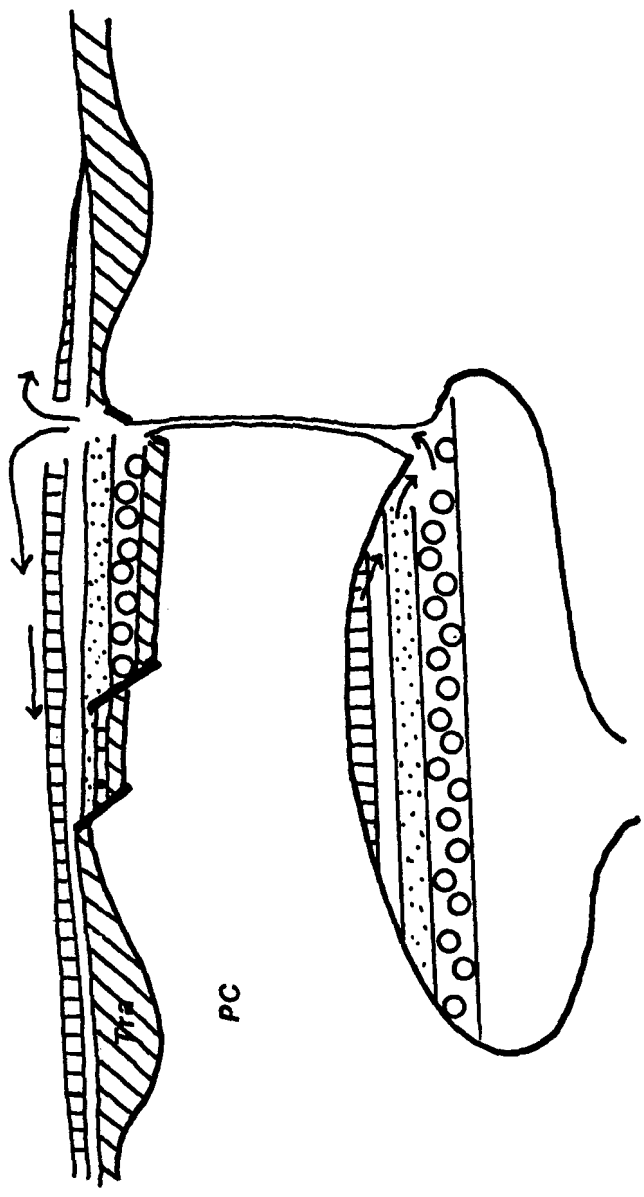


Fig. 48. Model for eruption of the Tertiary Bonanza magma chamber. Eruptions tap the chamber along the side, with successive eruptions causing drawdown from more roofward parts of the chamber.

One explanation for the Bonanza mineral trends is that these flows erupted at a slow rate from an unzoned magma chamber in which fractional crystallization was rapidly altering the magma chemistry, causing the magmas to become more evolved with time. The Uv would then represent a later-injected, more mafic batch of magma. An argument against this theory is the absence of cooling breaks between flows within the caldera, suggesting a rapid eruption rate (Huijsmans, 1985). K/Ar dates (Varga and Smith, 1984) also indicate rapid eruption, because the ages of the Tbu and the Tbl are the same (within analytical error).

A more plausible explanation is that the Bonanza volcanics represent a zoned magma chamber that was tapped along the side instead at the top of the chamber, with successive eruptions causing drawdown from progressively higher, more evolved parts of the chamber (Fig. 48). The deposits formed by such a processes would mimic the zonation within the magma chamber, and become increasingly felsic with stratigraphic height. (See Chapter 1 for a description of deposits produced from chambers tapped at the top.) The Uv most likely represents a new batch of mafic magma that was injected into the chamber late in the eruptive history.

CHAPTER 8

CONCLUSIONS

The following conclusions have been reached concerning the volcanic history of the Bonanza area. Because the study was focused on the Bonanza Tuff, only generalized observations can be made about the Rawley Andesite and the Upper volcanic lavas.

- 1) The first lava erupted in the Bonanza area was the intermediate-composition Rawley Andesite (37.6 million years BP). Generation of this lava was probably related to the subduction of the Pacific plate beneath the western edge of the North American plate.
- 2) In the 1.6 million years following the eruption of the Rawley Andesite, the Bonanza magma chamber developed chemical and thermal zonations which have been preserved in the phenocryst phases of the Bonanza Tuff. The process(es) that formed these zones cannot be determined exactly; however, low $^{87}\text{Sr}/^{86}\text{Sr}$ ratios of the Bonanza Tuff preclude any large-scale assimilation or crustal melting. Fractional crystallization is the probable cause, although alteration of the tuff prohibits any meaningful modelling to test this hypothesis.
- 3) The zoned chamber was sited at a depth of 9 km, and the magma had an average temperature of 1010°C and a water pressure of at least 0.9 kb. The magma was water-undersaturated, but did contain a significant amount of fluorine.
- 4) Magma in the zoned Bonanza chamber erupted five million years earlier than other silicic chambers in the San Juan volcanic field due to its location along the western edge of the Rio Grande rift system. Tensional faulting along the rift first began in the Bonanza area, causing a release of

pressure that precipitated upward migration of magma to shallow crustal levels. After the magma in the shallow chamber had evolved, continued faulting triggered the exsolution of volatiles and the early eruption of the Bonanza Tuff.

- 5) The Bonanza magma chamber was tapped along the side instead of at the top of the chamber. This caused the eruption of more evolved liquids with time as drawdown induced the extrusion of magma from increasingly roofward zones. Late in the eruptive history, a more mafic magma was injected into the Bonanza magma chamber and was erupted (34.7 million years BP) as the intermediate-composition upper volcanic lavas.
- 6) At the surface, the F₂-rich vapor phase of the magma did not exsolve fast enough to produce an eruption column with associated Plinian airfall deposits. Instead, Tbl and Tbu flows "boiled over" from a source vent near present-day Porphyry Peak, or perhaps from ring-fractures in this area produced by concurrent caldera collapse. The source vent shifted or widened periodically, tearing out clasts of the volcanic superstructure and granitic country rock that became incorporated into the pyroclastic flows. The later-erupted, more mafic Upper volcanic lavas contained less volatiles, and so were erupted in a quieter manner.
- 7) Winnowing of vitric fines during the eruption process caused depletions of SiO₂, Na₂O, K₂O, and incompatible trace elements in the whole-rock samples. A quantitative estimate of the effects of winnowing upon rock chemistry is not possible, however, because winnowing probably did not occur in the same proportions for each eruption. Minor chemical variations were also caused by preferential accumulation of lithics in some flows due to widening of the source vent and/or gravitational settling of lithics to the bottom of a flow.
- 8) Winnowing effects were later over-printed by post-depositional alteration. Hydrothermal silicification enriched intra-caldera and Tbu samples in silica, but depleted them in all other elements. Weathering of the rocks followed, whereby cation exchange with meteoric water leached glass of Na₂O, SiO₂, and perhaps some other cations, and caused relative enrichment of Al₂O₃. K₂O was enriched in the glass, creating the unusually high K₂O contents of the Bonanza rocks.

LIST OF REFERENCES

- Anderson, T., and Flett, J.S., 1903, Report on the eruption of Mount Lamington, Papua: Aust. Bur. Min. Resour. Geol. Geophys. Bull., v. 38, p. 1-117.
- Barth, T.F.W., 1934, Polymorphic phenomena and crystal structure: Am. Jour. Sci., v. 5, p. 273.
- _____, 1951, The feldspar geological thermometers: Neues Jahrb. Mineral., v. 82, p. 143-154.
- _____, 1956, Studies in gneiss and granite: Norske Vidensk. Acad. Oslo, I. Mat.-Naturv Klasse, v. 1, p. 263-274.
- _____, 1962, The feldspar geologic thermometer: Norsk. Geol. Tidsskr., V. 42, p. 330-339.
- Barton, M., and Hamilton, D.L., 1982, Water-undersaturated melting experiments bearing upon the origin of potassium-rich lavas: Mineral. Mag., v. 45, p. 267-278.
- Barton, M., and Wyers, G.P., 1987, Estimation of the conditions of crystallization of Tertiary volcanics from Patmos (Dodecanesos, Greece) and implications for the intracrustal evolutionary history of xenocryst bearing, primitive alkali basaltic magmas: J. Volc. Geotherm. Res., submitted for publication.
- Boettcher, A.L., 1973, Volcanism and orogenic belts - the origin of andesites: Tectonophysics, v. 17, p. 223-240.
- Bohlen, S.R., and Essene, E.J., 1977, Feldspar and oxide thermometry of granulites in the Adirondach Highlands: Contrib. to Mineral. Petrol., v. 62, p. 153-169.
- Bottinga, Y., Kudo, A., and Weill, D., 1966, Some observations on oscillatory zoning and crystallization of magmatic plagioclase: Am. Mineral., v. 51, p. 792-806.

- Bowen, N.L., 1928, The Evolution of Igneous Rocks: Dover Publications (1956 ed.), New York, 251 p.
- Bridwell, R.J., 1968, Geology of the Kerber Creek area, Saguache County, Colorado: Colo. School of Mines thesis #1177, 104 p.
- Brown, W.L., and Parsons, I., 1981, Towards a more practical two-feldspar geothermometer: Contrib. Mineral. Petrol., v. 76, p. 369-377.
- Bruns, D.L., 1971, Geology of the Lake Mountain NE quadrangle, Saguache County, Colorado: Colo. School of Mines thesis #1367, 79 p.
- Buddington, A.F., and Lindsley, D.H., 1964, Iron-titanium oxide minerals and synthetic equivalents: J. Petrol., v. 5, p. 310-357.
- Burbank, W.S., 1932, Geology and ore deposits of the Bonanza mining district, Colorado: U.S. Geol. Survey Prof. Paper 169, 166 p.
- Chronic, H., 1980, Roadside Geology of Colorado, Mountain Press Publishing Company, Missoula, p. 1-6, 218-222.
- Cook, D.R., 1960, Bonanza project, Bear Creek Mining Company: Am. Inst. Mining Metall. Engineers Trans., Mining sect., p. 285-295.
- Cox, K.G., Bell, J.D., and Pankhurst, R.J., 1979, The Interpretation of Igneous Rocks, George Allen and Unwin, Boston, 450 p.
- Deer, W.A., Howie, P.A., and Zussman, J., 1978, An Introduction to the Rock Forming Minerals, The Chaucer Press, Bungay, 528 p.
- Dickinson, W.R., 1968, Circum-Pacific andesite types: J. Geophys. Res., v.73, p. 2261-2269.
- _____, 1970, Relation of andesites, granites, and derivative sandstones to arc-trench tectonics: J. Geophys. Space Phys., v. 8, p. 813-860.
- Ewart, A., 1979, A review of the mineralogy and chemistry of Tertiary - Recent dacitic, latitic, rhyolitic, and related salic volcanic rocks: in Barker, F., ed., Trondhjemites, Dacites, and Related Rocks, Elsevier Scientific Publishing Company, New York, p. 13-121.

- _____, 1982, Petrogenesis of the Tertiary anorogenic volcanic series of southern Queensland, Australia, in light of trace element geochemistry and O, Sr, and Pb isotopes: *J. Petrol.*, v. 23, p 344-382.
- Ferry, J.M., 1978, Fluid interaction between granite and sediment during metamorphism, south-central Maine: *Am. Jour. Sci.*, v. 278, p. 1025-1056.
- Fisher, R.V., and Schmincke, H.-U., 1984, Pyroclastic Rocks: Springer-Verlag, New York, 528 p.
- Gerlach, D.C. and Grove, T.L., 1982, Petrology of Medicine Lake Highland volcanics: Characterization of endmembers of magma mixing. *Contrib. Mineral. Petrol.* v. 80, p. 147-159.
- Gibson, I.L., 1970, A pantelleritic welded ash-flow tuff from the Ethiopian rift-system: *Contr. Mineral. Petrol.*, v. 28, p. 89-111.
- Gill, J., 1981, Orogenic Andesites and Plate Tectonics, Springer-Verlag, New York, 390 p.
- Harloff, C., 1927, Zonal structures on plagioclase: *Leidse Geol. Meded.*, v. 2, p. 99-114.
- Hay, R.L., 1959, Formation of the crystal-rich glowing avalanche deposits of St. Vincent: *B.W.I.J. Geol.*, v. 67, p. 540-562.
- Heiken, G., and McCoy, F, Jr., 1984, Caldera development during the Minoan eruption, Thira, Cyclades, Greece. *J. Geophys. Res.* v. 89, p. 8441-8462
- Helgeson, H.C., Delaney, I.M., Nesbitt, H.W., and Bird, D.K., 1978, Summary and critique of the thermodynamic properties of rock-forming minerals: *Am. J. Sci.*, v. 278-A, p. 1-229.
- Hildreth, W., 1981, Gradients in silicic magma chambers: implications for lithospheric magmatism: *J. Geophys. Res.*, V. 86, p. 10153-10192.
- Huijsmans, J.P.P., 1985, Calc-alkaline lavas from the volcanic complex of Santorini, Aegean Sea, Greece: University of Utrecht thesis, the Netherlands, 316 p.
- Hurlbut, C.S., Jr., and Klein, C., 1977, Manual of Mineralogy (after James D. Dana), 19th Edition, John Wiley and Sons, New York, 532 p.

- Iiyama, J.T., 1966, Contribution a' l'étude des équilibres sub-solidus du système ternaire orthose-albite-anorthite à l'aide des réactions d'échange d'ions Na-K au contact d'une solution hydrothermale: Bull. Soc. Fr. Mineral Cristallogr, V. 89, p. 442-454.
- Irvine, T.N., and Baragar, W.R.A., 1971, A guide to the chemical classification of the common volcanic rocks: Can. J. Earth Sci., v. 8, p. 523-548.
- Jakes, P., and White, A.J.R., 1972, Major and trace element abundances in volcanic rocks of orogenic areas: Geol. Soc. America Bull., V. 83, p. 29-40.
- Karig, Daniel E., 1965, Geophysical evidence of a caldera at Bonanza, Colorado: U.S. Geol. Survey Prof. Paper 525- B. p. B9-B12.
- Katsui, Y., 1963, Evolution and magmatic history of some Krakatoan calderas in Hokkaido, Japan: Jour. Fac. Sci. Hokkaido University Series IV, v. 11, p. 631-650.
- Kempner, H.A.A., 1978, Bonanza! A Pictorial History of Colorado's Kerber Creek Country, Little London Press, Colorado Springs, 48 p.
- Knepper, D.H., Jr., and Marrs, R.W., 1971, Geological development of the Bonanza-San Luis Valley-Sangre de Cristo Range area, south-central Colorado: in James, H.L. (ed.), Guidebook of the San Luis Basin, Colorado, p. 249-264.
- Kozu, S., 1934, The great activity of Komagatake in 1929: Tschermak's Mineral. Petrol. Mitt., v. 45, p. 133-174.
- Kudo, A.M., and Weill, D.F., 1970, An igneous plagioclase thermometer: Contr. Mineral. Petrol., v. 25, p. 52-65.
- Larsen, E.S., Jr., and Cross, W., 1956, Geology and petrology of the San Juan region, southwestern Colorado: U.S. Geol. Survey Prof. Paper 258, 109 p.
- Leet, L.D., Judson, S., and Kauffman, M.E., 1978, Physical Geology, Prentice-Hall, Inc., Princeton, 490 p.
- Lewis, G.N., and Randall, M., 1961, Thermodynamics: Revised by K.S. Pitzer and L. Brewer, second ed., McGraw-Hill, New York, 723 p.

- Lindsley, D.H., 1963, Fe-Ti oxides in rocks as thermometers and oxygen barometers: Carnegie Inst. Wash. Yb., v. 62, p. 60-65.
- Lipman, P.W., 1965, Chemical comparison of glassy and crystalline volcanic rocks: U.S. Geol. Survey Bull. 1201-D. 24 p.
- Lipman, P.W., Doe, B.R., Hedge, C.E., and Steven, T.A., 1978, Petrologic evolution of the San Juan volcanic field, southwestern Colorado: Pb and Sr isotopic evidence: Geol. Soc. America Bull., v. 89, p. 59-82.
- Lipman, P.W., Steven, T.A., and Mehnert, H.H., 1970, Volcanic history of the San Juan Mountains, Colorado, as indicated by potassium-argon dating: Geol. Soc. America Bull., v. 81, p. 2329-2352.
- Luhr, J.F., Carmichael, I.S.E., and Verekamp, J.C., 1984, The 1982 eruptions of El Chichon volcano, Chiapas, Mexico: mineralogy and petrology of the anhydrite-bearing pumices: J. Volc. Geotherm. Res., v. 23, p. 69-108.
- MacKenzie, W.S., 1957, The crystalline modifications of $\text{NaAlSi}_3\text{O}_8$: Am. Jour. Sci., v. 255, p. 481-516.
- Mahood, G., and Hildreth, W., 1982, Geochem., Cosmochem. Acta., v. 47, p. 11-30.
- Marrs, R.W., 1973, Application of remote sensing techniques to the geology of the Bonanza volcanic center: Colo. School of Mines thesis #1531, 281 p.
- Martin, R.C., 1965, Ignimbrite lithology at Whakamaru, New Zealand: N.Z. Jour. Geol. Geophys., v.8, p.680-701.
- Mayhew, J.D., 1969, Geology of the eastern part of the Bonanza volcanic field, Saguache County, Colorado: Colo. School of Mines thesis #1226, 94 p.
- Moore, J.G., and Melson, W.G., 1969, Nuees ardentes of the 1968 eruption of Mayon Volcano, Philippines: Bull. Volcanol., v. 33, p. 600-620.
- Mysen, B.O., and Kushiro, I., 1978, Compositional variations of coexisting phases with degree of melting of peridotite in the upper mantle: Am. Mineral., v. 62, p. 843-856.

- Nairn, I.A., and Self, S., 1978, Explosive eruptions and pyroclastic avalanches from Ngauruhoe in February, 1975: J. Volcanol. Geotherm. Res., v. 3, p. 39-60.
- Noble, D.C., 1970, Loss of sodium from crystallized comendite welded tuffs of the Miocene Grouse Canyon Member of the Belted Range Tuff, Nevada: Geol. Soc. America Bull., v. 81, p. 2677-2688.
- Nordstrum, D.K., and Munoz, J.L., 1985, Geochemical Thermodynamics: The Benjamin/Cummings Publishing Co., Inc., Reading, 477 p.
- Orville, P.M., 1962, Comments on the two-feldspar geothermometer: Norsk. Geol. Tidaskr, v. 42, p. 340-346.
- _____, 1972, Plagioclase cation exchange equilibrium with aqueous chloride solution at 700° and 2000 bars in the presence of quartz: Am. Jour. Sci., v. 272, p. 234-272.
- Patton, H.B., 1915, Geology and ore deposits of the Bonanza district, Saguache County, Colorado: Colo. School of Mines thesis #1531, 279 p.
- Perchuck, L.L., and Ryabchikov, I.D., 1968, Mineral equilibria in the system mepherine-alkali feldspar-plagioclase and their petrologic significance: Jour. Petrol., v. 9, p. 123-167.
- Perry, H.A., 1971, Geology of the northern part of the Bonanza volcanic field, Saguache County, Colo.: Colo. School of Mines thesis #1362, 72 p.
- Plouff, D., and Pakiser, L.C., 1972, Gravity study of the San Juan Mountains, Colo.: U.S. Geol. Survey Prof. Paper 800-B, p. B183-B190.
- Powell, M., and Powell, R., 1977, Plagioclase-alkali feldspar geothermometry revisited: Mineralogical Magazine, v. 41, p. 253-256.
- Robie, R.A., and Waldbaum, D.R., 1968, Thermodynamic properties of minerals and related substances at 298.15°K (250°C) and one atmosphere (1.1013 bars) pressure and at high temperatures: U.S. Geol. Surv. Bull., v. 1299, p.

- Seck, H.A., 1971, Der Einfluss des Drucks auf die Zusammensetzung koexistierender Alkalifeldspate und Plagioclase im System $\text{NaAlSi}_3\text{O}_8$ - KAlSi_3O_8 - $\text{CaAl}_2\text{SiO}_8$ - H_2O : *contrib. Mineral. Petrol.*, v. 31, p. 67-86.
- Smith, R.L., 1960, Zones and zonal variations in welded ash flows: U.S. Geol. Survey Prof. Paper 354-F, p. 149-169.
- _____, 1979, Ash-flow magmatism: *Geol. Soc. America spec. Paper 180*, p. 5-27.
- Smith, R.L., and Bailey, R.A., 1968, Resurgent cauldrons: in Coats, R.R., Hay, R.L., and Anderson, C.A. (eds.), *Studies in volcanology*: *Geol. Soc. America Memoir 116*, p. 613-662.
- Sparks, R.S.J., and Walker, G.P.L., 1977, The significance of vitric-enriched air-fall ashes associated with crystal-enriched ignimbrites: *J. Volc. Geotherm. Res.*, v. 2, p. 329-341.
- Sparks, R.S.J., and Wilson, L., 1982, Explosive volcanic eruptions. V. Observations of plume dynamics during the 1979 Soufriere eruption, St. Vincent: *Geophys. J. Roy. Astron. Soc.*, v. 69, p. 551-570.
- Spencer, K.J., and Lindsley, D.H., 1981, A solution model for coexisting iron-titanium oxides: *Am. Mineral.*, v. 66, p. 1189-1201.
- Steven, T.A., and Lipman, P.W., 1976, Calderas of the San Juan volcanic field, southwestern Colorado: U.S. Geol. Soc. Prof. Paper 958, 35 p.
- Stewart, D.B., 1979, The formation of siliceous potassic glassy rocks: in Yoder, H.S., ed., The Evolution of the Igneous Rocks: Fiftieth Anniversary Perspectives, Princeton University Press, Princeton, p. 339-350.
- Stormer, J.C., Jr., 1975, A practical two-feldspar geothermometer: *Am. Mineralogist*, v. 60, p. 667-674.
- _____, 1983, The effects of recalculation on estimates of temperature and oxygen fugacity from analyses of multi-component iron-titanium oxides: *Am. Mineral.*, v. 68, p. 586-594.
- Stormer, J.C., and Whitney, J.A., 1985, Two feldspar and iron-titanium oxide equilibria in silicic magmas and the depth of origin of large volume ash-flow tuffs: *Am. Mineralogist*, v. 70, p. 52-64.

- Taylor, G.A., 1958, The 1951 eruption of Mount Lamington, Papua: Austr. Bur. Min. Resour. Geol. Geophys. Bull., v. 38, p. 1-117.
- Thompson, J.B., 1967, Thermodynamic properties of simple solutions: in P.H. Anderson, ed., Researches in Geochemistry, II, John Wiley and Sons, New York, 663 p.
- Thompson, J.B., and Waldbaum, D.R., 1969a, Mixing properties of sanidine crystalline solutions: III. Calculations based on two-phase data: Am. Mineral., v. 54, p. 811-838.
- Tweto, O., 1979, The Rio Grande rift system in Colorado: in Riecher, R.J., ed., Rio Grande Rift: Tectonics and Magmatism, American Geophysical Union, Washington D.C., 438 p.
- Varga, R.J., and Smith, B.M., 1984, Evolution of the early Oligocene Bonanza caldera, northeast San Juan volcanic field, Colorado: Jour. Geophys. Research, v. 89, p. 8679-8694.
- Waldbaum, D.R., and Thompson, J.B., 1969b, Mixing properties of sanidine crystalline solutions: IV. Phase diagrams from equations of state: Am. Mineral., v. 54, p. 1274-1298.
- Walker, G.P.L., 1972, Crystal concentration in ignimbrites: Contr. Mineral. Petrol., v. 36, p. 135-146.
- Wells, P.R.A., 1977, Pyroxene thermometry in simple and complex systems. Contrib. Mineral. Petrol., v. 62, p. 129-139.
- Williams, 1942, The geology of Crater Lake National Park: Carnegie Inst. Wash. Publ., v. 540, p. 1-162.
- Wilson, L., Sparks, R.S.J., Huang, T.C. and Watkins, N.D., 1978, The control of volcanic eruption heights by eruption energetics and dynamics. J. Geophys. Res., v. 83, p. 1829-1836.
- Wolf, T., 1878, Der Cotopaxi und seine litze Eruption am 26. Juni 1877: N. Jb. Min. Geol., p. 113-167.
- Wood, B.J., and Banno, S., 1973, Garnet-orthopyroxene and orthopyroxene-clinopyroxene relationships in simple and complex systems: Contr. Mineral. Petrol., v. 42, p. 109-124.

Wyllie, P.J., 1971, The Dynamic Earth, Wiley, New York, 416 p.

Zielinski, R.A., Lipman, P.W., and Millard, H.T., Jr., 1976, Minor element variations in hydrated and crystallized calc-alkaline rhyolites: in U.S. Geol. Survey Prof. Paper 1000, 175 p.